Stress adaptation of mitochondrial protein import by OMA1-mediated degradation of DNAJC15

Inaugural-Dissertation

zur Erlangung des Doktorgrades
der Mathematisch-Naturwissenschaftlichen Fakultät
der Universität zu Köln

vorgelegt von
Lara Kroczek

Köln, den 7. Juli, 2025

Tag der mündlichen Prüfung: 29.09.2025

Für meine Eltern

Table of contents

List of figures

List of abbreviations

%	percent
°C	degree Celsius
AA	amino acids
AAA	ATPases associated with diverse cellular activities
AGK	acylglycerol kinase
AIFM1	apoptosis-inducing factor 1
bp	base pair
bZIP	basic leucine zipper
DCMA	dilated cardiomyopathy with ataxia
eIF2α	eukaryotic translation initiation factor 2 subunit α
ER	endoplasmic reticulum
ERAD	endoplasmic reticulum-associated degradation
ERMES	endoplasmic reticulum-mitochondria encounter structure
ER-SURF	ER surface-mediated protein targeting
et al.	Latin *et alii*, meaning “and others”
g	gravity of Earth
GCN2	general control nonderepressible 2
GET	guided entry of tail-anchored
h	hour
HAX1	HCLS1-associated protein X-1
Hot13	helper of TIM protein 13
HRI	heme-regulated inhibitor
HSE	heat shock elements
HSP	heat shock protein
HSP7	hereditary spastic paraplegia
HSR	heat shock response
iBAQ	intensity-based absolute quantification
IM	inner mitochondrial membrane
IMS	intramembrane space of mitochondria
M	molar (mol/L)
MAIP1	m-AAA protease interacting protein 1
MCU	mitochondrial calcium uniporter
MICOS	mitochondrial contact site and cristae organizing system
min	minute
mitoCPR	mitochondrial compromised protein import response
mitoRQC	mitochondrial ribosomal quality control
mitoTAD	mitochondrial protein translocation-associated degradation
MMP	mitochondrial membrane potential
MPP	mitochondrial processing peptidase
MS	mass spectrometry
mtDNA	mitochondrial DNA
MTS	mitochondrial targeting sequence
nm	nanometer
OMM	outer mitochondrial membrane
OXPHOS	oxidative phosphorylation
PAM	presequence translocase-associated motor
PCR	polymerase chain reaction

PERK	PKR-like ER kinase
PHB	prohibitin
pmol	picomolar
POTRA	polypeptide transport-associated
RIDD	regulated IRE1-dependent decay
ROS	reactive oxygen species
RT	room temperature
s.	see
S1P	site-1 protease
S2P	site-2 protease
SAM	sorting and assembly machinery
SCA28	spinocerebellar ataxia
SPAX5	spastic ataxia neuropathy syndrome
TIM23	presequence translocase of the inner membrane
TMD	transmembrane domains
TOM	translocase of the outer membrane
uORFs	upstream open reading frames
UPR	unfolded protein response
UPR^{mt}	mitochondrial unfolded protein response
α	alpha
β	beta
µ	micro

1. Abstract

The diverse functions of mitochondria are reflected in the complexity of their proteome. To rapidly adapt to environmental and cellular demands, mitochondria dynamically rewire their proteome, a process facilitated by mitoproteases that function as quality control enzymes and regulatory factors through targeted protein processing and degradation. The stress-regulated mitochondrial peptidase OMA1 plays a central role in these adaptive responses by limiting mitochondrial fusion and promoting mitochondrial stress signaling and metabolic reprogramming.

Here, we demonstrate that cellular stress adaptation involves OMA1-mediated regulation of mitochondrial protein import and oxidative phosphorylation (OXPHOS) biogenesis. Specifically, OMA1 cleaves the mitochondrial co-chaperone DNAJC15, targeting it for degradation by the m-AAA protease AFG3L2. DNAJC15 functions as a co-chaperone of the presequence translocase of the inner membrane, and is the functional homolog of the yeast import regulator Pam18. Loss of DNAJC15 impairs the import of OXPHOS-related proteins via the TIM23 complex, thereby limiting OXPHOS biogenesis under conditions of mitochondrial dysfunction. The accumulation of non-imported mitochondrial preproteins at the endoplasmic reticulum triggers an unfolded protein response.

Our findings reveal OMA1-mediated alterations in protein import specificity as part of the mitochondrial stress response and suggest that this mechanism restricts OXPHOS biogenesis under stress conditions until mitochondrial function is restored or defective mitochondria are eliminated via mitophagy. The accumulation of mitochondrial proteins at the endoplasmic reticulum under conditions of impaired mitochondrial import highlights the interdependence of proteostasis regulation across different organelles.

2. Introduction

2.1 Mitochondria

2.1.1 Mitochondrial plasticity and quality control

Mitochondria, often referred to as the "powerhouses of the cell", are essential for ATP production through OXPHOS. However, their functions extend far beyond energy metabolism, encompassing the regulation of apoptotic pathways, the synthesis of iron-sulfur clusters, and participation in diverse metabolic processes. Given their dynamic nature, mitochondria must continuously adapt to fluctuating cellular and environmental conditions. This adaptation necessitates precise regulation of the mitochondrial proteome to allow different metabolic outputs and preserve organellar integrity.

Mitochondrial plasticity is governed at multiple levels, including transcriptional, translational, and post-translational regulation. Among these, proteolysis plays a pivotal role in maintaining mitochondrial homeostasis. Proteases serve not only as quality control enzymes by selective degradation of proteins, but also as regulatory factors, modulating protein function through targeted processing. This proteolytic control is critical for numerous mitochondrial processes, including genome maintenance and gene expression, membrane protein assembly, phospholipid metabolism, mitochondrial dynamics, as well as the regulation of cell death and stress response pathways [1]. A decline in mitochondrial quality control is associated with ageing and the development of age-related diseases, such as cancer, diabetes, or neurodegenerative diseases [2, 3]. Considering the multifaceted functions of mitoproteases, it becomes apparent that common mitochondrial diseases overlap with illnesses resulting from mutations in mitoproteases [1].

2.1.1.1 The m-AAA protease

ATPases associated with diverse cellular activities (AAA) proteases utilize energy from ATP hydrolysis via conserved AAA+ domains to degrade proteins in various subcellular compartments [4, 5]. Mitochondrial proteases are embedded in the inner mitochondrial membrane (IM) and assemble into hexameric and cylinder-shaped structures. While the proteolytic domain likely facilitates correct complex assembly, oligomerization and stabilization of the hexamer are mediated by both the

transmembrane and AAA-ATPase domains [6, 7]. Their chaperone-like activity ensures the recognition of misfolded or exposed non-structured protein motifs [6].

In human mitochondria, two distinct AAA proteases exist. Whereas the i-AAA protease, composed of YME1L subunits, faces the IMS, the m-AAA protease, formed by homo- or hetero-oligomeric complexes of AFG3L2 and paraplegin (*SPG7*) [8], is directed towards the matrix. Structurally, these proteases are delineated by three functional domains. An N-terminal domain responsible for membrane anchoring, a central AAA-ATPase domain that includes Walker A (ATP binding) and Walker B (ATP hydrolysis) motifs, and a C-terminal M41 metallopeptidase domain [6, 9].

Both AAA proteases intricately associate with membrane scaffolds from the SPFH family, including stomatin, prohibitin, flotillin, and HflC/K [10, 11], which form multimeric ring-like structures and modulate membrane protein turnover affecting the lipid and protein environment of AAA proteases [1]. The m-AAA protease engages with PHB1 and PHB2 subunits, whereas the i-AAA protease, in conjunction with PARL, assembles with SLP2 [12]. Notably, the PHB complex exerts a negative regulatory influence on protease activity by limiting substrate accessibility of the m-AAA protease [13-15].

Due to its pivotal role in cellular homeostasis, mutations or deletions in m-AAA protease subunits are implicated in various neurodegenerative disorders. It is important to state that the expression levels of *SPG7* and *AFG3L2* differ across tissues, contributing to cell-type specific pathologies. Loss of *SPG7* function, the most common group of genetic disorders linked to the m-AAA protease, leads to progressive motor impairment, manifesting as spasticity in the lower extremities, causing hereditary spastic paraplegia (HSP7), a disorder marked by corticospinal neuron degeneration [16]. In contrast, mutations in *AFG3L2* are associated with severe neuromuscular phenotypes, including defects in axonal development, delayed myelination, and impaired axonal radial growth. Pathologies linked to *AFG3L2* mutations include spinocerebellar ataxia (SCA28) and spastic ataxia neuropathy syndrome (SPAX5) [17, 18], both characterized by Purkinje cell degeneration. In the context of these diseases, it is important to note that *SPG7* alone is unable to form functional homo-oligomeric structures. Moreover, its maturation following mitochondrial import and subsequent cleavage by

mitochondrial processing peptidase (MPP) is highly dependent on the autocatalytic processing of AFG3L2 [8, 19].

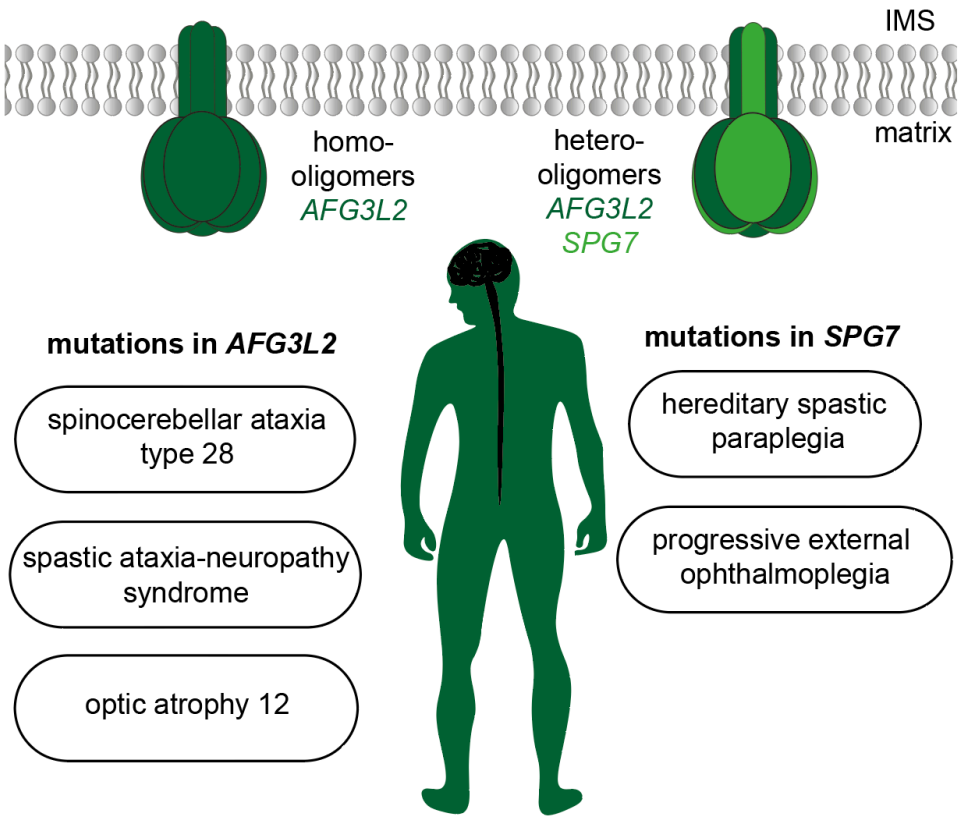

Figure 1. Diseases associated with mutations in the subunits of *AFG3L2* or *SPG7* in the m-AAA protease. The m-AAA protease assembles as a homo-oligomeric AFG3L2 complex (left) or a hetero-oligomeric *AFG3L2-SPG7* structure (right). Mutations in *AFG3L2* are linked to e.g. SCA28 and SPAX5 and OPA12, while *SPG7* mutations can cause HSP7 and PEO, reflecting tissue-specific expression and functional dependencies.

Mutations in the m-AAA protease are frequently associated with mitochondrial translation defects and impaired assembly of OXPHOS complexes, partially explained due to defective processing of MRPL32, a known substrate of the m-AAA protease and a component of the large mitochondrial ribosomal subunit [20]. Normally, MRPL32 undergoes cleavage of its unusually long mitochondrial targeting sequence (MTS) by the m-AAA protease, ensuring proper folding and integration into functional mitoribosomes. Upon impairment of AFG3L2 activity, mitochondrial translation is severely compromised due to the accumulation of immature MRPL32, further exacerbating translational defects.

Additionally, loss of AFG3L2 disrupts mitochondrial calcium homeostasis by compromising the regulation of EMRE, a key modulator of the mitochondrial calcium uniporter (MCU). Substrate-trapping experiments have identified m-AAA protease interacting protein 1 (MAIP1) as a cofactor involved in EMRE import. EMRE subsequently associates with MICU regulatory proteins to form a gatekeeping complex that controls calcium flux through MCU. EMRE is a substrate of AFG3L2 [21, 22] and excessive EMRE accumulation in the absence of a functional m-AAA protease leads to direct MCU binding lacking gatekeeper subunits. Consequently, a constitutively active calcium uniporter is formed, resulting in mitochondrial calcium overload and an increased susceptibility to calcium-induced cell death [22, 23]. Another crucial function of the m-AAA protease is its role in regulating TMBIM5 levels, a Ca^{2+}/H^{+} exchanger in the inner mitochondrial membrane, which inhibits the m-AAA protease [24]. Under hyperpolarization, TMBIM5 undergoes degradation by the m-AAA protease, relieving its inhibitory effect and triggering a remodeling of the mitochondrial proteome, including targeted degradation of complex I subunits [24]. This is consistent with findings demonstrating the turnover of OXPHOS subunits by the m-AAA protease, such as Cox1 [25], mt-ND1 [26], and NDUFA9 [27]. Furthermore, TIMMDC1, a complex I assembly factor, is stabilized by the IMS-residing protein C9orf72. This protein recruits the PHB-complex to inhibit m-AAA protease-mediated degradation of TIMMDC1, thereby directly influencing OXPHOS complex I assembly [28]. Recent studies have demonstrated that the m-AAA protease regulates the turnover of SLC25A39 in an iron-dependent manner. As a key transporter of glutathione (GSH) into the mitochondrial matrix, the AFG3L2-dependent degradation of SLC25A39 reduces both mitochondrial GSH and iron availability [29].

Furthermore, homologs in *Arabidopsis thaliana* and *Nicotiana tabacum* have revealed a crucial role of the Ycf2/FtsHi complex in preprotein translocation. The energy generated by the complex serves as the primary ATP source for protein translocation, further driven by its pulling force that facilitates the translocation of preproteins across the membrane [30, 31].

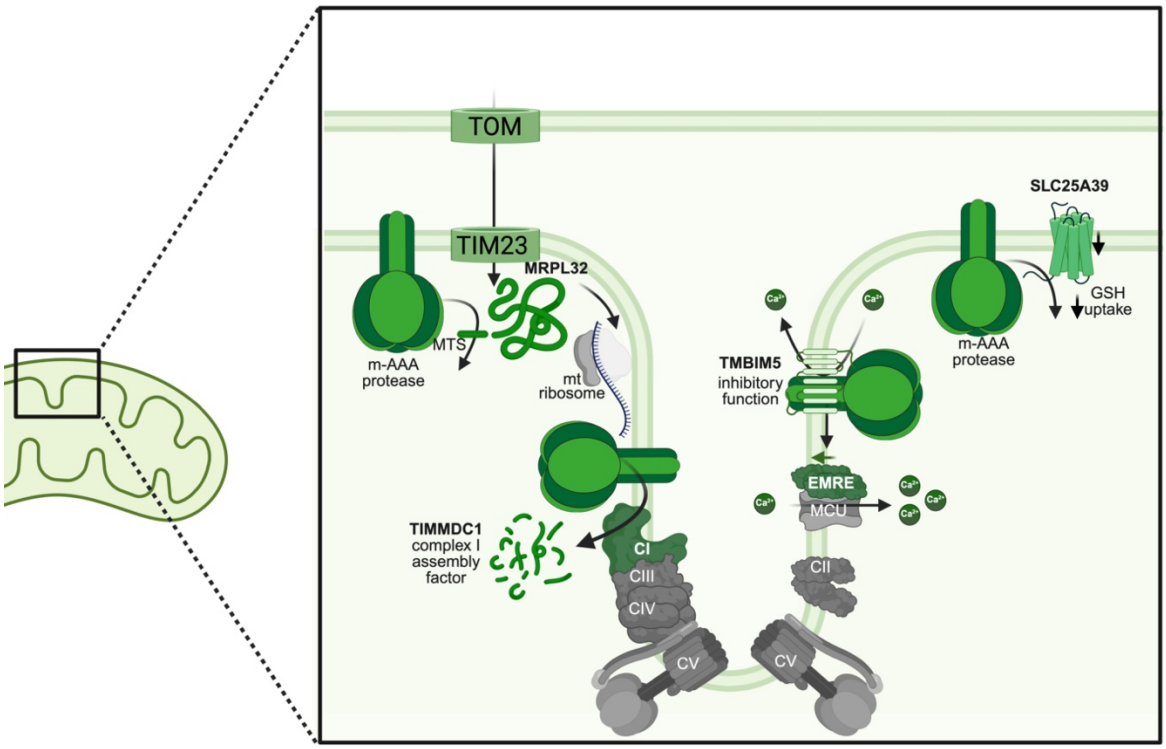

Figure 2. Mitochondrial proteostasis regulation by the m-AAA protease. The m-AAA protease regulates mitochondrial proteases by degrading and processing proteins localised in the IM or the matrix. Well-characterized substrates (bold) include MRPL32 and TIMMDC1, involved in mitochondrial translation and complex I assembly, respectively. Additionally, the protease degrades EMRE, TMBIM5, an inhibitor of AFG3L2, and SLC25A39, thereby limiting glutathione uptake into the mitochondrial matrix.

2.1.1.2 OMA1, a stress-activated protease

ATP-independent proteases, such as the metalloprotease OMA1, complement ATP-dependent proteases in maintaining mitochondrial quality control. Named for its overlapping activity with the m-AAA protease, OMA1 has emerged as a critical sensor and effector, integrating signals from various stress stimuli to regulate mitochondrial dynamics, proteostasis, stress responses, and apoptosis [32]. OMA1 is activated by diverse stress conditions and mitochondrial insults, including oxidative stress, heat stress, protein stress, reduced mitochondrial membrane potential (MMP), loss of mitochondrial DNA (mtDNA), impaired mitochondrial translation, defects in OXPHOS, and diminished ATP production [33-36]. In mammals it was shown that the N- and C-terminal extensions in OMA1 and redox-sensitive sites likely contribute to sensing those mitochondrial stressors [36, 37]. Upon activation, OMA1 can undergo autoproteolysis or its stability can further be regulated by YME1L-mediated degradation under certain stress conditions [36, 38-40].

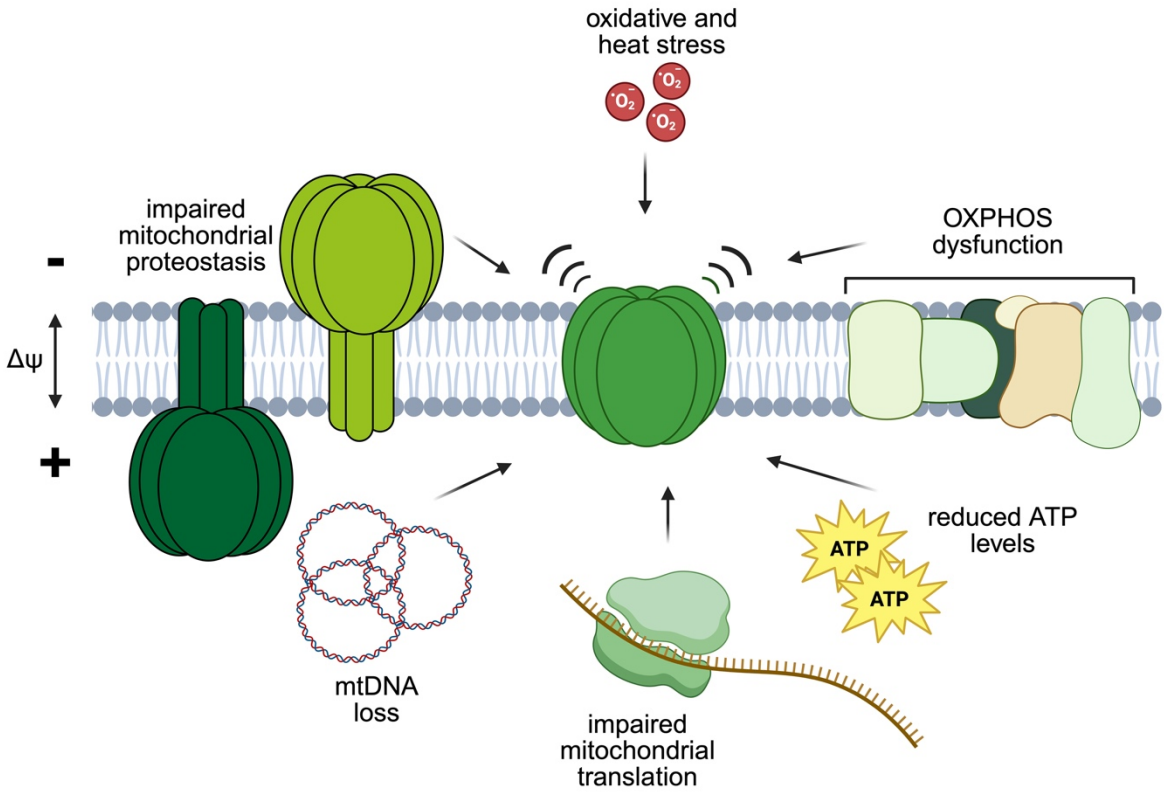

Figure 3. OMA1 is a mitochondrial, stress-responsive protease. Upon cellular and mitochondrial disturbances, that involve an impaired MMP, reduced ATP levels, oxidative stress, heat stress, mtDNA loss, impaired mitochondrial translation or impaired mitochondrial proteostasis, OMA1 gets activated.

OMA1 is involved in the regulation of mitochondrial dynamics via the regulation of both OPA1 and MIC19. Cleavage of OPA1, also processed by YME1L, limits mitochondrial fusion and leads to the accumulation of shorter isoforms that promote mitochondrial fragmentation [41], thereby increasing susceptibility to cytochrome *c* release and apoptosis in the presence of intrinsic apoptotic stimuli. OMA1 deficiency confers resistance to apoptotic stimuli [42-44]. This is further supported by an impaired OPA1 processing in OXPHOS-deficient hearts that disrupts autophagy, underscoring the role of long-OPA1 (L-OPA1) in limiting mitophagy [45]. Under basal conditions, absence of OPA1 cleavage does not affect mitochondrial dynamics [45], supporting the model in which L-OPA1 is sufficient to sustain mitochondrial fusion [46-48]. Short-OPA1 (S-OPA1), however, may enhance membrane fusion activity [46, 49]. Previous work identified a role of OPA1 processing in specifically disrupting the balance between lamellar and tubular cristae structures [50, 51].

OMA1 was further proposed to process MIC19, a protein essential for cristae architecture as a core component of the mitochondrial contact site and cristae organizing system (MICOS) complex [52]. Cleavage of MIC19 by OMA1 leads to destabilization of the SAM and MICOS complexes, which in turn results in the breakdown of cristae junctions and diminished ATP synthesis. It is noteworthy that mitochondrial network morphology in OMA1-deficient cells remains unaffected under basal conditions [42, 48, 53, 54].

A genome-wide CRISPR-Cas9 screen identified DELE1 as a OMA1 substrate. Under normal conditions, DELE1 is fully translocated across both mitochondrial membranes and subsequently degraded within the matrix [55]. However, upon mitochondrial stress, DELE1 becomes stalled in the import machinery, exposing its N-terminus to OMA1 for proteolytic processing in the IMS. This cleavage event enables the C-terminal fragment of DELE1 to retro-translocate into the cytosol, where it activates the integrated stress response (ISR) by promoting eukaryotic translation initiation factor 2 subunit α (eIF2α) phosphorylation [56-59].

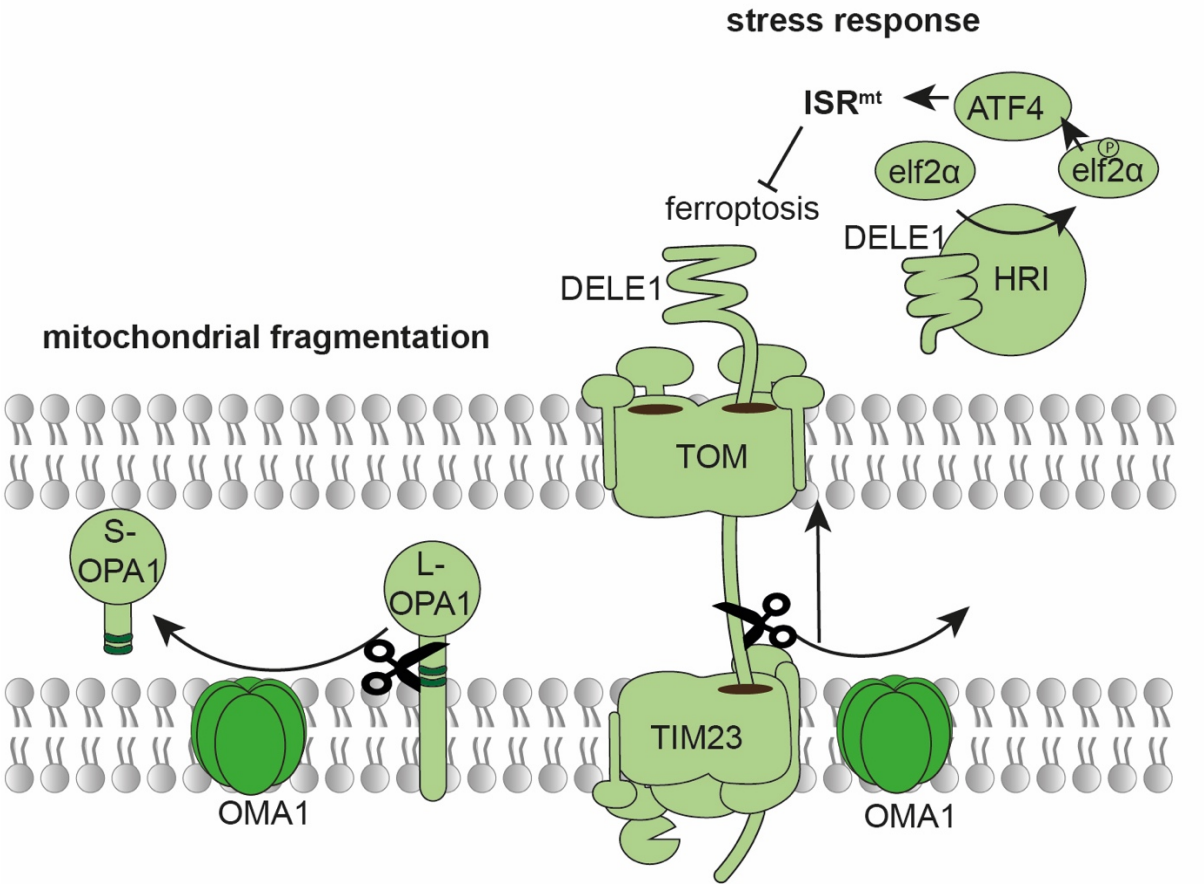

Figure 4. Regulation of mitochondrial dynamics and stress signaling by OMA1. OMA1 regulates mitochondrial dynamics by cleaving OPA1, promoting mitochondrial fragmentation in the IM. Under mitochondrial stress, OMA1 processes DELE1, enabling its cytosolic retro-translocation and activation of the ISR. Notably, impaired OPA1 processing did not affect the OMA1-DELE1 axis, proposing that the events occur independently [45].

The evidence supporting OMA1's role in stress responses is further substantiated by its regulation of substrates involved in mitophagy, the process by which damaged or dysfunctional mitochondria are recognized and eliminated. OMA1 has been shown to cleave mislocalised PINK1, a serine kinase initiating mitophagy [60]. A robust genetic interaction has been further observed between OMA1 and the E3 ubiquitin ligase Parkin, which is activated by PINK1 accumulation during mitochondrial stress. Parkin has been found to coordinate outer membrane fusion via MFN2 [61], thereby complementing OMA1's regulation of IM fusion through OPA1. The combined loss of OMA1 and Parkin in mice disrupts mitochondrial structure and significantly reduce lifespan [62]. Additionally, OMA1 regulates PGAM5 under stress in depolarized mitochondria and in the absence of PARL [11]. PGAM5 plays a critical role in mitochondrial dynamics, mitophagy, and cell survival. Furthermore, it has

been shown that OMA1 cleaves stalled protein intermediates in conditions of compromised protein import, thereby unblocking the import machinery for clearance by the VCP/p97 complex [63].

The protease OMA1 functions at the nexus of apoptotic signaling and cellular survival. Although nonessential under basal conditions, OMA1 assumes a pivotal role during metabolic challenges, such as the exposure to a high-fat diet or cold-induced thermogenesis [64]. In models of cardiac failure [65, 66], neurodegeneration [67], and hypoxia-reperfusion injury in the ischemic kidney, OMA1 exhibits a pro-apoptotic effect [68-70]. Conversely, OMA1 activation can initiate a protective ISR through the prevention of ferroptosis, which mitigates mitochondrial cardiomyopathy [71]. OMA1 has a pro-survival role in spinal axonopathy and ocular dysfunction [72]. Under DNA damage conditions, OMA1 is vital for the survival of the cells, as its loss reduces glycolysis and makes cells more prone to a p53-dependent apoptosis, independent of OMA1 activation or DELE1 or OPA1 involvement [73]. In the context of cancer biology, OMA1 exhibits context-dependent effects. In colorectal cancer, its activity supports tumor growth by inducing a metabolic shift toward hypoxic glycolysis [74]. Conversely, in metastatic breast cancer, loss of OMA1 correlates with enhanced proliferation, increased filopodia formation, and greater migratory capacity, indicating that OMA1 modulates distinct aspects of tumor progression [75].

Overall, the multifaceted roles of OMA1 underscore its significance as a central regulator of mitochondrial quality control and cellular fate. By sensing diverse mitochondrial stressors and modulating key proteins such as OPA1 and DELE1, OMA1 influences processes from mitochondrial dynamics to the induction of the ISR. Its diverse regulatory mechanisms and context-dependent functions highlight its potential as a therapeutic target in neurodegeneration, cardiovascular disease, cancer, and other pathologies.

2.2 Mitochondrial protein import

The functional diversity of mitochondria is reflected in the complex structure of its proteome. More than 1200 different proteins in humans make up the mitochondrial proteome [76]. Since only a minor fraction of those proteins is encoded by the mitochondrial genome [77], the majority of mitochondrial proteins are synthesized at

cytosolic ribosomes and translocated into mitochondria via multimeric protein complexes along a total of five pathways. The physiological properties of the proteins determine their way of mitochondrial entry. Most mitochondrial proteins enter mitochondria through the translocase of the outer mitochondrial membrane (TOM). Only some tail-anchored, α-helical OMM proteins insert directly into the OMM via the mitochondrial import (MIM) complex. After passing through TOM complex pores integration into the IM happens in a TIM22-, or TIM23-dependent manner, whereas integration into the OMM can happen via the sorting and assembly machinery (SAM). Proteins destined for the mitochondrial intermembrane space (IMS) are imported and folded with the assistance of the mitochondrial IMS import and assembly (MIA) pathway [78, 79]. In contrast, proteins targeted to the mitochondrial matrix or IM are imported via either the presequence pathway (TIM23) or, in the case of multispanning, hydrophobic carrier proteins, through the carrier translocase pathway (TIM22). Both import routes depend on an intact MPP. Additionally, matrix-destined proteins typically require ATP hydrolysis for translocation and possess an N-terminal presequence that forms a positively charged, amphipathic α-helix [80].

2.2.1 Protein entry into mitochondria

The translocation of most nuclear-encoded mitochondrial proteins is mediated by the TOM complex. This complex consists of multiple subunits, with TOMM40 forming the central channel. TOMM40 accommodates both hydrophobic and hydrophilic signals, facilitating the translocation of diverse substrate proteins [81, 82]. Structural analyses have revealed distinct electrostatic properties within the channel, offering insights into the mechanisms of protein translocation [83-85]. The channel interior is predominantly negatively charged, while the periphery and the central region of the dimer on the IMS side exhibit a primarily positive charge distribution [86]. This electrostatic architecture is thought to play a crucial role in guiding precursor proteins through the translocation pathway [85]. Substrate specificity is further refined by receptor proteins such as TOMM70. TOMM70 contains an N-terminal hydrophobic α-helix anchor with its C-terminal α-helical structure serving as the primary docking site for hydrophobic precursors proteins. Those proteins carry an internal targeting sequence, that need to be transferred to the subsequent import components by cytosolic chaperones [87]. Given its essential role in precursor recognition, mutations in TOMM70 have been linked to severe

neurological disorders characterized by pronounced OXPHOS deficiency, particularly reduced complex IV activity [88, 89]. The likely embryonic lethality associated with loss-of-function mutations in TOM subunits may explain their rarity in humans [90]. TOMM20 with its α-helix-rich structure and its hydrophobic groove functions as a receptor for mostly precursor proteins of the presequence pathway [91-94], that are simultaneously bound to the acidic cytosolic domain of TOMM22 [92, 95].

The dimeric structure of the TOM complex revealed phosphatidylcholine at the interface between the TOMM40 β-barrel channels [85]. In addition, TOMM22 is critical for maintaining the integrity of the complex, as its loss markedly disrupts TOM complex assembly [85]. Higher-order oligomers of TOMM40, including trimers and tetramers, have been observed, but their functional significance remains incompletely understood. Structurally, TOMM40 forms a β-barrel pore comprising 19 β-strands, with β-strands 1 and 19 interacting to facilitate dimerization [96]. This dimerization results in the formation of two independent channels, providing distinct translocation pathways and exit sites for imported proteins. The presence of an uneven number of β-strands is thought to reduce structural stability, facilitating necessary conformational changes during protein translocation [97, 98]. The stability and assembly of the TOM complex are further regulated by small TOM proteins, including TOMM5, TOMM6, and TOMM7 [99, 100]. TOMM7 regulates TOMM22 biogenesis by interacting with the SAM-Mdm10 complex, promoting its dissociation, an essential step for the proper assembly of TOMM22 [101]. Following passage through the TOM complex, the IMS-exposed domains of TOMM40 and TOMM22 ensure efficient transfer of precursor proteins to downstream translocases such as the TIM23 complex [84, 98, 102, 103]. Despite the central role of the TOM complex in mitochondrial protein import, some proteins bypass this pathway and enter mitochondria through TOM-independent mechanisms [94, 104].

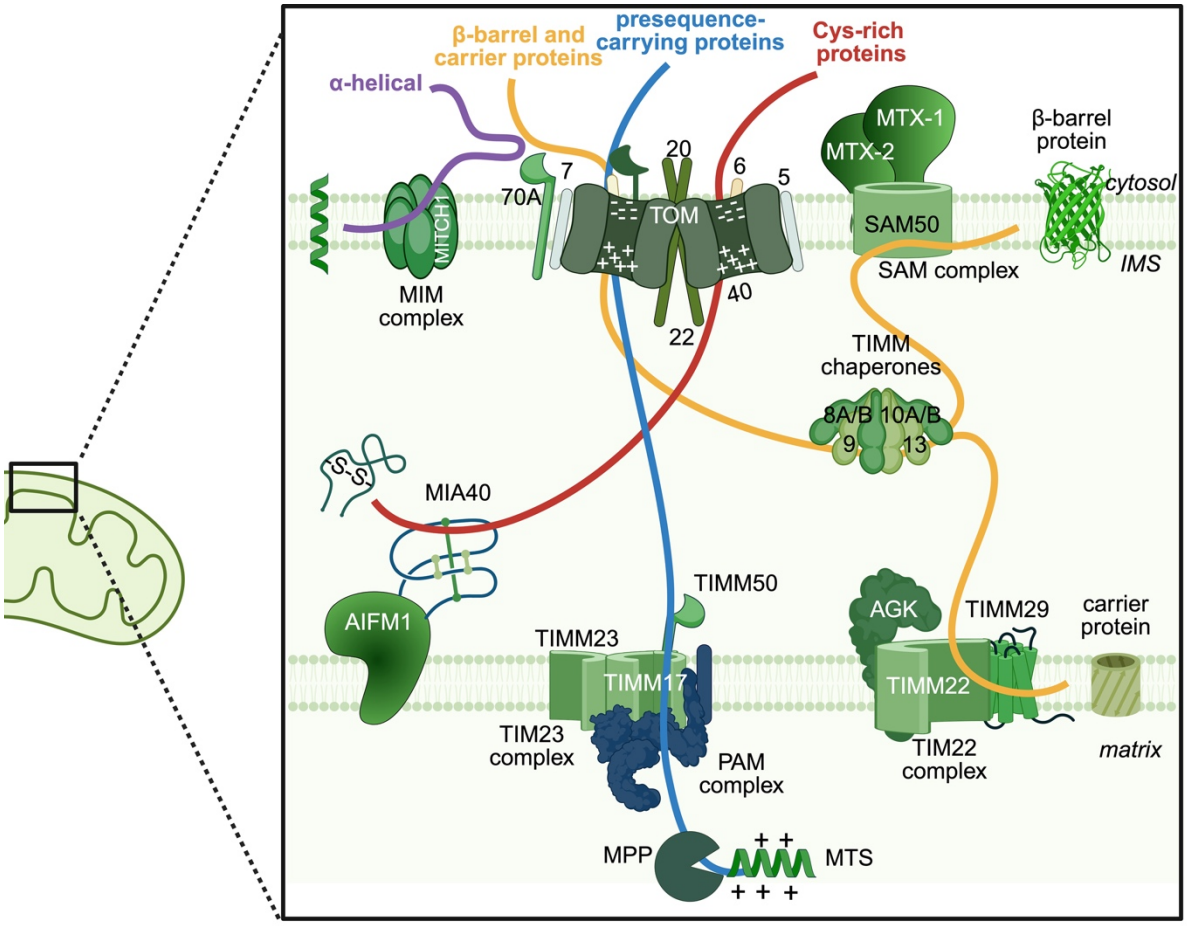

Figure 5. Schematic representation of mitochondrial import pathways. Mitochondrial protein import follows distinct pathways. β-barrel proteins (yellow) integrate into the OMM, while carrier proteins (yellow) are inserted into the IM. Cysteine-rich proteins (red) remain in the IMS, where they form disulfide bonds via MIA40-mediated oxidation. The MIM pathway (violet) directs α-helical proteins into the OMM. The presequence pathway (blue) targets proteins to the matrix or IM, guided by an N-terminal, positively charged α-helix.

2.2.1.1 The carrier pathway

The TIM22 complex plays a crucial role in inserting hydrophobic transmembrane proteins, such as metabolite carriers and members of the TIMM17/22/23 family, into the IM. These proteins lack a cleavable targeting sequence, but their transmembrane domains effectively function as signal peptides [105]. The core subunit, TIMM22, shares significant structural similarity with TIMM17 of the TIM23 complex; both form a half-channel that opens laterally into the lipid bilayer, facilitating the release of the mature protein into the IM [106]. Additional subunits of the TIMM22 complex include in yeast Tim54, Tim18 and sdh3 [105]. In humans, the TIM22 complex contains an additional subunit, called TIMM29, which supports the transfer of the carrier proteins to the TIM22 complex and is important for the stability

and complex assembly [107]. Another subunit of the TIM22 complex is AGK, that has a dual function as lipid kinase [108]. Like protein translocation via the TIM23 complex, membrane insertion via the TIM22 complex depends on a functional MMP, a process supported by an intramolecular disulfide bond within TIM22 that maintain the complex's integrity through the interaction with Tim18 [109].

In yeast, the sdh3 subunit, in addition to its role in the assembly of TIM22, is also a critical component of succinate dehydrogenase (complex II) in the OXPHOS pathway [110]. This dual function and the close proximity of translocase components to OXPHOS subunits suggests a possible role of them in maintaining the local proton gradient required for mitochondrial protein import [111]. Unlike TIM23, TIM22 operates independently of the presequence translocase-associated motor (PAM) complex enabling ATP hydrolysis by HSPA9.

Substrate proteins that are imported post-translationally must be preserved in an unfolded, import-competent state in the cytosol, specifically those proteins, that expose their N-terminal domains to the IMS and are characterized by multiple hydrophobic regions. Cytosolic chaperones, including those from the HSP70 and HSP90 families, bind these regions to prevent aggregation and facilitate transfer to the TOMM70 receptor [112]. TOMM70, with its binding sites for chaperones and precursor proteins, directs them to TOMM22 and further TOMM40, through which the proteins are translocated via its channel in a looped conformation that positions both termini toward the cytosol [113]. The N-terminal segment of TOMM40 extends into the IMS and recruits chaperone proteins, hexameric complexes of TIMM8, TIMM9, TIMM10 or TIMM12, which guide substrates to the TIM22 complex [114]. Human cells however have six small TIM proteins, encoding for the proteins TIMM8A, TIMM8B, TIMM9, TIMM10A, TIMM10B and TIMM13 [115]. In some cases, substrate proteins can undergo oxidation by the MIA40 complex [116], before being transferred to the Tim54 subunit, which is critical for their insertion of those proteins into the IM. Recent studies in yeast have identified Dbi1, a protein in the IM, as a new interactor of TIM22 substrates [117]. Initially found to bind unassembled Tim17, Dbi1 promotes disulfide bond formation in Tim17, independently of the classical disulfide relay system. Its role appears broader, affecting a range of membrane proteins with two transmembrane domains that are stabilized through disulfide bonds. The human homolog, DMAC1, has been identified in association with

intermediate stages of complex I assembly [117, 118]. Mutations in key components of the TIM22 pathway can lead to severe diseases, like mutations in AGK causing Sengers syndrome [119, 120]. AGK is, apart from its role in import regulation, required for maintaining mitochondrial cristae morphogenesis and proper phospholipid metabolism [108]. Mutations in AGK cause deficiencies contributing to cataracts, skeletal myopathy, and hypertrophic cardiomyopathy [121].

2.2.1.2 The sorting and assembly machinery

The SAM complex at the OMM plays a critical role in the insertion of β-barrel precursor proteins. These precursors are first recognized by receptors of the TOM complex and subsequently guided through the TOMM40-mediated pore via their hydrophobic binding sites [122-124]. To prevent aggregation in the IMS, chaperone complexes stabilize these precursors. Specifically, the TIMM9-TIMM10 hexameric complexes bind to hydrophobic domains, directing them to the SAM complex for membrane integration [125-127]. The SAM complex consists of several components, with SAM50 serving as the core subunit. SAM50, an integral outer membrane protein, oligomerizes to form an aqueous pore that facilitates the proper folding and insertion of β-barrel precursors [128-130]. Structurally, SAM50 comprises a β-barrel domain at its C-terminus and a polypeptide transport-associated (POTRA) domain at its N-terminus, which is located in the IMS and plays a crucial role in precursor transfer. The final step of precursor insertion involves a lateral release mechanism, where the last β-strand of the precursor replaces the first β-strand of SAM50, integrating the remaining β-strands through β-hairpin structures at the lateral gate. A large polar amino acid, such as lysine or glutamine of the last β-strand, was shown to serve as a signaling peptide. This induces a conductance increase of the SAM channel allowing the lateral release towards the OMM [131]. In addition to SAM50, the SAM complex includes two peripheral membrane proteins: Sam35 and Sam37 in yeast, known as MTX-1 and MTX-2 in humans. Sam35 facilitates precursor binding by protruding into the pore to recognize β-signal-containing precursors [132, 133]. Sam37, in cooperation with the POTRA domain of Sam50, supports the release of folded substrates into the lipid bilayer. Notably, Sam35 caps the Sam50 β-barrel, forming the stable core of the protein translocase [94, 134].

Beyond its role in β-barrel protein import, the SAM complex engages in essential interactions regulating OMM assembly. It associates with Mdm10, which is involved

in TOM22 precursor integration and the assembly of Tom40 with small Tom proteins. Mdm10 also serves as a key component of the endoplasmic reticulum-mitochondria encounter structure (ERMES). Tom7 modulates the distribution of Mdm10 between the SAM and ERMES complexes: when bound to Tom7, Mdm10 preferentially associates with ERMES [135, 136]. Furthermore, the SAM complex interacts with the TOM complex to facilitate precursor transitions, forming higher-order translocation supercomplexes [94, 137].

2.2.1.3 The mitochondrial intermembrane space import and assembly (MIA) pathway

The MIA pathway is essential for the import of cysteine-rich proteins into the IMS. Its core component, MIA40 (also known as CHCHD4 in humans), recognizes mitochondrial IMS sorting signals, which are primarily composed of conserved cysteine residues and hydrophobic patches [138, 139]. Canonical MIA40 substrates are generally small polypeptides characterized by specific targeting sequences and conserved cysteine-containing motifs, most commonly twin CX_3C or CX_9C motifs. These structural features are essential for recognition by MIA40 and for promoting oxidative folding within IMS. In contrast, non-canonical substrates may harbor motifs, such as $CX_{13}C$ or $CX_{14}C$ [140]. In yeast, Fcj1, an integral IM protein, recruits Mia40, the core component of the disulfide relay system, to the IMS side of the TOM complex [141]. This allows, that upon translocation through the TOM complex, Mia40 transiently interacts with incoming precursor proteins, forming intermolecular disulfide bridges that facilitate further translocation via the TIM23 and TIM22 complexes [116, 142]. MIA40 substrates include a wide range of evolutionarily conserved proteins involved in key pathways, such as the MICOS complex and respiratory chain assembly [76]. Furthermore, it has been also stated, that TIMM17, the core subunit of the TIM23 complex, relies on the formation of a disulfide bond, mediated by MIA40 interaction [143]. These substrates, typically small proteins, exhibit a simple helix-loop-helix structure or possess a bipartite mitochondrial targeting sequence. Upon binding to MIA40 via the hydrophobic cleft, containing a redox-active CPC (cysteine-proline-cysteine), intramolecular disulfide bridges form within the precursor proteins, promoting their release into the IMS [144]. The reoxidation of MIA40 is catalyzed by the sulfhydryl oxidase ALR/GFER (in yeast Erv1), which transfers electrons to cytochrome *c* oxidase within the OXPHOS machinery [145-147].

ALR functions as a homodimer, facilitating electron transfer between its monomers [148]. Additionally, MIA40 oxidation is regulated by the zinc-binding protein helper of TIM protein 13 (Hot13) [149]. Beyond its role as an oxidoreductase, MIA40 also functions as a holdase chaperone. This was demonstrated for the HCLS1-associated protein X-1 (HAX1), whose mitochondrial import depends on MIA40 despite lacking redox-active cysteines. Instead, HAX1 possesses a weak mitochondrial targeting sequence, and its non-covalent interaction with MIA40 is necessary for stabilization within the IMS and for preventing aggregation [150].

Structurally, the C-terminus of MIA40 is characterized by a high density of negative charges, which protect the protein from proteasomal degradation in the cytosol and contribute to its stability until they reach mitochondria [139, 151, 152]. At mitochondria, the slow MIA40 import is facilitated by apoptosis-inducing factor 1 (AIFM1) [153]. This interaction occurs via the unstructured N-terminal segment of MIA40 following AIFM1 dimerization in presence of NADH [154].

The physiological importance of AIFM1 is underscored by mutations associated with a broad spectrum of disorders, including Cowchock syndrome, combined oxidative phosphorylation deficiency 6, and progressive mitochondrial encephalomyopathy [155, 156,157]. Beyond its well-established role in apoptosis, where it translocates to the nucleus to promote DNA fragmentation and cell death [158], AIFM1 is essential for mitochondrial function. Pathogenic mutations impair oxidative protein folding, leading to defective activities of complexes I, III, and IV, as several subunits of these complexes require oxidation by the MIA40 pathway for proper maturation [90, 159].

2.2.1.4 The mitochondrial import (MIM) complex

The MIM complex plays a crucial role in the insertion of α-helical proteins into the OMM. Among its substrates are tail-anchored subunits of the TOM complex, including Tom20, Tom70, and small Toms, all of which require the MIM complex for proper integration [160, 161]. While Tom70 recognizes those multispanning proteins, it is not stated that those proteins pass through the Tom40 channel [162, 163]. In yeast, cytosolic chaperones such as Djp1 and Xdj1 have been shown to facilitate the delivery of MIM precursors by docking onto distinct TOM receptors [164, 165]. These chaperones guide the precursors to Tom70, from which they are directly transferred to the MIM complex for membrane insertion. Structurally, the MIM complex consists

of multiple Mim1 subunits and one or two Mim2 subunits, both of which are critical for complex stability. Notably, Mim1 oligomerization is essential for the efficient import of OMM proteins [160]. Additionally, negatively charged phospholipids have been found to enhance the MIM-dependent insertion of multispanning proteins, suggesting that lipid composition plays a key role in this process [166, 167].

The MIM complex functions either independently or in cooperation with other mitochondrial import machineries. It has been shown, that the coupling of MIM with the SAM complex is essential for the insertion of certain small TOM subunits [168]. Another example is Mcp3, which is first transported via Tom40, transferred to TIM23 components, cleaved by the inner membrane peptidase, and subsequently inserted into the OMM via the MIM complex. However, the precise mechanisms underlying this process remain incompletely understood and require further investigation [104]. Apart from the interaction of the MIM complex with the TOM complex, needed for the precursor handover, there are also some proteins, such as Msp1, known to be imported independent of any subunits of the TOM complex [169].

In mammals, MTCH2 was initially proposed to function as the mitochondrial outer membrane insertase for tail-anchored, signal-anchored, and multipass proteins [170, 171]. However, recent studies indicate that its paralog, MTCH1, rather than MTCH2, compensates for the growth defects caused by MIM complex depletion, suggesting that MTCH1 plays a more prominent role in mitochondrial membrane protein insertion [172]. Despite these insights, the mammalian import pathway remain poorly characterized, primarily relying on findings from yeast models. Structural investigations of the MIM complex will be crucial for elucidating its precise function in higher eukaryotes.

2.2.1.5 Presequence pathway

The presequence pathway is the primary route for importing proteins destined for the IM or the matrix. This pathway is characterized by the presence of an N-terminal MTS, which forms a positively charged amphipathic α-helix and drives translocation in an electrophoretic manner. The MTS typically ranges from 10 to 50 AA in length, though some proteins possess weak MTS that share characteristic features of a conventional MTS, but are poorly developed [173]. Additionally, certain proteins contain a non-cleavable internal targeting sequence with hydrophobic properties, enabling their sorting into the IM via a stop-transfer mechanism [174-178]. The initial

recognition of these targeting signals occurs at the TOM complex, where receptors such as TOMM20 and TOMM22 guide presequences through an acidic patch of the TOMM40 channel [103, 179]. Upon translocation into the IMS, precursor proteins interact with components of the TIM23 complex, notably TIMM50, which facilitates their transfer into the channel formed by the core subunit TIMM17 [180]. The subsequent sorting of proteins into either the IM or the matrix is mediated by distinct complexes: the TIM23^{sorting} complex directs proteins to the IM, whereas the TIM23^{motor} complex facilitates matrix localization [174, 181]. The TIM23^{sorting} complex is defined by the presence of TIMM21 and ROMO1 (Mgr2 in yeast). TIMM21 interacts via its C-terminal domain with both TIMM50 and TOMM22, forming a dynamic supercomplex [181, 182]. Additionally, TIMM21 has been shown to couple translocation with the assembly of respiratory chain complexes III and IV. The connection of protein import with the respiratory chain assembly assures the local maintenance of the MMP which is essential for directing the translocation and enhancing the energy efficiency of the translocase [183]. Mgr2 functions as a lateral gatekeeper, shielding the half-channel formed by TIMM17 and facilitating the lateral release of preproteins into the IM [184]. While the first transmembrane domain (TM1) of ROMO1 is essential for TIM23 complex stability, the second transmembrane domain (TM2) is critical for associating respiratory chain subunits with the TIM23 complex [173, 184, 185]. The TIM23^{motor} complex is essential for translocating matrix-destined proteins, a process that requires a functional MMP, which is thought to exert a pulling force on the positively charged presequences. However, the translocation of proteins into the mitochondrial matrix needs further energy, that is provided by the PAM complex through ATP hydrolysis mediated by mitochondrial HSP70 (mtHSP70, also called HSPA9 or Mortalin) [186]. TIMM44, which contains a lipid-binding segment tethering the protein to the matrix-facing side of the IM, is thought to recruit the PAM complex [187]. ATP hydrolysis is further regulated by additional components, including PAM16, which antagonizes ATPase activity, and Pam18 (DNAJC15 and DNAJC19 in humans), which stimulates ATPase function [188, 189]. Following ATP hydrolysis, HSPA9 is regenerated by the nucleotide exchange factor Mge1 (GRPEL1 and GRPEL2 in humans) for another round of protein translocation [173, 190]. As this mitochondrial protein import pathway is employed by the majority of mitochondrial proteins, mutations or disruptions in this process can have severe consequences. For example, dilated cardiomyopathy with ataxia (DCMA) is caused by a defect in

DNAJC19, a component of both the TIM23 and prohibitin (PHB) complexes. The loss of DNAJC19 results in impaired cardiolipin acylation and defective cristae morphogenesis, leading to clinical manifestations such as non-progressive cerebellar ataxia [191]. Mutations in mitochondrial translocase components have been linked to various other human diseases. PAM16 variants cause Mégarbané-Dagher-Melike spondylometaphyseal dysplasia, a skeletal disorder with short stature, platyspondyly, facial anomalies, and developmental delay [192-195]. TIMM50 mutations underlie 3-methylglutaconic aciduria type IX, characterized by seizures, intellectual disability, lactic acidosis, optic atrophy, and cardiomyopathy, alongside severe mitochondrial structural defects and impaired OXPHOS function due to severe impairment of the TIM23-dependent mitochondrial protein import [196-198]. Similarly, defects in the MPP are associated with neurological conditions such as spinocerebellar ataxia type 2 and multiple mitochondrial dysfunctions syndrome 6 due to faulty precursor protein processing and early impairment of the iron-sulfur protein biogenesis [199-201 90, 202].

2.2.2 The TIM23 complex

2.2.2.1 Structure and function of the TIM23 complex

The recently resolved structure of the TIM23 complex has fundamentally altered our understanding of the assembly and function of the TIM23 complex [203-205]. Notably, the core subunits TIMM17 and TIMM23, as well as the TIMM22 core subunit, all belong to the TIMM17 protein family, that is characterized by the presence of four transmembrane domains (TMDs) [206]. Both the N- and C-termini of these proteins are localised to the IMS. TIMM17 possesses an extended N-terminal segment, which is thought to bridge the TOMM40 and TIMM23 complexes. Structurally, all TIMM17 family proteins form a curved surface with a lateral cavity that opens into the lipid bilayer. TIMM17 and TIMM23 adopt a back-to-back orientation, with TIMM17 constituting the main translocation channel due to its larger cavity [203-205]. TIMM23, in contrast, primarily acts as a structural adaptor, ensuring the stability of the complex. The stability of TIMM23 is further supported by interactions with

cardiolipin, which may also facilitate interactions with TIMM17 and TIMM44. TIMM17 must be sealed by ROMO1 (in yeast Mgr2) for proper functioning of the translocation channel. While Mgr2 is not essential for viability, its presence significantly enhances the efficiency and fidelity of mitochondrial protein import. The channel itself is not water-filled but has been shown to locally reduce membrane thickness, creating a more favorable environment for polypeptide movement. This reduction in membrane thickness is thought to lower the energetic barrier for protein translocation [203-205]. TIMM17 plays a critical role in precursor translocation across the IM. The entry site of TIMM17 contains negatively charged residues that attract the positively charged presequences, a process independent of Mgr2. A hydrophobic patch along the channel together with Mgr2 further aids in precursor movement, forming a structured translocation path shielding TIMM17 from lipids. Following this, a hydrophilic lateral cavity within TIMM17 facilitates the final steps of precursor transport into the mitochondrial matrix [203-205].

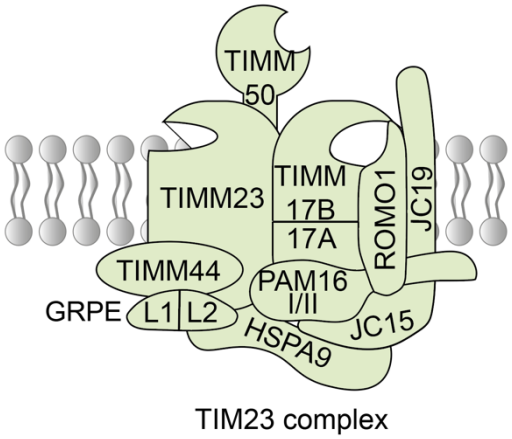

Figure 6. Structure of the human TIM23 complex. The TIM23 complex, embedded in the IM, consists of two half-channels formed by TIMM23 and TIMM17 homologs, with TIMM17 functioning as the translocation pore. This pore is shielded by ROMO1 to facilitate protein import into the mitochondrial matrix and by acting as a gate, enabling the insertion of proteins into the IM. The PAM complex, essential for ATP-driven translocation, comprises TIMM44, GRPE homologs, HSPA9, which mediates ATP hydrolysis, as well as PAM16 and J-domain protein homologs.

2.2.2.2 The role of the human J-proteins in mitochondrial protein import

J-domain proteins are essential regulators of mitochondrial protein import, primarily by stimulating the ATPase activity of HSP70 [188, 207, 208]. DNAJC15 and DNAJC19, human homologs to the yeast Pam18 protein, belong to class C J-domain proteins, characterized by their J-domain located at the C-terminus that faces to the mitochondrial matrix [209]. Structurally, DNAJC15 and DNAJC19 share common features, including an unstructured linker region upstream of their J-domain, followed by a transmembrane domain anchoring them to the IM that is highly conserved in vertebrates [210]. However, DNAJC15 uniquely possesses a long N-

terminal domain that extends into the IMS [207]. Despite their structural similarities, these proteins exhibit distinct, apparent half-lives: DNAJC15 is short-lived with an apparent half-time of 15.7 h, whereas DNAJC19 has a significantly longer half-life with an apparent half-time of 164.9 h [76]. The influence of these structural differences, along with the potential modulatory effects of proximal interacting proteins, on the stability and degradation dynamics of the complex remains to be elucidated.

DNAJC15 and DNAJC19 are homologous to Pam18, a yeast J-domain protein extensively studied for its role in mitochondrial protein import. At the TIM23 complex, Pam18 acts as a membrane-bound ATPase stimulator, increasing the affinity of mitochondrial Hsp70 for incoming precursor proteins [207]. Pam18 is recruited to the translocation machinery via interaction with Pam16, a functionally conserved process also observed in human mitochondria [211]. Pam18 forms a heterodimer with Pam16, linking it to both the presequence translocase and respiratory chain complexes. In the absence of Pam16, Pam18 forms homodimers that accumulate at the respiratory chain and primarily promote complex IV assembly. When not bound to the respiratory chain, Pam18 facilitates the import of TIM23 substrates [211]. It has been hypothesized that Pam18 can also play a role in sealing the lateral gate of Tim17, promoting the anterograde movement of polypeptides into the matrix, particularly of OXPHOS subunit intermediates [203-205]. This suggests a PAM-independent translocation mechanism necessary for protein insertion into the IM [212]. The Pam18 homologs DNAJC15 and DNAJC19 retain conserved functions in humans, forming dimeric and higher-order oligomeric complexes with PAM16 [207]. DNAJC15 exhibits stronger ATPase-stimulating activity than DNAJC19, aligning with its ability to rescue the lethal phenotype caused by *Pam18* deletion in yeast, a function DNAJC19 cannot fulfill [207]. Despite their shared role in mitochondrial protein translocation, they are recruited to distinct translocation machineries: DNAJC15 associates with the TIMM17A-containing translocase, whereas DNAJC19 interacts with TIMM17B [213, 214]. This specialization is further supported by the two human PAM16 homologs, PAM16-1 (MAGMAS-1) and PAM16-2 (MAGMAS-2), which display distinct binding preferences for these translocases. Notably, PAM16-2 preferentially interacts with DNAJC15 and exerts a stronger inhibitory effect than PAM16-1 [214, 215]

Beyond their roles in protein translocation, these J-domain proteins, specifically DNAJC15, are implicated in mitochondrial function and apoptosis. DNAJC15 has been further linked to a role in mitochondrial function and apoptosis by preventing the release of pro-apoptotic factors [207]. Additionally, it influences OXPHOS activity by interacting with complex I of the electron transport chain and regulating the distribution of active and inactive forms within supercomplex structures [216]. Other studies have linked DNAJC15 to lipid peroxidation and ferroptosis induction upon overexpression [217]. *In vivo* studies in *Dnajc15* depleted-mice reveal an increase in brown adipose tissue thermogenesis, involving the eIF2α stress response pathway [217, 218].

2.2.2.3 Proteolytic regulation of the TIM23 complex

To accomplish mitochondrial plasticity and integrity, mitoproteases regulate mitochondrial import through targeted proteolysis [1]. TIM23 is subject to strict regulation by those proteases which either degrade damaged import proteins or process them in a regulatory manner. In the paper by Morgenstern *et al.*, variations in the half-lives of mitochondrial proteins were unveiled, showcasing disparities even within the confines of the same protein complex [76]. These differences can be also seen in the TIM23 complex which shows that some translocation proteins are proteolytically regulated, such as TIMM17A [219, 220] or ROMO1 [221]. TIMM17A, a component of the TIMM23 complex, is degraded by the i-AAA protease YME1L in a stress-dependent manner. Its turnover increases in insults that initiate a downregulation of the mitochondrial translation through ISR-dependent eIF2α phosphorylation. Consequently, TIMM17A adapts mitochondrial protein import during pathologic conditions [219, 222]. This goes in line with YME1L further degrading TIMM17A and TIMM23 under conditions where mitochondrial protein import is impaired by a human clogger, assuming a protective role of YME1L [223]. Another proteolytically regulated protein by YME1L is ROMO1, which is attached to the mitochondrial membrane and maintains its integrity. Although it is dispensable for general import, ROMO1 is known to increase the import efficiency by shielding the half-channel build up by the two TIMM17 homologs and by recruiting TIMM21 to the TIMM23 complex. This supports the assembly of OXPHOS subunits by enabling lateral sorting [185, 203-205]. Additionally, ROMO1 regulates mitochondrial dynamics by its critical modulation of the YME1L import [221]. A recent multi-omics proteome

analysis identified the hypoxia-dependent regulation of the m-AAA protease AFG3L2, which modulates the mitochondrial proteome through the targeted degradation of PAM-complex components, including DNAJC15 and PAM16 [224]. The different half-lives of these subunits suggest that short-lived translocase components may function as regulatory sensors, controlling distinct checkpoints, while long-lived proteins such as TIMM17B and TIMM50 likely serve housekeeping roles [76].

2.3 Mitochondrial protein import stress

2.3.1 Quality control mechanisms in the cytosol

To prevent cytosolic protein aggregation, cells have evolved mechanisms to ensure the proper targeting of newly synthesized proteins to their respective organelles. Cytosolic Hsp70 and Hsp40 are essential for maintaining protein homeostasis by preventing the misfolding and aggregation of precursor proteins [225]. They achieve this by binding to exposed hydrophobic domains, thereby stabilizing proteins in an unfolded state to facilitate proper targeting and import. The Hsp40 family is defined by J-domain–containing proteins that determine substrate specificity, deliver client proteins to Hsp70, and stimulate its ATPase activity. In mitochondria, Hsp70 hydrolyzes ATP to regulate substrate binding and release at the OMM, thereby supporting chaperone-mediated protein import and contributing to mitochondrial proteostasis by preventing precursor aggregation and ensuring proper folding [226-228].

However, under persistent stress conditions that impair mitochondrial protein import, precursor proteins accumulate in the cytosol and can form aggregates. These aggregates may be solubilized by Hsp70 in cooperation with the co-chaperone Apj and the nucleotide exchange factor Sse1, which facilitate their subsequent targeting for proteasomal degradation [229]. The 26S ubiquitin-proteasome system (UPS) is essential for degrading misfolded and aggregated proteins before they become cytotoxic. It consists of a 19S regulatory particle, which unfolds proteins, and a 20S core particle, composed of multiple subunits that hydrolyze proteins into short peptides [230-232]. Proteasomal subunits share a conserved Rpn4-binding region in their promoters, acting downstream of HSF1 to enhance proteasome assembly [233, 234]. For proteasomal degradation, proteins must be ubiquitinated in a three-step process involving E1, E2, and E3 enzymes. Initially,

E1 activates ubiquitin through ATP-dependent AMP conjugation and transfers it to the E2 ubiquitin-conjugating enzyme. E3 then mediates the transfer of ubiquitin to lysine residues on the target protein, marking it for degradation [235]. This ubiquitin-dependent mechanism is also critical for mitochondrial quality control, enabling the retro-translocation and degradation of misfolded mitochondrial proteins [236-238]. In addition to proteasomal degradation, misfolded proteins in human cells can also be targeted for clearance through the ubiquitin-autophagy receptor p62, which directs them to the autophagic pathway [239]. If surveillance mechanisms fail and non-imported mitochondrial proteins aggregate, they can be sequestered into specialized cytosolic inclusions known as "mitostores" [240, 241]. The small heat shock protein Hsp42 facilitates sequestration, while Hsp104, in cooperation with other co-chaperones, promotes disaggregation, maintaining the proteins in a state that allows their re-import once the mitochondrial stress is resolved [228, 240, 241].

2.3.2 Quality control mechanisms at the TOM complex

Mitochondrial protein import relies on stringent quality control mechanisms to prevent the accumulation of stalled precursor proteins at the TOM complex. These surveillance pathways can be classified into constitutively active mechanisms, which continuously monitor TOM function, and inducible responses, which are activated upon mitochondrial stressors, such as import blockage or impaired co-translational translocation [242].

One such constitutively active surveillance pathway is the mitochondrial protein translocation-associated degradation (mitoTAD), which facilitates the recognition and proteasomal degradation of non-imported precursor proteins, even under non-stressed conditions. Recent studies have identified Ubx2 as a key component of mitochondrial surveillance, directly interacting with the TOM complex [243]. Previously characterized for its role in the ER-associated degradation (ERAD) pathway [244], Ubx2 exerts regulatory functions at both the ER and mitochondria [245]. Structurally, Ubx2 contains a Ubx domain, which recruits the AAA+ ATPase Cdc48 (in humans known as VCP or p97), and a UBA domain, which binds ubiquitylated target proteins. The recruitment of Cdc48 by Ubx2 to the TOM complex facilitates the extraction and clearance of stalled translocation intermediates [243, 244, 246]. In addition to Ubx2, an alternative quality control pathway involving Pth2 and Dsk2 plays a critical role in TOM surveillance. Pth2 interacts with the TOM complex, recognizing

ubiquitin-like domain-containing proteins, a process mediated by the TOM interactor Rsp5. Once bound to ubiquitylated precursor proteins, Pth2 recruits Dsk2, which directs the proteins to the proteasome for degradation. Given the constitutive activity of this pathway, Pth2 depletion leads to the accumulation of precursor proteins in the cytosol, even under non-stressed conditions, highlighting its essential role in maintaining mitochondrial protein homeostasis [247, 248].

Eukaryotic cells routinely translate nuclear-encoded mitochondrial proteins across cytosolic ribosomes that are often engaged in co-translational import [249, 250]. If translation is impaired, defective peptides may accumulate, leading to stalled ribosomes and arrested protein import [251]. This activates the ribosome-associated quality control (RQC) pathway: Rqc2 stabilises the 60S-nascent-tRNA complex and recruits Ltn1, an E3 ubiquitin ligase, that ubiquitylates aberrant nascent polypeptides, directing them for proteasomal degradation [251]. When ubiquitylation is delayed or ineffective, Rqc2 catalyses “CAT-tailing”, the addition of C-terminal alanine and threonine residues, to expose lysines and enhance Ltn1 engagement. However, excessive CAT-tailing can promote aggregation of stalled chains, especially those co-translationally imported into mitochondria, exerting toxic stress. Vms1 emerges as a specialized safeguard at this cytosolic-mitochondrial interface. It associates with the 60S subunit at the mitochondrial surface, functioning as a peptidyl-tRNA hydrolase that intercepts stalled nascent chains, terminates CAT-tail extension, displaces Rqc2, and promotes release of nascent peptides. This action enables mitochondrial protein import and degradation via internal proteostasis systems and prevents an accumulation of toxic CAT-tailed aggregates in the matrix. In cells lacking Ltn1 or Vms1, CAT-tailed proteins accumulate and aggregate within mitochondria, impairing respiratory growth and mitochondrial fitness [252-256]. Thus, while CAT-tailing is a general RQC mechanism to salvage stalled translation, the Rqc2-Ltn1-Vms1 axis is particularly critical during co-translational import of mitochondrial proteins and is activated upon mitochondrial import stress preventing the formation of toxic aggregates.

Another quality control response activated upon mitochondrial translocation blockage is the mitochondrial compromised protein import response (mitoCPR), which prevents the accumulation of precursor proteins at the organelle’s entry site [257]. Under conditions of mitochondrial import stress, increased expression of

Cis1 has been observed. Although Cis1 is a cytosolic, non-transmembrane protein, it relocalises to mitochondria and interacts with the TOM receptor Tom70 upon import impairment. If the stress persists, Cis1 recruits the AAA-ATPase Msp1 (in humans known as ATAD1) to facilitate protein extraction [258]. Msp1, previously characterized for its role in recognizing mislocalised ER proteins at the OMM, functions in import surveillance by extracting stalled precursor proteins from the TOM complex. These extracted proteins are subsequently relocalised to the cytosol and targeted for degradation via the proteasome [228, 257, 259-261].

2.3.3 Quality control mechanisms of the mitochondria with the help of the ER

When mitochondrial protein import is compromised, precursor proteins with hydrophobic transmembrane domains, particular members of the SLC25A family, are at high risk of mislocalization and cytotoxic aggregation. To mitigate this, the guided entry of tail-anchored (GET) pathway plays a critical role by redirecting membrane proteins to the ER [262]. Although originally characterized as a system for the post-translational insertion of C-terminal tail-anchored proteins into the ER membrane [263], subsequent studies revealed that the ATPase Get3 also recognizes and directs mislocalised mitochondrial precursors to the ER [262, 263]. In the absence of a functional GET pathway, these precursors are sequestered into cytosolic aggregates dependent on Hsp42, that associate with both mitochondria and the ER [262]. Once targeted to the ER, these GET-dependent ER localised proteins can engage with the ER surface-mediated protein targeting (ER-SURF) pathway, which facilitates their re-delivery to mitochondria [264]. This process involves the co-chaperone Djp1, the yeast homolog of the human protein DNAJB6. Djp1 and the tethering protein Lam6 interact with the TOM complex receptor TOMM70 and play a crucial role in the ER-SURF pathway, which utilizes the ER surface as a sorting platform for mitochondrial precursors [264-266]. This pathway is for example crucial for the efficient mitochondrial import of Oxa1 [264], as well as of the human PINK1 mRNA, which is translated on ribosomes near the endolysosomes and ER before being transferred via DNAJB6 to the mitochondrial surface [267].

This disturbed protein localization can further activate an ER-specific unfolded proteins response (UPR) response to maintain cellular proteostasis [265]. While this response may help restore protein homeostasis at later stages, an initial hypothesis

for mitochondrial precursor relocalisation to the ER suggests a buffering mechanism that prevents cytosolic protein overload [265]. However, it remains unclear whether these proteins are retained in an import-competent state or ultimately targeted for ERAD.

2.4 Cellular homeostasis and stress responses

2.4.1 Overview of cellular stress responses

Cells are frequently exposed to various stressors, which can originate from internal or external sources. These stressors can disrupt proteostasis, leading to impaired cellular function or even cell death. To mitigate this, cells have developed protective stress response mechanisms, which involve the activation of stress signaling pathways. However, if the stress persists, these signaling cascades can converge on cell death pathways.

2.4.1.1 Heat shock response

The heat shock response (HSR) is a critical mechanism for maintaining protein homeostasis, and its impairment has been implicated in various neurodegenerative diseases and cancers [268, 269]. Initially identified in response to temperature increments, which trigger the aggregation of denatured and misfolded proteins, the HSR is activated to remove these toxic aggregates [270]. A key regulator of this stress response is the transcription factor HSF1, whose activity is tightly controlled through structural and chaperone-mediated mechanisms. Under non-stressed conditions, HSF1 exists as an inactive monomer that trimerizes in response to heat shock, increasing its DNA binding affinity to heat shock elements (HSEs) [271-273]. This enables HSF1 to prevent protein misfolding or target misfolded proteins for degradation, thereby restoring protein homeostasis within the cell. The stress-induced proteins can be grouped into different classes, including molecular chaperones, components of the proteolytic system, nonphysiological covalent modifications of nucleic acids important for DNA repair, metabolic enzymes for reorganizing the energy supply, regulatory proteins such as transcription factors, and proteins involved in cellular structures such as the cytoskeleton and membrane modulating proteins to maintain membrane stability [274].

While higher-order oligomers of HSF1 may enhance transcription, their function *in vivo* remains poorly understood. HSF1 levels are tightly regulated through

mechanisms such as chaperone-mediated feedback, where HSP70 represses HSF1 transcriptional activity and trimer disassembly. Additionally, HSP90 has been implicated in these feedback mechanisms, showing a complex interplay between HSF1 and heat shock proteins in maintaining protein homeostasis [275].

2.4.1.2 Oxidative stress response

Reactive oxygen species (ROS) pose a threat to cells, necessitating mechanisms that maintain the balance between oxidative stress and antioxidant defense mechanisms. An imbalance can trigger cell death, as ROS contribute to cytochrome *c* release from mitochondria and activate transcription factors like NF-κB and p53, which upregulate pro-apoptotic inducers [276, 277]. Mitochondria play a central role, as auto-oxidation of reduced components in the electron transport chain is the primary ROS source [278]. When oxidative stress occurs, it activates cellular defense mechanisms that upregulate heat shock proteins, most notably Hsp27, which help counteract oxidative damage by boosting intracellular glutathione levels and reducing iron concentrations within the cell [279-281]. This response is partly due to overlapping stress pathways, such as UPR, originating from the ER causing PERK phosphorylation, which induces the transcription factor NRF2 and promotes gene expression involved in glutathione biosynthesis [282].

2.4.1.3 Unfolded protein response

Proteostasis is a fundamental process within cellular organelles, ensuring the proper synthesis, folding, and degradation of proteins to maintain cellular homeostasis. This is particularly critical in the lumen of the ER, where a complex network of chaperones, folding enzymes, and quality control mechanisms regulates protein maturation, prevents the accumulation of misfolded proteins, and orchestrates their degradation via the ERAD pathway or autophagy [283]. Under conditions of high protein demand, the folding process can become error-prone, leading to the accumulation of unfolded and misfolded proteins in the ER. The accumulation of unfolded proteins in the ER lumen are known to elicit an ER stress response, the activation of the UPR to restore protein homeostasis. The UPR enhances the removal of misfolded proteins, promotes their degradation, reduces overall protein synthesis, and selectively increases the production of chaperones and foldases to improve the folding capacity [284]. If the stress persists, JNK protein kinase activation can induce an apoptotic cell death [285].

Three highly conserved sensors detect ER stress and initiate UPR. These sensors typically consist of an ER luminal domain that recognizes unfolded proteins and a cytosolic region that transmits signals to effector proteins. One key sensor, IRE1, is a type I transmembrane protein with serine/threonine kinase and endoribonuclease domains. When unfolded proteins accumulate in the ER lumen, the chaperone BiP dissociates from IRE1's luminal domain, triggering its oligomerization, trans-autophosphorylation, and activation of its endoribonuclease function [286,287]. There are two isoforms of IRE1: IRE1α and IRE1β [288]. IRE1α predominantly interacts with BiP, whereas its interaction with IRE1β is comparatively reduced, likely due to the higher affinity of IRE1β for unfolded proteins at its luminal domain [289]. Functionally, IRE1α plays a central role in the splicing of XBP1 mRNA. In contrast, IRE1β is more prominently associated with regulated IRE1-dependent decay (RIDD), a mechanism that facilitates the degradation of selected mRNAs, including those encoding pro-survival proteins, particularly under conditions of prolonged ER stress [290, 291]. An inactivation of IRE1 has been linked to two phosphatases Dcr2 and Ptc2 [292, 293]. However, under ER stress conditions, these phosphatases seem to be not essential, suggesting the presence of compensatory phosphatases or an alternative, dephosphorylation-independent mechanism for IRE1 inactivation [292, 293].

PKR-like ER kinase (PERK), like IRE1, has a homologous luminal domain and depends on BiP binding for regulation. When unfolded proteins accumulate, BiP dissociates, leading to PERK oligomerization and trans-phosphorylation. This activates PERK's kinase function, resulting in the phosphorylation of eIF2α [294]. Phosphorylated eIF2α reduces global protein synthesis by interfering with initiator methionyl-tRNA, GTP, and the 40S ribosomal subunit, preventing GDP recycling by acting as an inhibitor of the nucleotide exchange factor, eIf2B [295, 296]. Despite this general translation suppression, certain stress-related proteins are selectively translated through mechanisms involving upstream open reading frames (uORFs). uORFs are regulatory elements located in the 5′ untranslated region of the messenger RNA and can be translated into short peptides. These peptides modulate the translation of the main coding sequence situated downstream [297]. ATF4, for example, is expressed and induces expression of genes involved in redox balance, amino acid metabolism, autophagy, and apoptosis. Furthermore, the levels of ATF3 increase and allows binding to the promoter of GADD34, a regulatory

subunit of protein phosphatase 1, which facilitates eIF2α dephosphorylation [298]. Unlike IRE1, which primarily mitigates ER stress without directly inducing apoptosis, sustained PERK activation can drive cell death by cleaved PARP [299, 300].

The third key sensor, ATF6, is a type II transmembrane protein involved in ER stress signaling. When misfolded proteins accumulate, BiP dissociates from ATF6, triggering its transport from the ER to the Golgi [301]. A member of the protein disulfide isomerase family, named ERp18, was shown to facilitate this process during stress [302]. In the Golgi, ATF6 undergoes sequential cleavage by site-1 protease (S1P) at an RXXL motif, generating an intermediate fragment that is further processed by site-2 protease (S2P) [301 303]. This releases a basic leucine zipper (bZIP) transcription factor, which translocates to the nucleus and activates stress response genes. Although ATF6 activates XBP1 expression, both regulate distinct transcriptional programs to reshape ER proteostasis with ATF6 driving ER expansion, even in the absence of XBP1 [304, 305]. ATF6 signaling enhances the expression of ER chaperones and enzymes that support protein translocation, folding, and secretion, with GRP78, GRP94, and Calnexin among its key targets [306]. ATF6 exists in two isoforms, ATF6α and ATF6β. While ATF6α is essential for a full stress response, ATF6β functions as a weak activator and can even act as a transcriptional repressor of ATF6α, limiting its activity during prolonged ER stress [307].

The differences in the reaction kinetics among ER stress sensors are not yet fully understood. However, evidence suggests that the UPR proceeds in distinct phases. For example, ATF6 is activated first to promote protein folding, followed by XBP1 splicing by IRE1 activation, which induces the ERAD pathway to target misfolded proteins for degradation [308, 309]. It has also been shown that IRE1 contributes to sustaining PERK expression during prolonged ER stress through XBP1 signaling [310]. In turn, PERK signaling attenuates IRE1 activity via the phosphatase RPAP2, thereby inhibiting activation of cytoprotective factors such as XBP1 and the ERAD pathway. This shift guides the response towards caspase activation and cell death if recovery mechanisms failed to function [311].

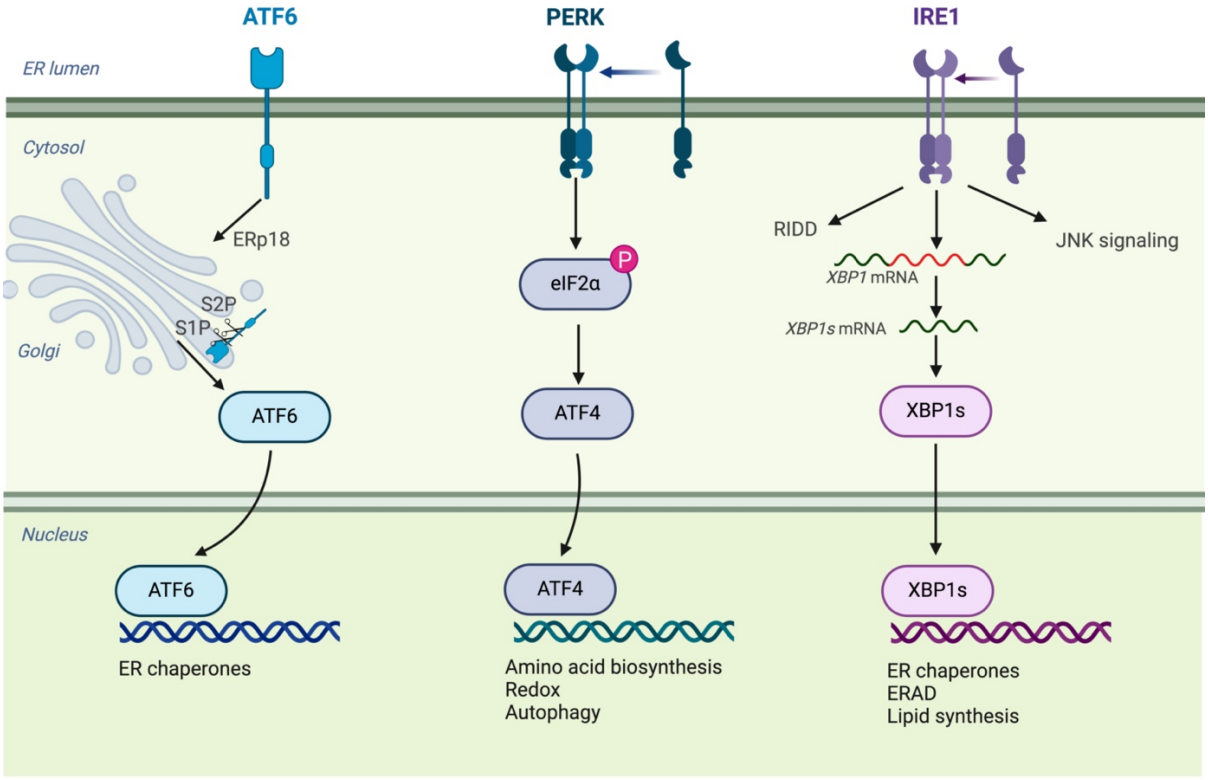

Figure 7. The UPR stress response. UPR signaling is mediated by the ER stress sensors ATF6, PERK, and IRE1, which coordinate adaptive and apoptotic responses. IRE1 splices XBP1 mRNA and promotes RIDD, while PERK phosphorylates eIF2α to attenuate translation and induce ATF4. ATF6 undergoes Golgi cleavage, releasing a transcription factor that enhances ER chaperone expression.

2.4.1.4 Integrated stress response

While the UPR is specifically activated by the accumulation of unfolded proteins in the ER, the ISR is named because it is activated by a broad range of cellular stressors. These stressors also engage kinases that overlap with those involved in the UPR [312].

ISR is a central mechanism for maintaining cellular homeostasis. In response to various stressors, specific kinases become activated and phosphorylate eIF2α to initiate the ISR. Disruptions in the ER function, for example, activate PERK, while viral infections are detected by PKR through the recognition of double-stranded RNA [313]. Amino acid deprivation and ribosome stalling, as well as an imbalance of cytosolic and mitochondrial NADH/NAD+ ratios leading to asparagine and aspartate depletion, trigger the general control nonderepressible 2 (GCN2) kinase [313, 314]. However, heme deficiency and mitochondrial stress lead to the autophosphorylation

of the heme-regulated inhibitor (HRI) kinase [315]. Once activated, these kinases induce eIF2α phosphorylation, which causes a global reduction in mRNA translation and conserves cellular resources under stress conditions [295, 296]. Nevertheless, certain genes are able to bypass this translational inhibition due to the presence of uORFs; among these are genes encoding key transcription factors such as ATF4 and CHOP that regulate stress-adaptive genes, including GADD34 [316]. Moreover, ATF4, in cooperation with ATF3, enhances amino acid metabolism by promoting the conversion of phosphoglycerate to serine [317-319], thereby increasing the availability of amino acids at the expense of glucose-derived energy production [320]. These transcription factors also upregulate enzymes of the folate cycle, such as SHMT and MTHFD2, which are essential for nucleotide biosynthesis and cell proliferation, while additional downstream targets contribute to cysteine synthesis and support the cellular redox balance [320].

The stress response to mitochondrial dysfunction depends on ATF4, that is primarily mediated by the GCN2 and HRI pathways. The initial steps of kinase activation involve the regulator DELE1 (s. chapter 2.1.1.2) [55, 321]. The effective activation of this response requires the oligomerization of the cleaved DELE1 [322]. Additionally, full-length DELE1 has been observed to stabilize on the mitochondrial surface under iron deficiency [59]. Depending on the cell lines, OMA1 has been shown to be dispensable for DELE1 cleavage, indicating that in this context, the mitochondrial protease HtrA2 is primarily responsible for processing DELE1 into its short form [323].

The progression of the mitochondrial-regulated ISR occurs in distinct stages, ranging from early activation to chronic effects. During the initial phase, the transcription of FGF21, GDF15, MTHFD2, and ATF5 is significantly upregulated, while overall protein synthesis is reduced, except for amino acid transporters and metabolic enzymes [324]. This transcriptional response supports glucose uptake and enhances mitochondrial one-carbon metabolism, supplying nucleotides for DNA maintenance and glutathione for antioxidant protection. In the subsequent stage, proteins involved in *de novo* serine synthesis, nucleotide pool balance, and mTORC1 activation are upregulated, while ATF5 remains active. ATF4 plays a key role in this phase by promoting serine synthesis, which is crucial for one-carbon metabolism and the trans-sulfuration pathway. In the final stage, the expression of ISR target genes declines, while ATF3 becomes activated, increasing the likelihood

of apoptosis induction [324, 325]. Overall, acute ISR activation plays a protective role by preventing ferroptotic cell death, mitigating cardiomyopathy, and supporting normal tissue development [56, 57, 326-328]. However, chronic activation of the mitochondrial ISR has been associated with pathological conditions, such as cancer [329, 330], Alzheimer's disease [331, 332], and Down syndrome [333]. These findings underscore the critical need for precise regulatory control to maintain cellular balance and prevent detrimental outcomes.

2.5 Aims of the thesis

A decline of mitochondrial function contributes to ageing and various other diseases. This dysfunction is frequently associated with a loss of mitochondrial plasticity, often resulting from impaired proteostasis. The stress-activated metallopeptidase OMA1 plays a central role in orchestrating the mitochondrial stress response and maintaining mitochondrial proteostasis under stress.

1. **Identification of novel OMA1 substrates**

OMA1 has been linked to cellular stress responses through DELE1 and to mitochondrial dynamics through the targeted processing of OPA1. To gain a more comprehensive understanding of how OMA1 regulates mitochondrial stress responses in light of its multifaceted functions, we identified and functionally characterized novel OMA1 substrates using proteomic approaches.

2. **Characterization of DNAJC15 in regulating mitochondrial protein translocation**

We identified DNAJC15, a mitochondrial co-chaperone involved in protein import, as a novel OMA1 substrate. Using interactome analyses, import assays, and genetic screening, we characterized how OMA1 regulates mitochondrial protein import through DNAJC15 processing.

3. **Investigation of the specific role of DNAJC15 and DNAJC19**

As a component of the TIM23 complex, DNAJC15 functions alongside its paralog DNAJC19. Although both co-chaperones share conserved J-domains, they differ markedly in their stability and regulatory mechanisms, suggesting distinct, context-dependent roles in mitochondrial protein import. We dissected the functional specialization of both paralogs by employing targeted depletion and SILAC-based mitochondrial proteomics to systematically compare their contributions to mitochondrial protein import.

4. Analysis of the cellular consequences resulting from impaired mitochondrial protein import upon acute DNAJC15 depletion

We analysed whether acute loss of J-domain containing proteins and the resulting import deficiencies elicit broader cellular stress responses. Specifically, we assessed the activation of canonical pathways, such as the ISR or the UPR, by combining RNA sequencing with mitochondrial fractionation assays.

3. Material and methods

3.1 Cell culture and genetic manipulation

3.1.1 Cell culture

HeLa (CCL-2) cells were purchased from American Type Culture Collection (ATCC) and cultured in Dulbecco‘s Modified Eagle‘s Medium (DMEM), containing 4.5 g/L D-Glucose (Thermo Fisher, Cat# 61965-059) and 10% v/v fetal bovine serum (FBS) (Sigma, Cat# F7524). Cells were maintained at 37°C and 5% CO_2 in a humidified incubator. Cell counting was performed using the viability marker trypan blue (Thermo Fisher, Cat# T10282) with the Countess automated cell counter (Thermo Fisher, Cat# AMQAF2001). Prior to each experiment, cells were seeded at equal densities and continuously monitored for Mycoplasma contamination.

3.1.2 Plasmid and siRNA transfection

For transient transfection of siRNA or esiRNA, a reverse transfection was conducted with a total cell number of $4x10^5$ cells per well in a 6-well plate. The experiments were conducted 48 h or 72 h after transfection with RNAiMAXX transfection reagent (Invitrogen, Cat# 56532). The following siRNA/esiRNA targeting sequences against human proteins were utilized: siRNA AFG3L2 (SASI_HS01_0023-1520, Merck), esiRNA TIMM44 (EHU009281, Merck), esiRNA HSPA9 (EHU011841, Merck), siRNA DNAJC19 (SASI_Hs01_00055864, Sigma) siRNA DNAJC15 (SASI_Hs01_00246981, Sigma), esiRNA TIMM17B (EHU032651, Merck), esiRNA TIMM17A (EHU023551, Merck), siRNA TIMM21 (EHU031871, Merck), siRNA PAM16 (SASI_Hs01_00168312, Sigma), esiRNA TIMM23 (EHU106141, Merck), esiRNA ROMO1 (EHU224321, Merck), esiRNA TIMM50 (EHU043281, Merck), esiRNA GRPEL1 (EHU006111, Merck), esiRNA GRPEL2 (EHU065941, Merck), esiRNA OMA1 (EHU072451, Merck), esiRNA ATAD1 (EHU107311, Merck), esiRNA DNAJA1 (EHU114481, Merck), esiRNA DNAJB6 (EHU108351, Merck). For negative control, esiRNA eGFP negative control (Merck, Cat# EHUEGFP) and stealth RNAi siRNA negative control (Invitrogen, Cat# 12935300) were obtained. The efficiency of protein depletion was evaluated through immunoblotting.

3.1.3 Generation of stable cell lines

Complementary cDNAs encoding human DNAJC15, S-DNAJC15 and DNAJC15Δ2 were cloned into the PiggyBac vector (PB-Cuo-MCS-IRES-GFP-EF1α-CymR-Puro)

using the Q5 site-directed mutagenesis kit (NEB, Cat# E0554S). After plasmid transfection with Genejuice Transfection Reagent (Merck, Cat# 70967) and 0.2 µg/µL of the PiggyBac Transposase Expression Vector (PB210PA-1-SBI), cells were selected with puromycin (InvivoGen, Cat# ant-pr-1) for 4 days after reaching full confluence. Experiments were performed with the puromycin-selected polyclonal fraction in a *DNAJC15*$^{-/-}$ HeLa cell background. Expression was induced with 8 or 15 µg/mL of 4-Isopropylbenzoic acid (Aldrich, Cat# 268402) and confirmed by immunoblotting.

3.1.4 CRISPR-Cas9 gene editing

To generate *DNAJC15*$^{-/-}$ and *DNAJC19*$^{-/-}$ and *AFG3L2*$^{-/-}$ *SPG7*$^{-/-}$ and *OMA1*$^{-/-}$ HeLa cells, cells were transfected with px335 plasmid (Addgene Cat# 42335), which contained guide RNAs for a nickase Cas9 deletion. The gRNAs for *DNAJC15* were 5‘ACTTGCAGCCCTCGGCCAAA and 5‘GTGGTGTCATCGCTCCAGTT. The gRNAs for *DNAJC19* were 5‘CGGGAAGCAGCATTAATACT and 5‘TCAGTGGTGGCTATTATAGA. The gRNAs for *OMA1* were 5’CCATATAGTAAATAAGTATCAGG and 5’TGGGAGTAAATCAGTGTGACAGG. The gRNAs for *AFG3L2* and *SPG7* were 5’GCTGCTACCACACGCTCTTC and 5’GGTACATCAAGGCTAGCCGC, respectively. Following 3 consecutive transfections on subsequent days, cells were seeded as single cells in 96-well plates and examined for protein expression after a two-week growth period. Deletions were further confirmed by PCR and subsequent genomic sequencing analysis.

3.2 Cell-based functional assays

3.2.1 IncuCyte-based cell growth assays

Cells were grown at equal densities in 96-well plates, with 5,000 cells per well. All experiments were repeated as independent biological replicates. Cell proliferation was monitored by phase microscopy imaging at 10x magnification using the IncuCyte System (Sartorius GmbH, Göttingen, Germany). To assess cell growth, the slope of log-transformed phase area was determined. Significance was assessed by an unpaired two-tailed t-test. Data were visualized using GraphPadPrism Version 10.4.1 (532).

3.2.2 Protein stability assays

Cells were grown at equal densities in 6-well plates at 400,000 cells per well. Plasmid and siRNA transfection was performed for 48 h and the media was changed to complete DMEM media containing either 0.1 mg/mL Emetine (Sigma, Cat# E2375) or 100 µg/mL Cycloheximide (Sigma, Cat# C7698) for the indicated time points. Cells were collected and washed with PBS. Quantification of the protein decay was acquired using ImageJ (version: 2.1.0/1.53c) and visualized with GraphPadPrism Version 10.4.1 (532).

3.3 Molecular and biochemical techniques

3.3.1 Antibodies

The following antibodies were used for immunoblotting: DNAJC15 (ProteinTech, Cat# 16063-1-AP, 1:500), TUBULIN (Sigma, Cat# T6074, 1:2000), AFG3L2 (Sigma, Cat# HPA004480, 1:1000), ACTIN (Santa Cruz, Cat# SC-47778, 1:3000), SDHA (abcam, Cat# ab14715, 1:5000), OMA1 (Santa Cruz, Cat# SC-515788; 1:1,000) and OPA1 (BD Biosciences, Cat# 612607, 1:2000). Corresponding species-specific HRP-coupled antibodies were used for immunoblot (Biorad; Cat# 1706515 and Cat# 1706516).

3.3.2 SDS-PAGE and immunoblotting

Cells were harvested and washed with ice-cold PBS, before lysing with lysis buffer (50 mM Tris-HCl pH 7.4, 1 mM EDTA, 0.1 (w/v) SDS, 1% (w/v) Triton-X-100, 0.5% (w/v) sodium deoxycholate, 150 mM (w/v) NaCl) containing complete EDTA-free protease inhibitor cocktail (Roche, Cat# 64755100). Protein concentration was determined using a Bradford assay (BioRad, Cat# 5000006). Samples were boiled for 5 min at 95°C prior to SDS-PAGE. Total proteins from cells (100 µg) were separated using 14% SDS-PAGE, followed by transfer to nitrocellulose membrane and immunoblotting with the indicated antibodies. Western blot images were acquired using an Intas ChemoStar ECL Imager HR6.0 (Intas, Cat# 114801) and ChemoStar Ts software.

3.3.3 Measurement of cellular respiration

Oxygen consumption rate was measured in a Seahorse Extracellular Flux Analyzer XFe96 (Agilent) according to the manufacturer's instructions for cells grown in DMEM-GlutaMAXX containing 25 mM glucose. For each well, 3.6 x10^3 cells were

plated and incubated for 24 h at 37°C and 5% CO_2 in a humidified incubator prior to measurement. Oxygen consumption rate was assessed after the addition of the corresponding OXPHOS inhibitors (oligomycin - 2µM, FCCP - 0.5 µM, rotenone and antimycin A - 0.5 µM), included in the Seahorse XF Cell Mito Stress Test Kit (Agilent, Cat# 103015-100).

For respiration measurements using OROBOROS, oxygen consumption was analysed at 37°C using isolated mitochondria (400 µg), which were suspended in 2.1 mL of respiratory buffer (MiR05 buffer: 110 mM sucrose, 0.5 mM EGTA, 20 mM Taurine, 3 mM $MgCl_2$, 60 mM K-lactobionate, 10 mM KH_2PO_4, 20 mM HEPES-KOH; pH 7.1) or for cells (10^6 cells) in DMEM, containing 4.5 g/L D-glucose (Thermo Fisher, Cat# 61965-059) and 10% (v/v) FBS (Sigma, Cat# F7524). Measurements were performed with an Oxygraph-2k system (OROBOROS INSTRUMENTS, Innsbruck, Austria). Substrate-driven oxygen consumption was assessed in the presence of succinate (10 mM), pyruvate (10 mM), glutamate (5 mM), and malate (5 mM). Oxygen consumption rate was determined under three conditions: the phosphorylating state after addition of ADP (1.2 mM), the non-phosphorylating state after treatment with oligomycin (10 µM for mitochondria, 20 µM for cells), and the uncoupled state induced by the addition of carbonyl cyanide m-chlorophenylhydrazone (CCCP), which was added in incremental steps up to a concentration of 50 µM (for mitochondria) and 500 µM (for cells), to achieve maximal respiratory capacity. To ensure accurate assessment of respiratory chain-dependent oxygen consumption, antimycin A (500 nM) was added at the end of each experiment to account for residual oxygen consumption.

3.3.4 Quantitative PCR

Cells were harvested and washed with ice-cold PBS prior to cell lysis using the lysis buffer provided in the RNA isolation kit (Macherey-Nagel, Cat# 740955.250). The experiment was performed according to the manufacturer's instructions. RNA isolation was quantified using a NanoDrop spectrophotometer (Thermo Fisher, Cat# ND-ONE-W), and complementary DNA (cDNA) was synthesized using the GoScript Reverse Transcriptase kit (Promega, Cat# A2791), according to the manufacturer's protocol, with a total RNA concentration of 50 µg/mL. Quantitative PCR was performed using SYBR Green PCR mix (Applied Biosystems, Cat# 4367659), containing 0.5 µM of each primer and 20 ng of cDNA for 40 cycles at 95°C for

denaturation and 60°C for the elongation step. Hypoxanthine-guanine phosphoribosyltransferase (HPRT) was used as a housekeeping gene to normalize expression levels, which were determined using the ΔΔCt method. The sequences are the following: For HPRT, we used 5‘TGACACTGGCAAAACAATGCA and 5‘GGTCCTTTTCACCAGCAAGCT, for ATF4, we used 5‘AGGTCTCTTAGATGATTACC and 5‘CAAGTCGAACTCCTTCAAATC, for ASNS, we used 5‘AAAGGTCCCAGATCATATTG and 5‘ATATGACTTCATCCAGAGCC, for MTHFD2, we used 5‘GTGGATTTTGAAGGAGTCAG and 5‘CTTTAGACTTCAGCACTTCTC, for PYCR1, we used 5‘ACAAGATAATGGCTAGCTCC and 5‘CAATGTGTCTGTCCTCAATG, for SHMT2, we used 5‘CATTTGAGGACCGAATCAAC and 5‘CACCTGATACCAGTGAGTAG, for DNAJC15, we used 5‘ATGAGTAGGCGAGAAGCTGGTC and 5‘GGGTGATTCAAAATCATGACTCTC, for PDIA6, we used 5‘TCAGAAAGGCGAGTCTCCTGTG and 5‘CCTCTTGGCAATGTCCTCGTTG, for HSPA5, we used 5‘CTGTCCAGGCTGGTGTGCTCT and 5‘CTTGGTAGGCACCACTGTGTTC, for DNAJB11, we used 5‘ACGCTGGAAGTAGAAATAGAGCC and 5‘TCGGAACCGTAAATCTCCAGGC and for MANF, we used 5‘CAGCCACCAAAATCATCAATGAGG and 5‘TCCACTGTGCTCAGGTCGATCT.

3.3.5 Immunofluorescence of fixed cells

HeLa cells were fixed with 4% (w/v) paraformaldehyde for 10 min. After fixation, cells were washed with PBS for 10 min and cell permeabilization was achieved by incubating cells with 0.1% (w/v) Triton-X-100 in PBS for 5 min, followed by PBS washes for each 10 min. Nonspecific binding sites were blocked by incubating the cells with 2% (w/v) bovine serum albumin (BSA) in PBS for 30 min at room temperature. A mixture of primary antibodies in (w/v) 2% BSA in PBS was applied and incubated overnight at 4°C. After incubation, cells were washed thoroughly with PBS for 10 min, repeating the wash step three times. The secondary antibody solution was prepared in 2% (w/v) BSA in PBS, using antibodies conjugated to fluorophores with emission maxima of either 488 nm or 569 nm. Secondary antibodies were added and incubated in the dark for 45 min. After incubation, cells were washed three times with PBS for 10 min to remove excess secondary antibodies. For mounting, a drop of Prolong Gold Mounting Media was added to a

clean glass slide. The mounted samples were allowed to dry for 1 h at room temperature and stored at 4°C for at least two days.

3.4 Subcellular sample preparation

3.4.1 Subcellular fractionation

Cell pellets were resuspended in homogenization buffer (20 mM HEPES-KOH pH 7.4, 220 mM Mannitol, 70 mM Sucrose, 1 mM EGTA pH 7.4) containing complete EDTA-free protease inhibitor cocktail (Roche, Cat# 64755100). The suspension was kept on ice for 15 min. Cell disruption was performed by applying 20 strokes in a glass mortar and PTFE pestle at 1,000 rpm using a rotating homogenizer (Schuett Biotec, Cat# 3201011). Two consecutive centrifugation steps at 600xg for 5 min were conducted to remove nuclei. Mitochondrial fractions were pelleted at 8,000xg for 10 min at 4°C. When indicated in the figure legend, mitochondria were treated with 20 µg/mL Proteinase K (Southern Cross Science, Cat# 0219350491) for 20 min at 4°C, followed by reaction termination with 2 mM PMSF (Roche, Cat# 10837091001). For further subcellular fractionation, the supernatant of the mitochondrial-containing fraction was centrifuged at 40,000xg for 1 h, to yield the heavy microsome fraction. Additional centrifugation of the remaining supernatant at 100,000xg for 1 h allowed isolation of the light microsomal fraction. The supernatant, containing the soluble fraction was precipitated with acetone.

3.5 Proteomic sample preparation

Proteomics sample lysis and processing were carried out by Dominique Diehl (Max Planck Institute for Biology of Ageing), and mass spectrometric measurements were performed by Hendrik Nolte (Max Planck Institute for Biology of Ageing). Neo-N-terminal proteomics analyses were conducted by Yvonne Lasarzewski (Max Planck Institute for Biology of Ageing).

3.5.1 Neo-N-terminal proteomics

Cells were lysed and proteins were reduced (10 mM TCEP) and alkylated (20 mM CAA) in the dark for 45 min at 45°C. TMT labels (TMT10plex Label Reagent Set plus TMT11-131C, #A37725, or TMT6plex Label Reagent Set) were equilibrated to RT and solubilized in LC-MS grade acetonitrile according to manufacturer's protocol. For 30 µg protein input, 20 µL of TMT labels were added and incubated for 1 h at 25°C on a thermomixer at 300 rpm. The reaction was stopped adding 100

mM Tris-HCL buffer to a final concentration of 20 mM. Samples were pooled to a total of 100 µg and subjected to SP3-based protein digestion. Peptides were incubated with activated NHS-magnetic beads (Pierce™ NHS-Activated Magnetic Beads, # 88826) according to the manufactor's instructions to capture free amine groups of internal peptides (peptide N-term). The supernatant was removed, acidified and desalted using SDB-RP stage tips and resuspended in 10 mM ammonium hydroxide and 5% acetonitrile. Peptides were then separated via offline high-pH peptide fractionation. The instrumentation consisted out of a ZirconiumTM Ultra HPLC and a PAL RTC autosampler system using the binary buffer system. A) 10 mM ammonium hydroxide and B) 80% acetonitrile and 10 mM ammonium hydroxide. Peptides were separated according to their hydrophobicity using an in-house packed column (length = 40 cm, inner diameter = 175 µm, 2.7-µm beads, PoroShell, Agilent Technologies) column. The instruments communicated and were controlled using the software Chronos (Axel Semrau GmbH). The total gradient length was 40 min and in total 12 (*SPG7*$^{-/-}$, *AFG3L2*$^{-/-}$, *SPG7*$^{-/-}$ *AFG3L2*$^{-/-}$, and WT) or 36 (*OMA1*$^{-/-}$, and WT) fractions were collected (1/30 s) and subsequently concentrated using a SpeedVac to complete dryness.

3.5.2 DSP interaction analysis

Cells were seeded at a density 15x10^6 cells in a 15 cm cell culture dish. DNAJC15 expression was induced with 15 µg/mL of 4-isopropylbenzoic acid (Aldrich, Cat# 268402) and confirmed using immunoblotting. After 48 h of incubation in a humidified incubator, cells were washed twice with PBS. PBS containing 2 mM DSP (Thermo Fisher, Cat# 22585) was then added and the cells were incubated for 30 min at RT to allow cross-linking. For quenching, a 100 mM Tris pH 7.4 solution was added and the cells were incubated for a further 15 min at RT. Cells were then harvested, and lysed (20 mM HEPES-NaOH, 150 mM NaCl, 2 g/g digitonin (Merck, Cat# 300410)). Protein concentration was determined using Bradford reagent (BioRad, Cat# 5000006). For the subsequent immunoprecipitation, 1.4 mg of total protein was used as input, with DNAJC15 antibody (Proteintech, Cat# 16063-1-AP) pre-bound to Protein G magnetic beads (Thermo Fisher, Cat# 10003D). The Protein G and antibody mixture was washed, 2x for 10 min with 0.1% Sodium Deoxycholate and 3x washed with PBS including a 10 min incubation step with PBS. After adding the lysate, the mixture was incubated for 120 min. After several washes with

washing buffer (10 mM HEPES-NaOH, pH 7.5, 150 mM NaCl, 0.1% (w/v) Triton-X-100), proteins were eluted by incubating the beads in Laemmli buffer (50 mM Tris-HCL, pH 6.8, 2% (w/v) SDS, 10% (v/v) glycerol, 0.01% (w/v) bromophenol blue, 60 mM DTT) at 70°C for 10 min at 300 rpm.

3.5.3 SILAC-based mitoproteomics

HeLa cells were cultured in DMEM medium without arginine, lysine and glutamine (Silantes, Cat# 282006500), supplemented with Glutamine and 10% (v/v) dialyzed FBS. Cells were adapted for seven doublings to heavy isotope media $^{13}C_6{}^{15}N_4$ arginine (Silantes, Cat#201604102) and $^{13}C_6{}^{15}N_2$ lysine (Silantes, Cat# 211604102), to middle isotope media $^{13}C_6{}^{15}N$ arginine (Silantes, Cat# 201204102) and $^{12}C_4{}^{15}N$ lysine (Silantes, Cat# 211104113), to light isotope media $^{12}C^{15}N$ arginine (Silantes, Cat# 201004102) and $^{12}C^{15}N$ lysine (Silantes, Cat# 211004102). The same medium was used for the corresponding siRNA transfection. After 48 h of incubation, cells were trypsinized, and cell counts were performed using the viability marker trypan blue (Thermo Fisher, Cat# T10282) with the Countess automated cell counter (Thermo Fisher, Cat# AMQAF2001). Equal numbers of cells were pooled, and subcellular fractionation was performed.

3.5.4 Acetone precipitation

Four times the volume of ice-cold (-20°C) acetone was added to the supernatant and incubated overnight for 16 h. The samples were centrifuged at 20,000xg for 10 min at 4°C. The pellet was washed twice with 400 µL of 80% (v/v) ice-cold acetone. The pellet was dried under the fume hood for 5 min and then resuspended in 100 µL 4% (w/v) SDS in 100 mM HEPES-KOH (pH = 8.5).

3.5.5 SP3 digestion protocol

For total proteome analysis, 60 µL of 4% (w/v) SDS in 100 mM HEPES-NaOH (pH = 8.5) was pre-warmed to 70°C and added to the cell pellet for a further 10 min incubation at 70°C on a thermomixer (shaking: 550 rpm). Protein concentration was determined using the 660 nm Protein Assay (Thermo Fisher, Cat# 22660). 20 µg of protein was subjected to tryptic digestion. For immunoprecipitations, the LDS buffer eluate was directly used. Proteins were reduced (10 mM TCEP) and alkylated (20 mM CAA) for 45 min at 45°C in the dark. Samples were subjected to an SP3-based digestion [334]. Washed SP3 beads (SP3 beads (Sera-Mag(TM) Magnetic

Carboxylate Måodified Particles (Hydrophobic, GE44152105050250), Sera-Mag(TM) Magnetic Carboxylate Modified Particles (Hydrophilic, GE24152105050250) from Sigma Aldrich) were mixed equally, and 3 µL of bead slurry was added to each sample. Acetonitrile was added to a final concentration of 50% and washed twice using 70% ethanol (V = 200 µL) on a custom-made magnet. After a further acetonitrile wash (V = 200µL), 5 µL of digestion solution (10 mM HEPES-NaOH pH = 8.5 containing 0.5 µg Trypsin (Sigma, # T6567-1mg) and 0.5 µg LysC (Wako, # 129-02541) was added to each sample and incubated at 37°C overnight. Peptides were desalted on a magnet using 2 x 200 µL of acetonitrile. Peptides were eluted in 10 µL 5% (v/v) DMSO in LC-MS water (Sigma Aldrich, #900682) in an ultrasonic bath for 10 min and subjected to StageTip desalting using the SDB-RPS material (Affinisep, AttractSPE®Disks SDB-RP, #SPE-Disks-Bio-DVB-47.20) [335]. Formic acid and acetonitrile were added to a final concentration of 2.5% (v/v) and 2% (v/v), respectively. Samples were stored at -20°C prior to LC-MS/MS analysis.

3.5.6 Liquid chromatography and mass spectrometry for Neo N-terminal proteome

LC-MS/MS instrumentation consisted out of an Easy-LC 1200 (Thermo Fisher Scientific) coupled via a nano-electrospray ionization source to an QExactive HF-x mass spectrometer (Thermo Fisher Scientific). For peptide separation an in-house packed column (inner diameter: 75 µm, length: 20 cm) was used. A binary buffer system (A: 0.1% (v/v) formic acid and B: 0.1% (v/v) formic acid in 80% (v/v) acetonitrile) was applied as follows: Linear increase of buffer B from 4% (v/v) to 28% (v/v) within 33 min, followed by a linear increase to 55% (v/v) within 5 min. The buffer B content was further ramped to 95% (v/v) within 2 min. 95 % (v/v) buffer B was kept for further 3 min to wash the column. Prior each sample, the column was washed using 6 µL buffer A and the sample was loaded using 7 µL buffer A. The mass spectrometer operated in a data-dependent mode and acquired MS1 spectra at a resolution of 60000 (at 200 m/z) using a maximum injection time of 20 ms and an AGC target of 3e6. The scan range was defined from 350-1650 m/z and data type was set to profile. MS2 spectra were acquire in a Top15 mode at a 45000 resolution (at 200 m/z) using an isolation window of 0.8 m/z and a normalized collision energy

of 32. The first mass was set to 110 m/z. Dynamic exclusion was enable and set to 20 s.

3.5.7 Liquid chromatography and mass spectrometry for data independent acquisition (whole proteome, immunoprecipitation)

The LC-MS/MS instrumentation consisted of an Easy-LC 1200 (Thermo Fisher Scientific) coupled via a nano-electrospray ionization source to an Exploris 480 mass spectrometer (Thermo Fisher Scientific, Bremen, Germany). An Aurora Frontier column (60 cm length, 1.7 µm particle diameter, 75 µm inner diameter, Ionopticks). A gradient based buffer system (A: 0.1% (v/v) formic acid and B: 0.1% (v/v) formic acid in 80% (v/v) acetonitrile) based gradient was used at a flow rate of 185 nL/min as follows: a linear increase of buffer B from 4% (v/v) to 28% (v/v) within 100 min, followed by a linear increase to 40% within 10 min. The buffer B content was further increased to 50% (v/v) within 4 min and then to 65% (v/v) within 3 min. 95% (v/v) buffer B was maintained for a further 3 min to wash the column. The RF lens amplitude was set to 45% (v/v), the capillary temperature to 275°C and the polarity to positive. MS1 profile spectra were acquired at a resolution of 30,000 (at 200 m/z) over a mass range of 450-850 m/z and an AGC target of 1×10^6.

For MS/MS independent spectra acquisition, 34 equally spaced windows were acquired with an isolation m/z range of 7 Th, and the isolation windows overlapped by 1 Th. The first fixed mass was 200 m/z. The isolation center range covered a mass range of 500–740 m/z. Fragmentation spectra were acquired with a resolution of 30,000 at 200 m/z using a maximum injection time setting of ‘auto’ and stepped normalized collision energies (NCE) of 24, 28, and 30. The default charge state was set to 3 and the AGC target was 3e6 (900% - Exploris 480). MS2 spectra were acquired in centroid mode. FAIMS was activated with an inner electrode temperature of 100°C and an outer electrode temperature of 90°C. The compensation voltage was set at -45 V.

3.6 Transcriptomics

3.6.1 RNA sequencing data

For eukaryotic mRNA sequencing, samples were processed by Novogene. Sequencing was performed on the Illumina NovaSeq X Plus platform (PE150) using a paired-end 150 bp (PE150) read strategy. Messenger RNA was purified from total

RNA using poly-T oligo-attached magnetic beads. After fragmentation, the first strand cDNA was synthesized using random hexamer primers followed by the second strand cDNA synthesis. The library was ready after end repair, A-tailing, adapter ligation, size selection, amplification, and purification. The library was checked with Qubit and real-time PCR for quantification and bioanalyser for size distribution detection. Quantified libraries will be pooled and sequenced on Illumina platforms, according to effective library concentration and data amount.

3.7 Data Analysis

3.7.1 Statistics and reproducibility

All the independent experiments or biological samples are represented in the graphs. Instant Clue software 12.2 and GraphPadPrism V.10.4.1 was used to analyse all the datasets [336]. Data are represented by 95% confidence interval of the mean to show statistically significant differences between the groups. To compare two groups, $P < 0.05$ was considered significant, or if indicated otherwise. No statistical method was used to pre-determine sample size. The investigators for proteomics and metabolomics measurement were blinded to allocation during experiments and samples were randomized. The investigators were not blinded for all other experiments, and samples were not randomized. The center line of the visualized boxplots represents the median; edges of the box represent 25th and 75th quantiles; whiskers show minimum and maximum values excluding outliers. Outliers are defined by a greater distance from the median and 1.5x the interquartile range, if not indicated otherwise.

3.7.2 RNA sequencing

rRNA transcripts were removed from the annotation file by depleting all lines with 'rrna' tag on it. cDNA index was build using kallisto (kallisto/0.46.1) and RSeQC/4.0.0 used to identify mapping strand: A strand was identified by having more than 60% of reads mapped to it. Cases with less than 60% of reads in each strand are defined as unstranded. After normalization of read counts by making use of the standard median-ratio for estimation of size factors, pair-wise differential gene expression was performed using DESeq2/1.24.0. After removal of genes with less then 10 overall reads $\log_2$ fold changes were shrank using approximate posterior estimation for GLM coefficients.

3.7.3 Neo N-terminal proteome

Raw files were analysed using MaxQuant (1.6.7 and 1.6.12) [337], and the implemented Andromeda search engine. TMT 10-plex (WT and OMA1 knockout) or TMT-6plex (*SPG7*$^{-/-}$, *AFG3L2*$^{-/-}$, *SPG7*$^{-/-}$ *AFG3L2*$^{-/-}$, and WT) was set as a quantification setting. ArgC with semi-specificity (free N-terminus) was used. MS2 spectra were correlated against the Uniprot human reference proteome (UP000005640, number sequences: 21K, downloaded: 2022.08). Match-between runs algorithm was enabled. To identify novel Neo-N termini, the peptides.txt file of the MaxQuant output folder was utilized and TMT intensities between conditions were compared using a two-sided t-test. Raw files were analysed using MaxQuant (1.6.4) [337] and the implemented Andromeda search engine. TMT-10plex was set as a quantification setting. ArgC with semi-specificity (free N-terminus) was used. MS2 spectra were correlated against the Uniprot human reference proteome. Match-between runs algorithm was enabled. To identify novel Neo-N termini, the peptides.txt file of the MaxQuant output folder was utilized and TMT intensities between conditions were compared using a two-sided t-test in the Perseus software.

3.7.4 Whole proteome and crosslinking interaction studies

The Spectronaut (18.7.240325.55695) directDIA+ (Deep) analysis tool was used to correlate the acquired MS2 spectra in data-independent mode with the Uniprot reference human proteome (UP000005640, number sequences: 21K, downloaded: 2022-08). The MaxLFQ algorithm was used. The precursor, peptide and protein q-value cutoff were 0.01 in the Pulsar search. A total number of two missed cleavages of 2 were allowed, and the minimal peptide length was seven amino acids. Acetyl (Protein N-term), and Oxidation (M) were defined as variable modifications, and Carbamidomethyl at cysteines was set as a fixed modification. The mean precursor and mean peptide quantities were used for agglomeration to protein quantities. The log2 protein group LFQ intensities were used for a pairwise comparison using a two-tailed unpaired t-test followed by a permutation-based FDR calculation (FDR < 0.05 is considered significantly different, s0 = 0.1, number of permutations = 500). The experiment was performed with 5 (whole proteome) and 4 (interaction studies) biologically independent replicates.

3.7.5 SILAC-based subcellular fractionation

The Spectronaut (18.7.240325.55695) directDIA tool was used to analyse the acquired raw files. channel 2 (Arg6, Lys4) and channel 3 (Arg10, Lys8) were defined. The option 'exclude interference' was enabled to exclude fragments with the same mass of different SILAC channels (e.g. co isolated b-ions). Otherwise, the default settings were utilized. The SILAC protein group ratio was then calculated by aggregating the precursor data to the mean of the log_2 SILAC ratio at the elution group level and further calculating the median of the peptides log_2 SILAC ratio to obtain the protein group H/L, H/M and M/L ratios. The ratio distributions were then shifted to a median of 0. Significantly different protein groups were identified using a one-sample t-test on the log_2 protein group SILAC ratio. The *P* values were adjusted using the Benjamini-Hochberg correction (adj. *P* value < 0.05) in the Instant Clue software.

3.7.6 Quantification and statistical analysis

Densitometry data were generated by Fiji for Western blot quantification. Representative images from at least three independent experiments are shown. Graphs were generated using Prism (GraphPad). Volcano plots and heat maps were generated using InstantClue [336]. Error bars represent the standard deviation of the mean. Statistical significance of the data was assessed by using the two-sided unpaired t-test or the Whitney-Mann U-test, comparing control and test conditions, as described in the figure legend. Data was visualized in Instant Clue [338].

3.7.7 Data availability

RNA sequencing data will be uploaded to Gene Expression Omnibus (GEO). The proteomics data were uploaded to the following PRIDE projects under the IDs: The Neo-N termiome of *OMA1*$^{-/-}$ HeLa cells are available under the identifier PXD061134 (Username: reviewer_pxd061134@ebi.ac.uk Password: C1UmPFkOoRRa). The Neo-N termiome of *AFG3L2*$^{-/-}$, *SPG7*$^{-/-}$, *AFG3L2*$^{-/-}$ *SPG7*$^{-/-}$, and WT HeLa cells is available on PRIDE under the identifier PXD061137 (Username: reviewer_pxd061137@ebi.ac.uk, Password: OnCsk8N9f9Nd). The SILAC-based subcellular fraction proteomics experiment is available under the identifier: PXD061449 (Username: reviewer_pxd061449@ebi.ac.uk, Password: lGlE5bQioK63), and PXD061185 (Username: reviewer_pxd061185@ebi.ac.uk, Password: wQyII8xL8IaW). TIMM17A and TIMM17B knock-down in WT and

DNAJC15$^{-/-}$, HeLa cells were deposited to PRIDE under the identifier PXD061131 (Username: reviewer_pxd061131@ebi.ac.uk, Password: rb0G6SG536x0). The DNAJC15 DSP crosslinking interactome is available under the PRIDE identifier PXD061165 (Username: reviewer_pxd061165@ebi.ac.uk, Password: lyEQh0beALaX).

3.7.8 AI-Tools

Schematics were generated using Bio-Render and Adobe Illustrator. DeepL Write and OpenAI assisted with grammar and spelling during the writing of this thesis.

4. Publication

4.1 Stress adaptation of mitochondrial protein import by OMA1-mediated degradation of DNAJC15

Authors contributions:

The following chapter of this thesis has already been published on BioRxiv (https://doi.org/10.1101/2025.03.04.641455) and represents the main work of my Ph.D. project. This publication was a collaborative effort of multiple authors. My personal contributions to the publication included:

Conceptualization; execution of experiments, data curation; formal analysis; validation; investigation; graphical representation; methodology; writing - original draft; writing - review and editing.

Stress adaptation of mitochondrial protein import by OMA1-mediated degradation of DNAJC15

Lara Kroczek[1#], Hendrik Nolte[1#], Yvonne Lasarzewski[1], Thibaut Molinié[2], Daniel Curbelo Pinero[1], Kathrin Lemke[1], Elena Rugarli[2,3,4], and Thomas Langer[1,4,*]

[1] Max Planck Institute for Biology of Ageing, Cologne, Germany

[2] Institute for Genetics, University of Cologne, Cologne, Germany

[3] Center for Molecular Medicine, University of Cologne, Cologne, Germany

[4] Cologne Excellence Cluster on Cellular Stress Responses in Aging-Associated Diseases (CECAD), University of Cologne, Cologne, Germany

[#]These authors contributed equally.

[*]Corresponding author.

Max Planck Institute for Biology of Ageing, Joseph-Stelzmann-Str. 9b, 50931 Cologne, Germany

Phone: +49 221 37 970 500

Email: tlanger@age.mpg.de

Mitochondria adapt to cellular stress to ensure cell survival. The stress-regulated mitochondrial peptidase OMA1 orchestrates these adaptive responses, which limit mitochondrial fusion and promote mitochondrial stress signaling and metabolic rewiring. Here, we show that cellular stress adaptation involves OMA1-mediated regulation of mitochondrial protein import and OXPHOS biogenesis. OMA1 cleaves the mitochondrial chaperone DNAJC15 and promotes its degradation by the m-AAA protease AFG3L2. Loss of DNAJC15 reduces the import of OXPHOS-related proteins via the TIMM23-TIMM17A protein translocase, limiting OXPHOS biogenesis under conditions of mitochondrial dysfunction. Non-imported mitochondrial preproteins accumulate at the endoplasmic reticulum and induce an ATF6-related unfolded protein response. Our results demonstrate stress-dependent changes in protein import specificity as part of the OMA1-mediated mitochondrial stress response and highlight the interdependence of proteostasis regulation between different organelles.

4.2 Introduction

Mitochondrial stress responses orchestrated by the mitochondrial peptidase OMA1 ensure the adaptation of mitochondrial functions to meet changing physiological demands and maintain cell survival. Mitochondrial deficiencies, such as OXPHOS defects or dissipation of the membrane potential, activate OMA1 in the mitochondrial inner membrane (IM) and trigger the mitochondrial integrated stress response (ISR^{mt}) by processing of DELE1, which promotes metabolic reprogramming and enhances the cellular defence against oxidative stress [34, 36, 37, 56-58]. At the same time, OMA1 activation limits mitochondrial fusion through excessive processing of the dynamin-like OPA1 leading to the fragmentation of the mitochondrial network under stress [44, 48, 339 340]. Recent studies have demonstrated that OMA1 can also perform quality control functions by degrading polypeptides that block protein translocases [63]. The activation of OMA1 destabilizes the protease and causes its degradation, terminating the OMA1-mediated stress response after restoration of mitochondrial functions [33, 36]. Although impairment of OMA1-mediated stress pathways by *Dele1* deletion or prevention of Opa1 processing is well tolerated in mice [341], protective effects have been observed under pathophysiological conditions, such as mitochondrial (cardio-) myopathies [64, 326, 342, 343]. However, the consequences of OMA1 deficiency and of impaired OMA1-mediated stress responses are cell and tissue specific and depend on the physiological context [65-69, 72].

Here, to better understand how OMA1 affects mitochondrial proteostasis and stress responses, we performed a proteomic survey for proteolytic substrates of OMA1. We demonstrate that OMA1 cleaves the mitochondrial chaperone DNAJC15 facilitating its degradation by the mitochondrial m-AAA protease. The loss of DNAJC15 alters protein import by TIM23 protein translocases in the IM and limits the accumulation of OXPHOS-related mitochondrial matrix and IM proteins. Non-imported mitochondrial preproteins accumulate at the endoplasmic reticulum (ER) and trigger an ATF6-related unfolded protein response. These results demonstrate that OMA1 allows to adapt mitochondrial protein biogenesis to stress and reveal an intricate network of cellular stress responses to proteostasis disturbances.

4.3 Results

4.3.1 OMA1 cleavage facilitates DNAJC15 degradation by the m-AAA protease

To identify novel OMA1 substrate proteins, we searched for amino-terminal peptides of mitochondrial proteins that accumulate in an OMA1-dependent manner in a proteome-wide survey in wild-type (WT) and *OMA1*$^{-/-}$ human cervical cancer cells (Fig. 8a). Among the four MitoCarta 3.0 annotated peptides [344], that were significantly decreased in *OMA1*$^{-/-}$ cells, was one amino-terminal peptide of the protein DNAJC15 (MCJ), a co-chaperone of the human TIM23 translocase in IM [207, 213, 345] (Extended Data Fig. 1a). We detected a peptide corresponding to amino acids 20-35, indicating OMA1 cleavage of DNAJC15 (Q9Y5T4) after amino acid 19.

DNAJC15 has been identified as a short-lived mitochondrial protein [76, 224] and we have recently observed the accumulation of DNAJC15 in HeLa cells lacking the m-AAA protease subunit AFG3L2, raising the possibility that the m-AAA protease mediates proteolysis of DNAJC15 [76, 224]. Cycloheximide (CHX)-chase experiments confirmed the rapid turnover of DNAJC15, which was completely halted in cells lacking both m-AAA protease subunits, AFG3L2 and SPG7 (Fig. 8b, c; Extended Data Fig. 1b). We noted that DNAJC15 accumulated in a shorter form in these cells (Fig. 8b). Analysis of the neo-amino-terminal proteome of m-AAA protease-deficient cells revealed accumulation of the amino-terminal peptide 20-35 of DNAJC15 (Fig. 8a), suggesting that OMA1 mediates cleavage of full-length DNAJC15 (hereafter termed L-DNAJC15) after amino acid 19 into a shorter form (hereafter termed S-DNAJC15) that is degraded by the m-AAA protease. Consistently, L-DNAJC15 accumulated in *AFG3L2*$^{-/-}$*SPG7*$^{-/-}$ cells upon depletion of OMA1 (Fig. 8b, c).

To confirm these findings, we generated *DNAJC15*$^{-/-}$ HeLa cell lines expressing DNAJC15, S-DNAJC15 (lacking amino acids 2-19) or a DNAJC15 variant lacking amino acids 19 and 20 (hereafter referred to as DNAJC15Δ2) (Extended Data Fig. 1c). Experiments in *DNAJC15*$^{-/-}$ cells expressing DNAJC15 variants lacking 2, 6, or 10 amino acids at the OMA1 cleavage site had shown that deletion of amino acid 19 and 20 completely abrogated OMA1 cleavage, even after membrane hyperpolarization, which is known to activate OMA1 (Extended Data Fig. 1d, e). S-DNAJC15 was targeted to mitochondria and stabilized upon depletion of the m-AAA

protease in cells expressing DNAJC15 or S-DNAJC15 (Fig. 8d, e). Remarkably, impaired OMA1 cleavage led to a significant stabilization of DNAJC15Δ2, which accumulated in WT and m-AAA protease-deficient cells (Fig. 8f, g).

We conclude from these experiments that cleavage of DNAJC15 by OMA1 after amino acid 19 leads to the destabilization of DNAJC15 and rapid proteolysis by the m-AAA protease.

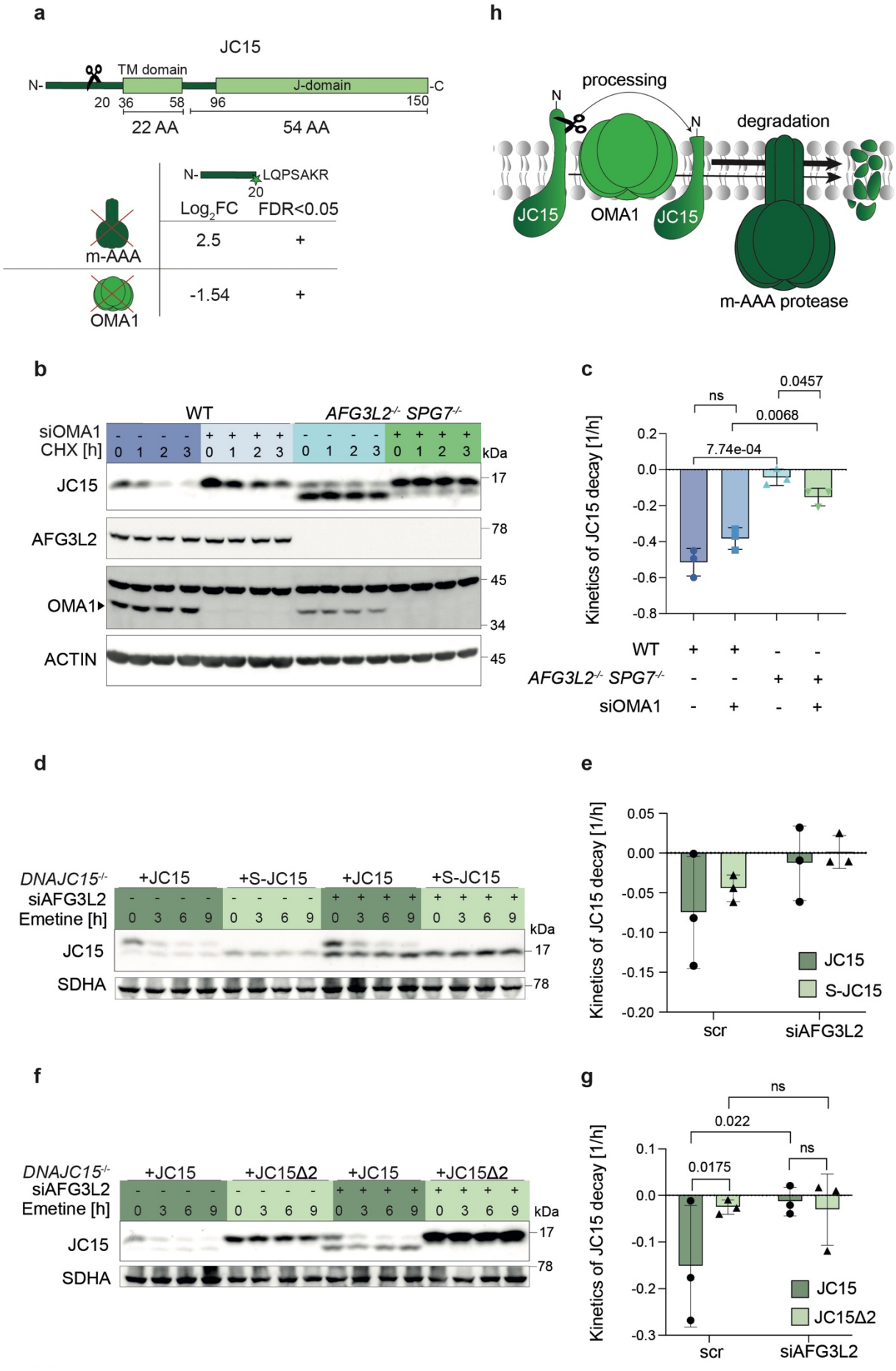
a
JC15
TM domain
J-domain
N-
-C
20
36
58
96
150
22 AA
54 AA
N-
LQPSAKR
20
Log2FC
FDR<0.05
m-AAA
2.5
+
OMA1
-1.54
+
h
processing
N
N
degradation
JC15
OMA1
JC15
m-AAA protease
b
WT
AFG3L2-/- SPG7-/-
siOMA1
CHX [h]
0 1 2 3 0 1 2 3 0 1 2 3 0 1 2 3
kDa
JC15
17
AFG3L2
78
OMA1
45
34
ACTIN
45
c
ns
0.0457
0.0068
7.74e-04
Kinetics of JC15 decay [1/h]
0.2
0.0
-0.2
-0.4
-0.6
-0.8
WT + + - -
AFG3L2-/- SPG7-/- - - + +
siOMA1 - + - +
d
DNAJC15-/-
+JC15
+S-JC15
+JC15
+S-JC15
siAFG3L2
Emetine [h]
0 3 6 9 0 3 6 9 0 3 6 9 0 3 6 9
kDa
JC15
17
SDHA
78
e
Kinetics of JC15 decay [1/h]
0.05
0.00
-0.05
-0.10
-0.15
-0.20
JC15
S-JC15
scr
siAFG3L2
f
DNAJC15-/-
+JC15
+JC15Δ2
+JC15
+JC15Δ2
siAFG3L2
Emetine [h]
0 3 6 9 0 3 6 9 0 3 6 9 0 3 6 9
kDa
JC15
17
SDHA
78
g
ns
0.022
ns
0.0175
Kinetics of JC15 decay [1/h]
0.1
0.0
-0.1
-0.2
-0.3
JC15
JC15Δ2
scr
siAFG3L2

Figure 8. OMA1 cleavage of DNAJC15 facilitates degradation by the m-AAA protease. a, Comparison of the Neo-N-terminal proteome data sets of wild-type (WT) HeLa cells with *OMA1*$^{-/-}$ and *AFG3L2*$^{-/-}$ *SPG7*$^{-/-}$ cells reveals the OMA1-dependent cleavage of DNAJC15 (JC15) at amino acid position 19 (UniProt ID: Q9Y5T4) (n = 5, biologically independent samples). **b**, Stability of DNAJC15 in WT and *AFG3L2*$^{-/-}$ *SPG7*$^{-/-}$ HeLa cells depleted of OMA1 (siOMA1) for 72 h after inhibition of cytosolic translation with Cycloheximide (CHX). A representative experiment is shown (n = 3, biologically independent samples). **c**, Degradation rates of DNAJC15 in (b) normalized to time point 0 h. Data are means +/- SD (n = 3, biologically independent samples). *P* values were calculated using a two-sided unpaired t-test. **d**, Stability of DNAJC15 in *DNAJC15*$^{-/-}$ cells expressing DNAJC15 (JC15) or DNAJC15 cleaved by OMA1 (S-JC15) and depleted of AFG3L2 (siAFG3L2) after inhibition of cytosolic translation with emetine. **e**, Degradation rates of DNAJC15 in (d) normalized to time point 0 h. Data are means +/- SD (n = 3, biologically independent samples). Statistics were calculated with a two-way ANOVA test. **f**, Stability of DNAJC15 in *DNAJC15*$^{-/-}$ cells expressing DNAJC15 (JC15) or a non-cleavable DNAJC15 variant lacking amino acid 19 and 20 (JC15Δ2) and depleted of AFG3L2 after inhibition of cytosolic translation with emetine. **g**, Degradation rates of DNAJC15 in (f) normalized to time point 0 h. Data are means +/- SD (n = 3, biologically independent samples). *P* values were calculated using a two-way ANOVA test. **h**, Schematic representation of the OMA1-mediated DNAJC15 processing leading to a degradation by the m-AAA protease.

4.3.2 Genetic interactions link DNAJC15 to mitochondrial protein import

Complementation studies in yeast have shown functional conservation of DNAJC15 with its yeast ortholog Pam18 (Tim14) [207, 214], suggesting that proteolysis of DNAJC15 by OMA1 and the m-AAA protease regulate mitochondrial protein import. While Pam18 (Tim14) is essential for cell growth and mitochondrial protein import in yeast [188, 208, 346], the basal characterization of *DNAJC15*$^{-/-}$ cells did not reveal global changes in cell growth or oxygen consumption, nor did it reveal broad changes in the cellular proteome (Extended Data Fig. 2a-c). Human cells express two Pam18 paralogs, DNAJC15 and DNAJC19. Both proteins are highly homologous in the J-domain and the transmembrane region, but DNAJC15 exposes an extended amino-terminal region to the mitochondrial intermembrane space (IMS), which is cleaved by OMA1 (Extended Data Fig. 2d). We therefore hypothesized that DNAJC19 could compensate for the loss of DNAJC15. Indeed, depletion of DNAJC19 abolished cell proliferation of *DNAJC15*$^{-/-}$ cells but did not affect the growth of WT HeLa cells (Fig. 9a). Re-expression of DNAJC15 or DNAJC15Δ2 restored cell growth (Fig. 9b-c), whereas only partial recovery was observed after expression of S-DNAJC15 (Fig. 9d-e). Thus, DNAJC15 and

DNAJC19 show functional redundancy, suggesting that both play a role in mitochondrial protein import.

We extended the analysis of the genetic interaction landscape of DNAJC15 to other components of the human TIM23 translocase [345]. Consistent with their central role during protein translocation through TIM23 complexes, downregulation of PAM16, HSPA9, or GRPEL1 strongly inhibited cell growth in WT cells independent of the presence of DNAJC15 or DNAJC19 (Fig. 9f). Similarly, TIMM23, TIMM44, ROMO1 depletion limited the proliferation of WT cells (Fig. 9f). Cell growth was further reduced in the absence of DNAJC15, providing additional genetic support for a protein import function of DNAJC15.

Notably, depletion of TIMM17A strongly impaired the growth of *DNAJC15*$^{-/-}$ cells, while only moderately affecting WT and *DNAJC19*$^{-/-}$ cell growth (Fig. 9g-i). Re-expression of DNAJC15, DNAJC15Δ2 or S-DNAJC15, restored the growth of *DNAJC15*$^{-/-}$ cells depleted of TIMM17A (Extended Data Fig. 2e-h). In contrast, DNAJC15 did not genetically interact with the TIMM17A-homolog TIMM17B (Fig. 9h, i). TIM17 proteins are an essential part of the protein translocation channel in TIM23 complexes [203-205]. Since both human TIMM17 homologs have been found as part of distinct protein-conducting complexes [213], these results suggest that DNAJC15 exerts translocase-specific functions during mitochondrial protein import.

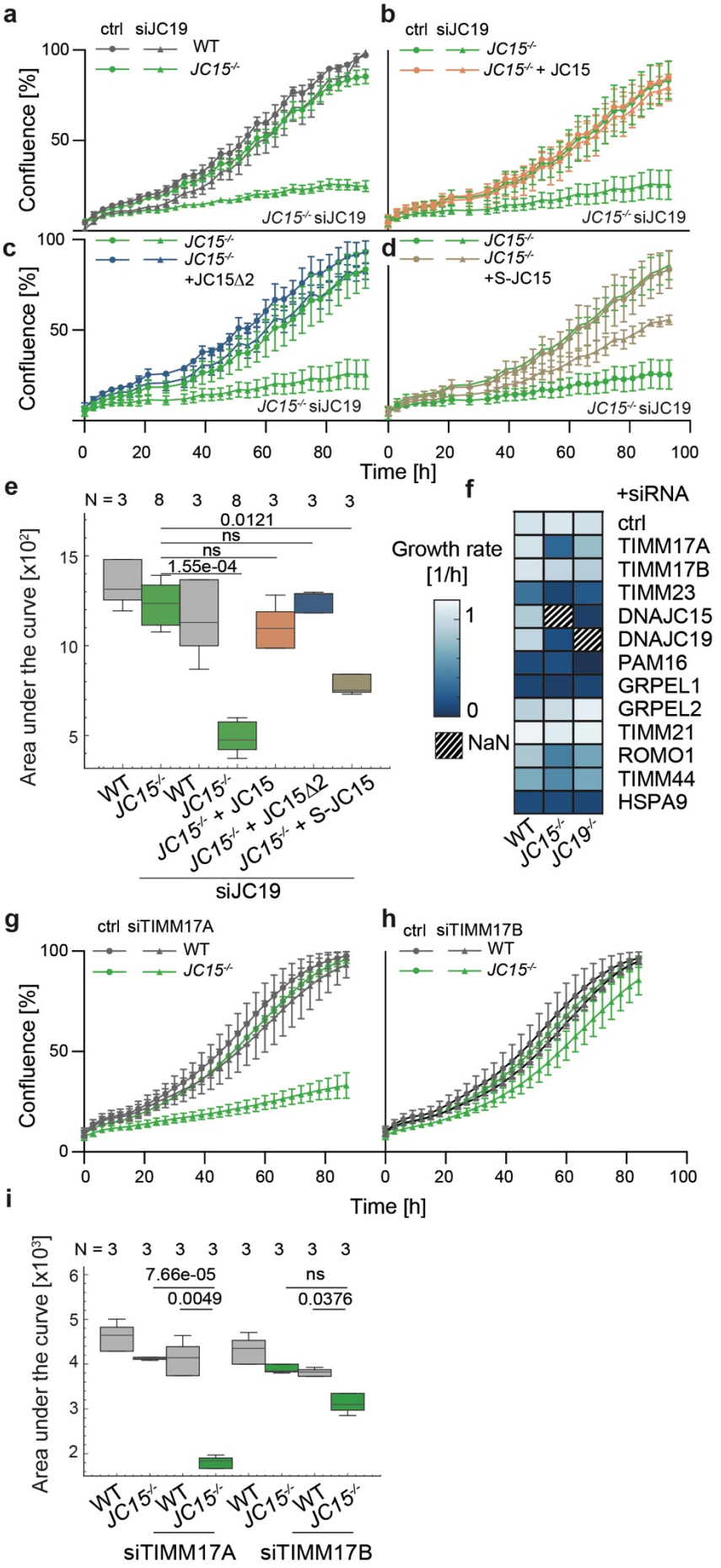
a
ctrl siJC19
WT
JC15-/-
Confluence [%]
JC15-/- siJC19
b
ctrl siJC19
JC15-/-
JC15-/- + JC15
JC15-/- siJC19
c
JC15-/-
JC15-/-
+JC15Δ2
JC15-/- siJC19
d
JC15-/-
JC15-/-
+S-JC15
JC15-/- siJC19
Time [h]
e
N = 3 8 3 8 3 3 3
0.0121
ns
ns
1.55e-04
Area under the curve [x10²]
WT
JC15-/-
WT
JC15-/-
JC15-/- + JC15
JC15-/- + JC15Δ2
JC15-/- + S-JC15
siJC19
f
+siRNA
Growth rate [1/h]
1
0
NaN
ctrl
TIMM17A
TIMM17B
TIMM23
DNAJC15
DNAJC19
PAM16
GRPEL1
GRPEL2
TIMM21
ROMO1
TIMM44
HSPA9
WT
JC15-/-
JC19-/-
g
ctrl siTIMM17A
WT
JC15-/-
Confluence [%]
h
ctrl siTIMM17B
WT
JC15-/-
Time [h]
i
N = 3 3 3 3 3 3 3 3
7.66e-05
0.0049
ns
0.0376
Area under the curve [x10³]
WT
JC15-/-
WT
JC15-/-
WT
JC15-/-
WT
JC15-/-
siTIMM17A
siTIMM17B

Figure 9. Genetic interactions of DNAJC15 with subunits of the TIM23 complex. a, Cell growth of wild-type (WT) and *DNAJC15*$^{-/-}$ HeLa cells after siRNA-mediated depletion of DNAJC19 (WT, n = 3; *DNAJC15*$^{-/-}$ n = 8, biologically independent samples). Data are means +/- SD. **b**, Cell growth of WT and *DNAJC15*$^{-/-}$ HeLa cells expressing DNAJC15 (JC15) after siRNA-mediated depletion of DNAJC19 (n = 3, biologically independent samples). Data are means +/- SD. **c**, Cell growth of WT and *DNAJC15*$^{-/-}$ HeLa cells expressing non-cleavable DNAJC15 (JC15Δ2) after siRNA-mediated depletion of DNAJC19 (n = 3, biologically independent samples). Data are means +/- SD. **d**, Cell growth of WT and *DNAJC15*$^{-/-}$ HeLa cells expressing OMA1-cleaved DNAJC15 (S-JC15) after siRNA-mediated depletion of DNAJC19 (n = 3, biologically independent samples). Data are means +/- SD. **e**, Quantification of cell growth determining the area under the curve in (a-d). *P* values were calculated using a Mann-Whitney U-test. Quantile box plot show median, 25th and 75th percentiles (WT, n = 3; *DNAJC15*$^{-/-}$, n = 8, *DNAJC15*$^{-/-}$ + JC15, n = 3; *DNAJC15*$^{-/-}$ + JC15Δ2, n = 3; *DNAJC15*$^{-/-}$ + S-JC15, n = 3, biologically independent samples). **f**, Heatmap of growth rates of WT, *DNAJC15*$^{-/-}$ and *DNAJC19*$^{-/-}$ HeLa cells after siRNA depletion of the indicated subunits of the TIM23 complex. Data are means (n = 3, biologically independent samples). **g-i** Cell growth of WT and *DNAJC15*$^{-/-}$ HeLa cells after siRNA-mediated depletion of TIMM17A (g) or TIMM17B (h) for 72 h (n = 3, biologically independent samples). Data are means +/- SD. Quantification of cell growth monitoring the area under the curve in (g-h) are shown in (i). *P* values were calculated using a two-sided unpaired t-test. Quantile box plot show median, 25th and 75th percentiles.

4.3.3 The interactome of DNAJC15

To define the molecular environment of DNAJC15 within mitochondria, we employed immunoprecipitation coupled with chemical crosslinking to isolate untagged DNAJC15 and associated proteins. LC-MS/MS analysis revealed a significant enrichment of 185 proteins, 179 of them being mitochondrial (according to MitoCop [76]), the vast majority of which are localised to the mitochondrial matrix and IM (Fig. 10a, b). Consistent with previous reports [207], PAM16 emerged as the strongest interactor of DNAJC15 (Fig. 10c). Moreover, we identified TIMM23, TIMM44, HSPA9, TIMM50, TIMM21 and DNAJC19 as significant DNAJC15 interactors, further supporting the association of DNAJC15 with the TIM23 complex (Fig. 10c).

An interaction network based on MitoCop pathways revealed close proximity of DNAJC15 to mitochondrial quality control and biogenesis factors (Fig. 10d). These include the m-AAA protease subunit AFG3L2 and its interactors MAIP1 and TMBIM5 (GHITM), the i-AAA protease YME1L as well as the CLPB chaperone and the scaffold proteins PHB1, PHB2 and STOML2 (SLP2), which are associated with AAA proteases and affect OXPHOS biogenesis (Fig. 10e) [11, 191, 347-349]. Strikingly,

the vast majority of proteins in the vicinity of DNAJC15 function in mitochondrial gene expression and respiratory chain biogenesis (Fig. 10d), highlighting the emerging coupling between protein translocation and OXPHOS biogenesis [183, 211]. Strikingly, the most highly enriched interactors of DNAJC15 included enzymes involved in the coenzyme Q metabolism, components involved in the respiratory complex I assembly and subunits of complex I, in particular those in the Q module and the ND4 module (Fig. 10d).

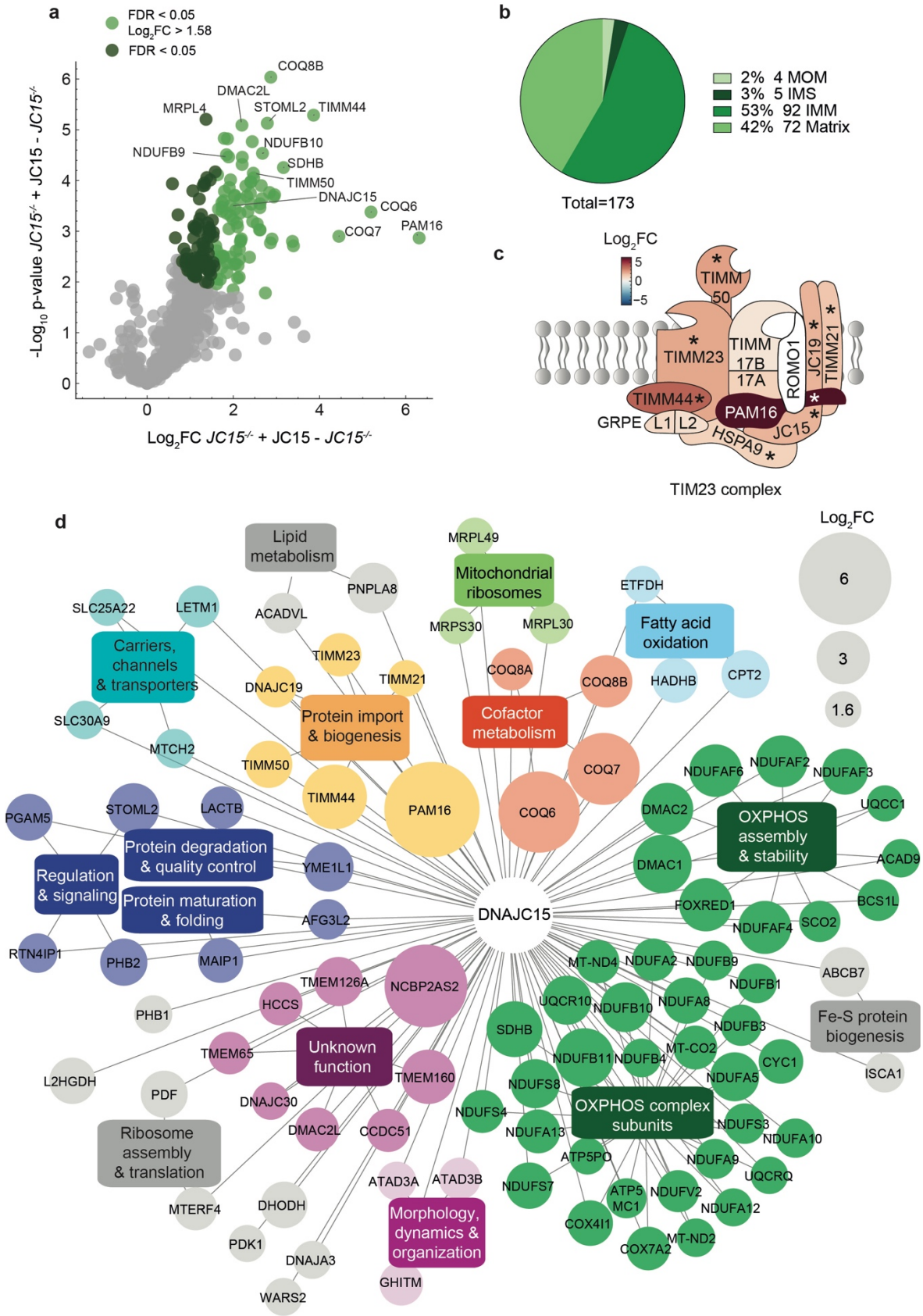
a
FDR < 0.05
Log2FC > 1.58
FDR < 0.05
COQ8B
DMAC2L
MRPL4
STOML2
TIMM44
NDUFB10
NDUFB9
SDHB
TIMM50
DNAJC15
COQ6
COQ7
PAM16
-Log10 p-value JC15-/- + JC15 - JC15-/-
Log2FC JC15-/- + JC15 - JC15-/-
b
2% 4 MOM
3% 5 IMS
53% 92 IMM
42% 72 Matrix
Total=173
c
Log2FC
TIMM 50
TIMM 23
TIMM 17B
17A
ROMO1
JC19
TIMM21
TIMM44
PAM16
GRPE
L1
L2
HSPA9
JC15
TIM23 complex
d
Log2FC
Lipid metabolism
Mitochondrial ribosomes
Fatty acid oxidation
Carriers, channels & transporters
Protein import & biogenesis
Cofactor metabolism
OXPHOS assembly & stability
Protein degradation & quality control
Protein maturation & folding
Regulation & signaling
Unknown function
Ribosome assembly & translation
Morphology, dynamics & organization
OXPHOS complex subunits
Fe-S protein biogenesis
DNAJC15
MRPL49
PNPLA8
ACADVL
SLC25A22
LETM1
MRPS30
MRPL30
ETFDH
HADHB
CPT2
COQ8A
COQ8B
TIMM23
TIMM21
DNAJC19
SLC30A9
MTCH2
TIMM50
TIMM44
PAM16
COQ6
COQ7
NDUFAF6
NDUFAF2
NDUFAF3
UQCC1
DMAC2
DMAC1
ACAD9
FOXRED1
NDUFAF4
SCO2
BCS1L
PGAM5
STOML2
LACTB
YME1L1
AFG3L2
RTN4IP1
PHB2
MAIP1
PHB1
TMEM126A
HCCS
NCBP2AS2
TMEM65
TMEM160
L2HGDH
PDF
DNAJC30
DMAC2L
CCDC51
MTERF4
DHODH
PDK1
DNAJA3
WARS2
ATAD3A
ATAD3B
GHITM
MT-ND4
NDUFA2
NDUFB9
NDUFB1
ABCB7
UQCR10
NDUFB10
NDUFA8
NDUFB3
SDHB
MT-CO2
NDUFB11
NDUFB4
CYC1
NDUFA5
ISCA1
NDUFS8
NDUFS4
NDUFA13
NDUFS3
NDUFA10
ATP5PO
NDUFA9
UQCRQ
NDUFS7
ATP5 MC1
NDUFV2
NDUFA12
COX4I1
MT-ND2
COX7A2

Figure 10. The DNAJC15 interactome. DNAJC15 immunoprecipitation in *DNAJC15*$^{-/-}$ HeLa cells expressing DNAJC15 and in *DNAJC15*$^{-/-}$ HeLa cells after chemical crosslinking (DSP, 2 mM) under non-denaturing conditions. **a**, Volcano plot showing the mitochondrial proteins interacting with DNAJC15 (according to MitoCarta 3.0). 174 significantly mitochondrial interactors are highlighted in green (FDR < 0.05, n = 4, biologically independent samples) with those that are 1.5x enriched in dark green (FDR < 0.05, $\log_2$FC < 1.58). **b**, Pie chart visualizing the known submitochondrial localization of the 173 significant mitochondrial DNAJC15 interaction partners (according to MitoCarta 3.0) (FDR < 0.05). **c**, Schematic visualization of the TIM23 complex subunits interacting with DNAJC15. The red scale indicates fold-enrichment between *DNAJC15*$^{-/-}$ cells expressing DNAJC15 and *DNAJC15*$^{-/-}$ cells ($\log_2$FC). The asterisk indicates all significantly affected proteins (FDR < 0.05, n = 4, biologically independent samples). **d**, String analysis of mitochondrial DNAJC15 interactors with a fold-enrichment higher than 1.58 (FDR < 0.05). The box size is adapted to their fold-enrichment ($\log_2$FC) in *DNAJC15*$^{-/-}$ HeLa cells expressing DNAJC15 compared to *DNAJC15*$^{-/-}$ HeLa cells. Pathways associated with only one gene name were removed.

4.3.4 DNAJC15 controls mitochondrial protein import specificity

Since the genetic and protein interaction landscapes linked the function of DNAJC15 to mitochondrial protein import, we directly monitored mitochondrial protein biogenesis using stable isotope labelling with amino acids in cell culture (SILAC) combined with cellular fractionation. We labelled WT HeLa cells with different stable isotopes of lysine and arginine prior to transfection with DNAJC15-specific, DNAJC19-specific or scrambled siRNA (Fig. 11a). This allowed pooling of the three samples prior to cell fractionation to reduce experimental variation. We then isolated the mitochondrial fraction by differential centrifugation and removed potential non-imported mitochondrial preproteins with exogenously added protease. The total cell fraction and mitochondrial fractions with and without protease treatment were subjected to LC-MS/MS analysis in four independent biological replicates (Fig. 11a). In total, 8342 proteins were quantified, covering 952 (83.8%) MitoCarta 3.0 annotated proteins. The SILAC ratios of individual proteins between depleted and non-depleted cells reflected changes in their steady-state levels under the different experimental conditions.

Depletion of DNAJC15 or DNAJC19 only moderately affected the distribution of mitochondrial proteins in the total cell fraction (Fig. 11b, c). We observed an only moderate increase of 110 and 77 mitochondrial proteins in cells depleted of DNAJC15 or DNAJC19, respectively (Fig. 11b, c). Thus, mitochondrial proteins are synthesized at similar rates regardless of the presence or absence of DNAJC15 or

DNAJC19. Strikingly, however, 188 MitoCarta 3.0 annotated proteins were reduced in the untreated mitochondrial fraction after DNAJC15 depletion, along with a significant systematic down-shift in the distribution of mitochondrial proteins in DNAJC15-depleted cells relative to wild-type cells (Fig. 11b, c). After protease treatment of the mitochondrial fraction the steady-state level of a further 75 proteins were significantly reduced, indicating that these proteins were not imported but remained associated with the outer mitochondrial membrane (OM) in DNAJC15-depleted mitochondria (Fig. 11b, c). In contrast, the depletion of DNAJC19 did not significantly reduce stead-state levels of mitochondrial proteins (Fig. 11c).

The loss of DNAJC15 impaired mainly the import of proteins, which are localised to the matrix and IM, and of a few IMS and OM localised proteins (Fig. 11d). Many of matrix and IM proteins are targeted to mitochondria by an amino-terminal mitochondrial targeting sequence (MTS). Consistently, we observed the downregulation of MTS peptides in the mitochondrial fraction of DNAJC15-depleted cells (Fig. 11d). Gene enrichment analysis of significantly changed proteins revealed broad effects on mitochondrial proteins with diverse functions in mitochondrial gene expression, protein biogenesis and metabolism (Fig. 11e). Among the downregulated mitochondrial proteins, proteins associated with mitochondrial ribosome assembly and RNA granules were most affected as shown by a MitoPathway analysis (Fig. 11f). These results show that DNAJC15 supports the mitochondrial import of many matrix and IM proteins with OXPHOS-related functions. Consistently, 73 proteins, which were present at reduced levels after DNAJC15 depletion, are also significantly enriched in the interactome of DNAJC15 and may bind to DNAJC15 during membrane translocation into mitochondria (Fig. 11g).

The mitochondrial proteins that were significantly decreased after DNAJC15 have a decreased half-life when compared to the median stability of the mitochondrial proteome (Fig. 11h, i) [76], while we did not observe differences in other parameters, such as protein abundance, protein length or MTS length and score (Extended Data Fig. 3a-d). It is therefore conceivable that, along with differences in import specificity, the high turnover of mitochondrial proteins may also contribute to the observed proteomic changes after impairment of protein import in DNAJC15-depleted mitochondria.

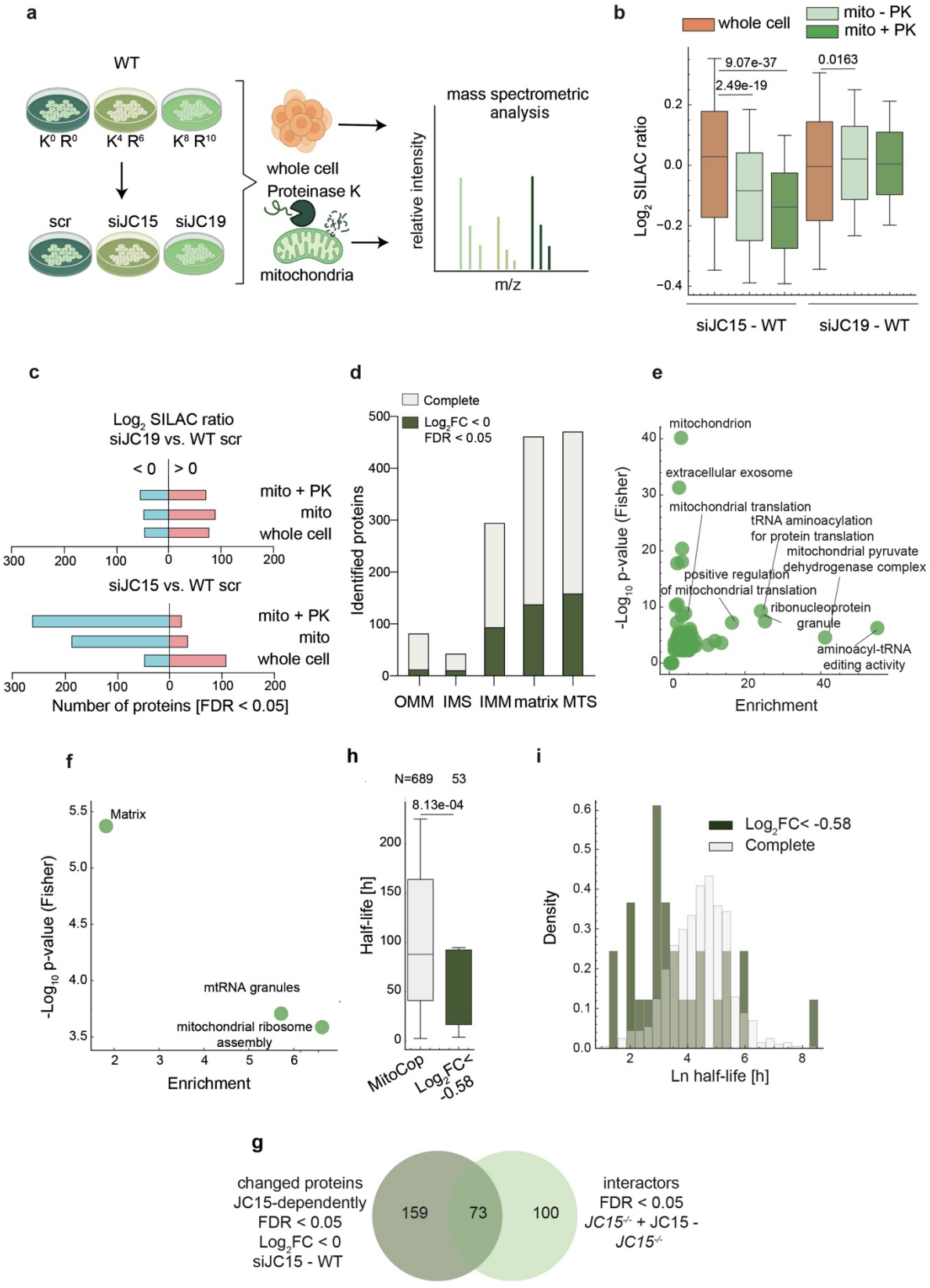
a
WT
K⁰ R⁰
K⁴ R⁶
K⁸ R¹⁰
scr
siJC15
siJC19
whole cell
Proteinase K
mitochondria
mass spectrometric analysis
relative intensity
m/z
b
whole cell
mito - PK
mito + PK
9.07e-37
2.49e-19
0.0163
Log2 SILAC ratio
siJC15 - WT
siJC19 - WT
c
Log2 SILAC ratio
siJC19 vs. WT scr
< 0
> 0
mito + PK
mito
whole cell
siJC15 vs. WT scr
Number of proteins [FDR < 0.05]
d
Complete
Log2FC < 0
FDR < 0.05
Identified proteins
OMM
IMS
IMM
matrix
MTS
e
mitochondrion
extracellular exosome
mitochondrial translation
tRNA aminoacylation for protein translation
mitochondrial pyruvate dehydrogenase complex
positive regulation of mitochondrial translation
ribonucleoprotein granule
aminoacyl-tRNA editing activity
-Log10 p-value (Fisher)
Enrichment
f
Matrix
mtRNA granules
mitochondrial ribosome assembly
-Log10 p-value (Fisher)
Enrichment
h
N=689
53
8.13e-04
Half-life [h]
MitoCop
Log2FC< -0.58
i
Log2FC< -0.58
Complete
Density
Ln half-life [h]
g
changed proteins
JC15-dependently
FDR < 0.05
Log2FC < 0
siJC15 - WT
159
73
100
interactors
FDR < 0.05
JC15-/- + JC15 - JC15-/-

Figure 11. Mitochondrial import defects after depletion of DNAJC15. a, Wild-type (WT) HeLa cells were labelled with different radioisotopes using stable isotope labelling with amino acids in cell culture (SILAC) for a minimum of five splits, to adapt cellular pools of stable isotope labeled lysine and arginine. Differently labelled cells were depleted of DNAJC19 (JC19) and DNAJC15 (JC15) for 48 h and an equal number of cells corresponding to the three different conditions were pooled prior to subcellular fractionation, to minimize experimental variation. Samples were analysed by LC-MS/MS (n = 5, biologically independent samples). **b**, Boxplot visualizing the distribution of mitochondrial proteins (MitoCarta 3.0) in the whole cell and in the mitochondrial fractions, which were treated with Proteinase K (PK) when indicated. Mann-Whitney U-test was performed. Quantile box plot show median, 25th and 75th percentiles were adapted to 0.5x fold (n = 5, biologically independent samples). **c**, Mitochondrial proteins (MitoCarta 3.0) significantly affected in the different fractions (FDR < 0.05) after depletion of DNAJC19 (siJC19, upper panel) and DNAJC15 (siJC15; lower panel), separated according to their SILAC ratio compared to WT (SILAC ratio > 0 for upregulation and SILAC ratio < 0 for downregulation). **d**, Fraction of significantly changed mitochondrial proteins (FDR < 0.05) within all identified proteins of various mitochondrial subcompartments and among proteins harboring a mitochondrial targeting sequence (MTS). **e**, Gene ontology enrichment analysis of all significant protein groups in the mitochondrial, Proteinase K-treated fraction after DNAJC15 depletion relative to WT (FDR < 0.02). **f**, Mitochondrial pathways enrichment analysis (MitoCarta 3.0) of significantly changed mitochondrial proteins after DNAJC15 depletion relative to WT (FDR < 0.02). **g**, Venn-diagram visualizing the overlap of significantly changed mitochondrial proteins after DNAJC15 depletion in HeLa cells (mitochondrial fraction treated with Proteinase K; Fig. 11d, n = 5, biologically independent samples) and DNAJC15 interactors (Fig. 10c) (FDR < 0.05, n = 4, biologically independent samples). **h**, Boxplot visualizing the half-life distribution of the mostly affected proteins ($log_2FC < -0.58$) compared to MitoCoP-annotated proteins. Mann-Whitney U-test was performed (n = 5, biologically independent samples). Half-life was extracted from Morgenstern *et al.* [76]. **i**, Density plot visualizing the Ln half-life distribution of the mostly affected proteins ($log_2FC < -0.58$) (n = 5, biologically independent samples). Half-life was extracted from Morgenstern *et al.* [76].

4.3.5 DNAJC15 cooperates with TIMM17A in protein import

Previous biochemical experiments suggested the existence of distinct TIM23 complexes in the IM containing either TIMM17A or TIMM17B [213]. We therefore depleted TIMM17A or TIMM17B from WT and *DNAJC15*$^{-/-}$ HeLa cells and analysed the mitochondrial proteome by LC-MS/MS (Fig. 12a). 204 and 50 mitochondrial proteins were significantly reduced after depletion of TIMM17A and TIMM17B, respectively (Fig. 12b). Notably, depletion of TIMM17A in *DNAJC15*$^{-/-}$ cells decreased the steady-state levels of an additional 135 mitochondrial proteins, many of them linked to the assembly of OXPHOS complexes and mitochondrial ribosomes, leading to a significant shift in mitochondrial mass (Fig. 12b; Extended

Data Fig. 3e-h). TIMM17B depletion in *DNAJC15*$^{-/-}$ cells reduced the steady-state levels of further 73 proteins (Fig. 12b; Extended Data Fig. 3e-h). A two-way ANOVA of the data set identified 42 mitochondrial proteins with significantly changed steady-state levels and revealed a significant downregulation of many mitochondrial ribosome and OXPHOS-related proteins only in cells lacking both TIMM17A and DNAJC15 but not in cells lacking TIMM17B and DNAJC15 (Fig. 12c; Extended Data Fig. 3f). These experiments are consistent with the genetic interaction of DNAJC15 with TIMM17A but not TIMM17B and suggest that DNAJC15 cooperates with TIMM17A-containing complexes in the mitochondrial import of OXPHOS-related proteins into the matrix and IM.

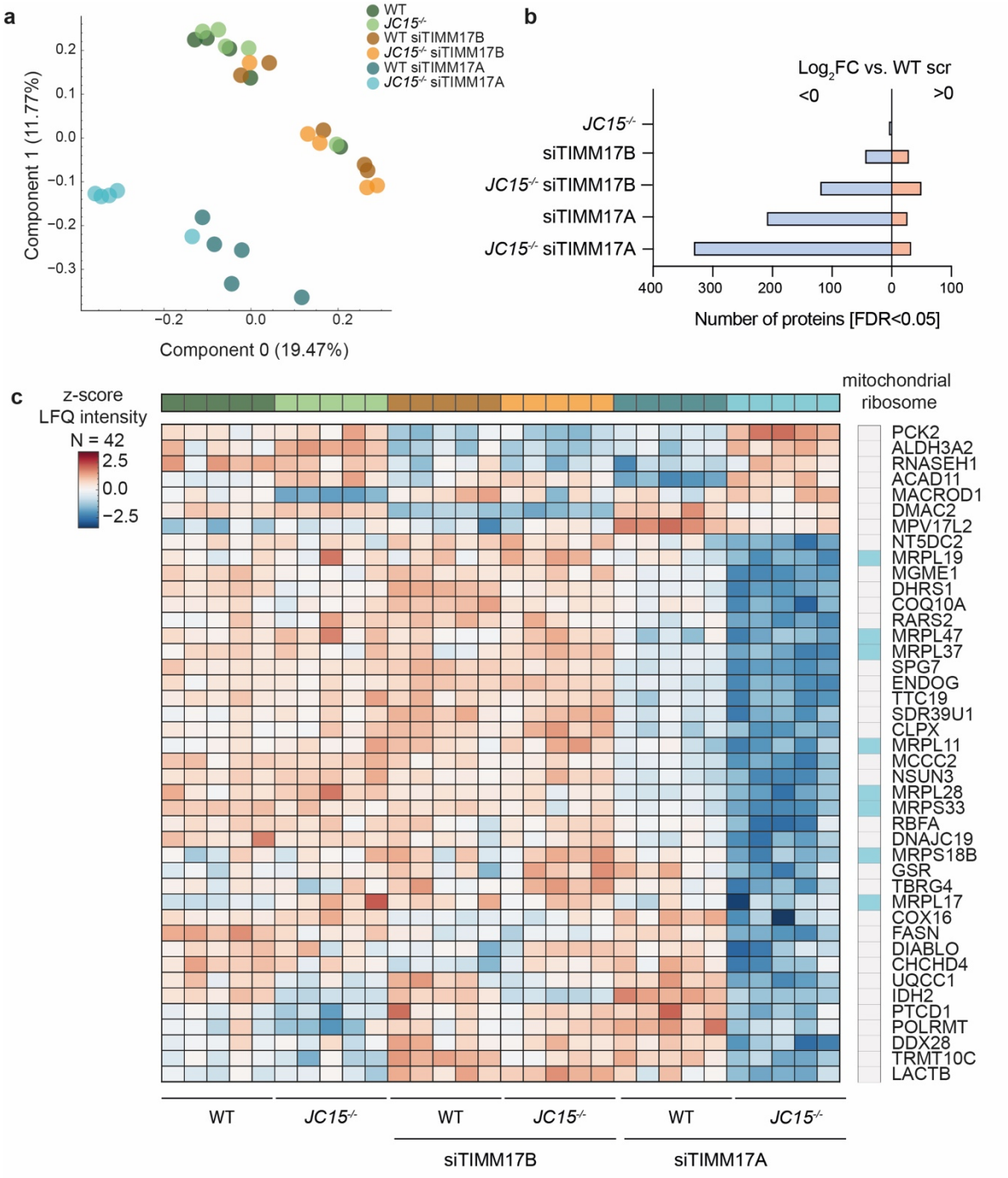

Figure 12. Cooperation of DNAJC15 with TIMM17A for the mitochondrial import of OXPHOS-related proteins. a, Principal component analysis (PCA) of cellular proteomes of wild-type (WT) and *DNAJC15*$^{-/-}$ HeLa cells after siRNA-mediated depletion of TIMM17A and TIMM17B for 72 h. (n = 5, biologically independent samples). **b**, Mitochondrial proteins significantly affected by the different treatments (FDR < 0.05), separated in up-, (log2FC > 0) and downregulated (log2FC < 0) proteins. **c**, Heat-map of the two-way ANOVA significant protein groups (-$\log_{10}$ *P* value > 2.9). Proteins corresponding to the significantly enriched gene ontology term 'mitochondrial ribosome' are highlighted. Dataset was filtered for minimum required values of more than 3 (n = 5, biologically independent samples).

4.3.6 DNAJC15 preserves mitochondrial OXPHOS activity

Given the profound effect of DNAJC15 on the steady-state levels of numerous proteins involved in mitochondrial gene expression and OXPHOS biogenesis, we determined cellular oxygen consumption rates in isolated mitochondria depleted of DNAJC15. Consistent with previous findings [213], loss of DNAJC15 significantly impaired complex I activity for both phosphorylation-coupled und uncoupled states (Fig. 13a). Similarly, we observed moderately reduced complex II activity in DNAJC15-depleted mitochondria (Fig. 13b). It should be noted that the activities of respiratory complexes were not affected in the absence of DNAJC15 at the cellular level (Fig. 13c, Extended Data Fig. 2b), probably due to the moderately increased mitochondrial mass in the cells indicated by our proteomic analysis (Fig. 13c). We conclude from these experiments that DNAJC15 mediates the import of many matrix and IM proteins, whose function is linked to mitochondrial gene expression and OXPHOS biogenesis.

The binding of DNAJC15 to OXPHOS-related proteins is consistent with a role of DNAJC15 for their import and rationalizes the impaired mitochondrial respiration after depleting DNAJC15 (Fig. 10d). However, this interaction analysis does not distinguish between binding partners of DNAJC15 and an association of DNAJC15 with newly imported polypeptides during or after completion of translocation. Indeed, the yeast DNAJC15 homolog Pam18 has dual functions in protein translocation and assembly of respiratory chain complexes [211]. As the amino-terminal region of DNAJC15 that is cleaved by OMA1 is required for the association of the chaperone with TIM23 complexes [213], we investigated how OMA1 cleavage affects the interactome of DNAJC15. However, the rapid turnover of S-DNAJC15 during chemical crosslinking precluded the direct identification of S-DNAJC15 interacting proteins (Extended Data Fig. 3i, j). We therefore compared the DNAJC15 interactome in *DNAJC15*$^{-/-}$ cells expressing DNAJC15 or non-cleavable DNAJC15Δ2. We identified 96 mitochondrial proteins as interacting partners of DNAJC15Δ2, all of which were also found in association with DNAJC15. Interacting proteins that did not depend on OMA1 cleavage, included the majority of TIM subunits, such as PAM16, TIMM44, TIMM23 and TIMM50, supporting an import function of L-DNAJC15 (Fig. 13e). Additional 83 proteins were detected exclusively in association with cleavable DNAJC15 (Fig. 13d). A direct comparison of the

interactomes of DNAJC15 and DNAJC15Δ2 revealed that binding of coenzyme Q biosynthetic enzymes was most strongly affected and significantly reduced if OMA1 cleavage is impaired (Fig. 13f), suggesting that these proteins bind preferentially to S-DNAJC15.

These results show that OMA1 cleavage alters the interactome of DNAJC15. Whereas L-DNAJC15 supports protein translocation by TIM23 complexes, S-DNAJC15 appears to preferentially bind proteins involved in coenzyme Q synthesis, which is crucial for OXPHOS biogenesis. This finding is reminiscent of the dual function of the yeast homolog Pam18 in protein translocation and assembly of respiratory chain complexes [211].

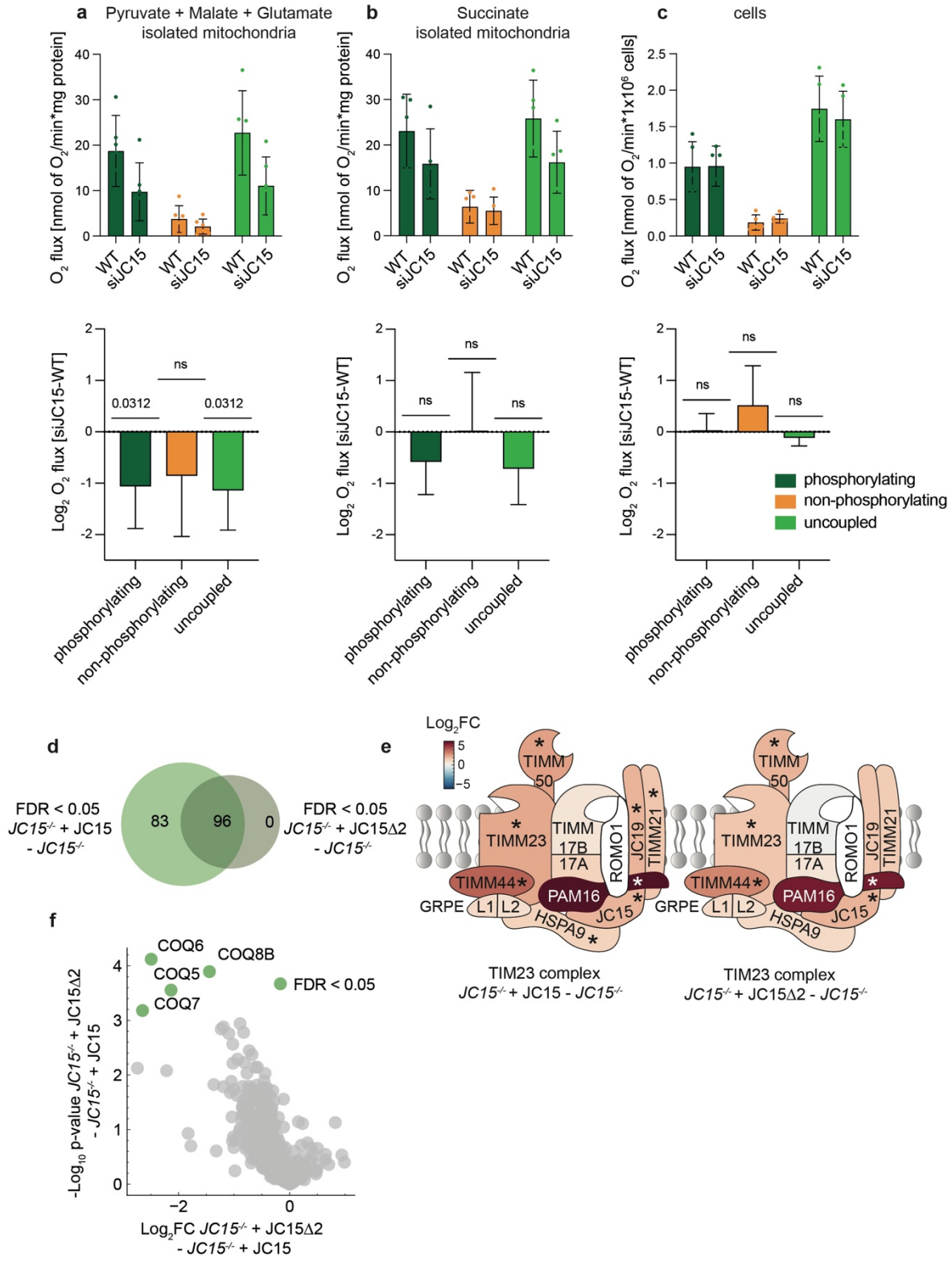
a
Pyruvate + Malate + Glutamate
isolated mitochondria
b
Succinate
isolated mitochondria
c
cells
O2 flux [nmol of O2/min*mg protein]
O2 flux [nmol of O2/min*1x10^6 cells]
WT
siJC15
Log2 O2 flux [siJC15-WT]
0.0312
ns
phosphorylating
non-phosphorylating
uncoupled
d
FDR < 0.05
JC15-/- + JC15
- JC15-/-
83
96
0
FDR < 0.05
JC15-/- + JC15Δ2
- JC15-/-
e
Log2FC
5
0
−5
TIMM 50
TIMM23
TIMM 17B
17A
ROMO1
JC19
TIMM21
TIMM44
PAM16
GRPE
L1
L2
HSPA9
JC15
TIM23 complex
JC15-/- + JC15 - JC15-/-
TIM23 complex
JC15-/- + JC15Δ2 - JC15-/-
f
COQ6
COQ8B
COQ5
COQ7
FDR < 0.05
-Log10 p-value JC15-/- + JC15Δ2
- JC15-/- + JC15
Log2FC JC15-/- + JC15Δ2
- JC15-/- + JC15

Figure 13. Impaired mitochondrial import after loss of DNAJC15 limits OXPHOS activity. Oxygen flux was measured in intact mitochondria isolated from DNAJC15-depleted HeLa cells and wild-type (WT) cells (a, b) or in cells (c) using an Oroboros respirometer. **a**, Oxygen flux in the presence of mitochondrial complex I substrates (pyruvate 10 mM, glutamate 5 mM, malate 5 mM) under phosphorylating conditions (ADP+P_i), non-phosphorylating conditions (oligomycin, 10 µM), and after uncoupling with CCCP. Statistical significance in the log_2 fold-changes in the oxygen flux between DNAJC15-depleted cells and WT cells (lower panel) was assessed using the Wilcoxon t-test. Data are means +/- SD (n = 5, biologically independent samples). **b**, Oxygen flux in the presence of mitochondrial complex II substrate (succinate 10 mM) and rotenone (140 nM) under phosphorylating and non-phosphorylating conditions and after uncoupling as in (a) (n = 4, biologically independent samples). Data are means +/- SD (n = 4, biologically independent samples). **c**, Oxygen flux in cells under phosphorylating and non-phosphorylating conditions and after uncoupling and statistical evaluation as in (a). Data are means +/- SD (n = 4, biologically independent samples). **d**, Venn diagram visualizing the overlap of the significantly identified interactors of DNAJC15 and DNAJC15Δ2 (FDR < 0.05). **e**, Schematic visualization of the TIM23 complex subunits interacting with DNAJC15. The red scale indicates fold-enrichment between *DNAJC15*$^{-/-}$ cells expressing DNAJC15 or DNAJC15Δ2 relative to *DNAJC15*$^{-/-}$ cells (log_2FC). The asterisk indicates all significantly affected proteins (FDR < 0.05, n = 4, biologically independent samples). **f**, Volcano plot showing the mitochondrial proteins losing interaction with DNAJC15 after mutating of the OMA1-cleavage site (according to MitoCarta 3.0). Four significantly mitochondrial interactors are highlighted in green (FDR < 0.05; n = 4, biologically independent samples).

4.3.7 Mitochondrial proteins mislocalised to the ER upon loss of DNAJC15 trigger an ATF6-related stress response

Since the loss of DNAJC15 reduced the steady-state levels of many mitochondrial proteins within the organelle but not at the cellular level, we performed further cell fractionation experiments to determine the localization of the non-imported mitochondrial proteins (Fig. 14a). After SILAC labelling and downregulation of DNAJC15 and DNAJC19, we isolated mitochondria by low-speed centrifugation (8,000xg; fraction A; Fig. 4a) and further fractionated the supernatant by differential centrifugation, to enrich the endoplasmic reticulum (ER) and plasma membrane (40,000xg; fraction B) or other vesicular structures (100,000xg; fraction C). The remaining supernatant was designated as the cytosolic fraction (fraction D) (Fig. 14a). LC-MS/MS analysis of the cell fractions confirmed the enrichment of different organellar structures in the different fractions (Extended Data Fig. 4a-c) and showed an accumulation of 130 mitochondrial proteins in the fraction B containing the ER membrane only after depletion of DNAJC15 (Fig. 14b, c;

Extended Data Fig. 4d). IM proteins and matrix proteins, which are imported along the TIM23^{motor} pathway [350], were enriched among proteins accumulating in fraction B (Extended Data Fig. 4e-g). 53 mitochondrial proteins that accumulated in fraction B were also significantly downregulated in fraction A. This is consistent with the observed protein import deficiency in the absence of DNAJC15. In contrast, we did not observe reduced steady-state levels of mitochondrial proteins in fraction A or accumulation of mitochondrial proteins in fraction B after depletion of DNAJC19 (Fig. 14d). Thus, these experiments suggest that non-imported mitochondrial preproteins accumulate at the ER specifically in cells lacking DNAJC15.

The accumulation of misfolded proteins and disturbances in ER proteostasis trigger ER stress responses [351, 352]. Therefore, we performed RNA sequencing under DNAJC15-depleted conditions and used a gene set profiling approach, which was developed to identify the activation of stress-responsive signaling pathways [353, 354]. These pathways included the integrated stress response (ISR), heat shock response (HSR), oxidative stress response (OSR), and the different branches of the ER unfolded protein response (UPR) mediated by IRE1 or ATF6 (Fig. 14e).

Loss of DNAJC15 did not induce an ISR, as indicated by the unaltered expression of the known target genes of the ISR or the ISR^{mt} (Fig. 14e; Extended Data Fig. 5a, b). OMA1, which can trigger the ISR^{mt} through DELE1 processing, was not activated in these cells nor was OPA1 processing increased (Extended Data Fig. 5c). However, DNAJC15 depleted cells exhibited the expected ISR upon oligomycin treatment, demonstrating that these cells are not refractory to ISR induction (Extended Data Fig. 5b). Similar to the ISR, the loss of DNAJC15 did not induce either the OSR or the HSF1-dependent HSR, which was observed after HSP90 inhibition and perturbation of mitochondrial proteostasis leading to UPR^{mt} [355]. In contrast, we observed activation of the ATF6-mediated UPR, as indicated by the increased expression of 11 downstream genes (Fig. 14f), whereas the IRE1/XBP1-mediated UPR was not induced (Fig. 14e).

We conclude from these experiments that the loss of DNAJC15 impairs mitochondrial protein import and leads to the accumulation of mitochondrial preproteins at the ER, disrupting ER proteostasis and triggering an ATF6-related UPR.

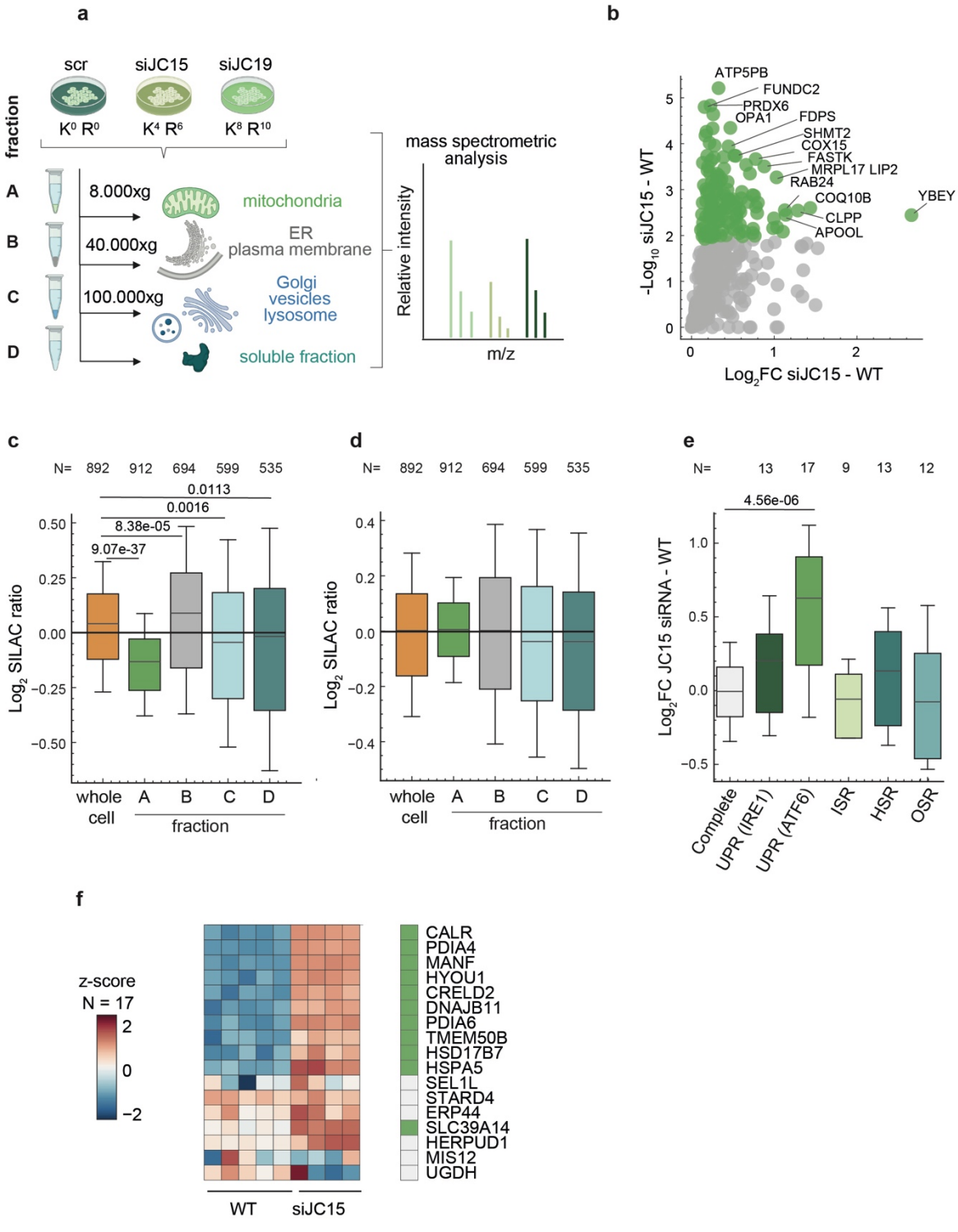
a
scr
siJC15
siJC19
K⁰ R⁰
K⁴ R⁶
K⁸ R¹⁰
fraction
A
B
C
D
8.000xg
40.000xg
100.000xg
mitochondria
ER
plasma membrane
Golgi
vesicles
lysosome
soluble fraction
mass spectrometric analysis
Relative intensity
m/z
b
ATP5PB
FUNDC2
PRDX6
OPA1
FDPS
SHMT2
COX15
FASTK
MRPL17 LIP2
RAB24
COQ10B
YBEY
CLPP
APOOL
-Log10 siJC15 - WT
Log2FC siJC15 - WT
c
N= 892 912 694 599 535
0.0113
0.0016
8.38e-05
9.07e-37
Log2 SILAC ratio
whole cell
A
B
C
D
fraction
d
N= 892 912 694 599 535
Log2 SILAC ratio
whole cell
A
B
C
D
fraction
e
N= 13 17 9 13 12
4.56e-06
Log2FC JC15 siRNA - WT
Complete
UPR (IRE1)
UPR (ATF6)
ISR
HSR
OSR
f
z-score
N = 17
2
0
−2
CALR
PDIA4
MANF
HYOU1
CRELD2
DNAJB11
PDIA6
TMEM50B
HSD17B7
HSPA5
SEL1L
STARD4
ERP44
SLC39A14
HERPUD1
MIS12
UGDH
WT
siJC15

Figure 14. Non-imported mitochondrial proteins after DNAJC15 loss induce an UPR at the ER. **a**, Subcellular fractionation of SILAC-labelled cells depleted of DNAJC15 and DNAJC19 (s. Fig. 4a) by differential centrifugation, followed by LC-MS/MS analysis. (n = 5, biologically independent samples). **b**, Volcano plot of mitochondrial proteins accumulating in the 40,000xg fraction (significant proteins, FDR < 0.05, are labelled in green) (n = 5, biologically independent samples). The 130 most significantly proteins are labelled in green. **c**, Boxplot visualizing the distribution mitochondrial proteins (MitoCarta 3.0) in the different cellular fractions as a SILAC ratio (log_2) between DNAJC15-depleted and wild-type (WT) cells (n = 5, biologically independent samples). Mann-Whitney U-test was performed. Quantile box plot show median, 25th and 75th percentiles are adapted to 0.5x fold (n = 5, biologically independent samples). N indicates the number of proteins identified in each fraction. **d**, Boxplot visualizing the distribution of mitochondrial proteins (MitoCarta 3.0) in all different fractions as in (c) after DNAJC19 depletion (n = 5, biologically independent samples). N indicates the number of proteins identified in each fraction. **e**, Gene expression analysis of WT HeLa cells and HeLa cells depleted of siDNAJC15 for 48 h by RNA sequencing. Box plot visualizing different transcriptionally-regulated stress responses according to gene sets regulated downstream of the following signaling pathways [354]: the unfolded protein response (UPR) depending on IRE1 or ATF6; the integrated stress response (ISR); the heat shock response (HSR) and the oxidative stress response (OSR). Mann-Whitney U-test was performed. Quantile box plot show median, 25th and 75th percentiles (n = 5, biologically independent samples). **f**, Heat-map of ATF6-related UPR targets [354] whose expression in DNAJC15-depleted relative to WT cells (log_2FC) is shown. Genes whose expression was significantly changed after DNAJC15 depletion (*P* value < 0.05) are shown in green.

4.4 Discussion

We identify DNAJC15 turnover as a functional component of the OMA1-mediated mitochondrial stress response, operating across multiple regulatory tiers, including modulation of mitochondrial dynamics and engagement of cytosolic signaling pathways such as the ISR. Under conditions of mitochondrial dysfunction, OMA1-mediated cleavage of DNAJC15 at its N-terminus facilitates its subsequent degradation by the m-AAA protease complex. This proteolytic cascade attenuates the import of nuclear-encoded proteins involved in OXPHOS biogenesis, thereby reducing the mitochondrial burden during stress. We propose that this regulatory mechanism serves to transiently suppress OXPHOS assembly, enabling the cell to conserve resources and maintain proteostasis until mitochondrial function is recovered or irreversibly damaged organelles are eliminated via mitophagy [356].

DNAJC15, together with its paralogue DNAJC19, supports mitochondrial protein import through TIM23 complexes as part of the import motor at the matrix side of the IM [213]. Consistently, we identified PAM16 (MAGMAS), DNAJC19, HSPA9, TIMM23, TIMM44 and TIMM21 in the vicinity of DNAJC15. DNAJC15 binding to TIM23 complexes did not depend on OMA1 cleavage, identifying L-DNAJC15 as the import competent form. PAM16 recruits DNAJC15 (and DNAJC19) to TIM23 complexes and ensures HSPA9-dependent protein import [213-215]. DNAJC15 and DNAJC19 interact genetically, suggesting at least partially redundant functions. However, in contrast to DNAJC19, loss of DNAJC15 broadly affects protein biogenesis and impairs the import of proteins with OXPHOS-related functions. Depletion of TIMM17A but not of TIMM17B aggravates this effect and further reduces the import of OXPHOS-related proteins into DNAJC15-deficient mitochondria, suggesting that DNAJC15 cooperates with TIMM17A in protein import. Indeed, previous biochemical experiments have identified different protein translocases harboring TIMM17A and TIMM17B that cooperate with DNAJC15 and DNAJC19 [213]. Notably, in contrast to their paralogues, TIMM17A and DNAJC15 are unstable proteins [76, 219]. Our results suggest that the proteolytic removal of this protein translocase as part of the OMA1-mediated stress response allows modulation to the mitochondrial import specificity to cope with unfavourable stress conditions [357].

The regulation of DNAJC15 by proteolysis highlights the importance of the relative steady-state levels of components of the translocation machinery for protein import. Consistently, overexpression of PAM16, as observed in cancer, has been shown to affect the recruitment of DNAJC15 and DNAJC19 to the respective protein translocases [214]. It is therefore conceivable that different relative expression levels of translocase subunits in different cells may explain the apparently discrepant effects of DNAJC15 depletion on OXPHOS activities in immune cells [216, 358-360] (Extended Data Fig. 6).

How does DNAJC15 specifically affect the biogenesis of OXPHOS-related proteins and OXPHOS biogenesis? While TIMM17A- and TIMM17B-containing translocases may exhibit different substrate specificities, we noted overall shorter half-lives of mitochondrial proteins that accumulated in mitochondria in a DNAJC15-dependent manner. It is therefore conceivable that a generally reduced import capacity after DNAJC15 degradation and rapid proteolysis of already imported mitochondrial proteins contribute to the observed changes in the mitochondrial proteome.

Loss of DNAJC15 does not inhibit protein import into mitochondria or completely block translocation by precursor stalling, but leads to accumulation of mitochondrial preproteins at the ER. Disruption of ER proteostasis in the absence of DNAJC15 triggers an ATF6-related UPR, demonstrating coupling of mitochondrial and ER proteostasis. Similarly, perturbations in the mitochondrial lipid transport can alter the lipid composition in the ER and trigger a UPR [361]. The accumulation of mitochondrial preproteins at the ER is reminiscent of studies in yeast suggesting that some mitochondrial preproteins encounter the ER membrane on their way to the mitochondria [264, 265]. Accordingly, the accumulation of mitochondrial preproteins at the ER upon loss of DNAJC15 during mitochondrial stress would allow a rapid recovery of mitochondrial import upon relief of the stress. While it remains to be established whether ER-associated preproteins remain competent for mitochondrial import, our findings reveal a close link in organellar proteostasis regulation and an integrated cellular stress response to mitochondrial dysfunction.

5. Discussion

The mitochondrial stress protease OMA1 limits mitochondrial fusion by processing OPA1 and activates cytosolic stress signaling through DELE1 cleavage in response to mitochondrial dysfunction [41, 56-59]. Here, the functional repertoire of OMA1 was extended to the regulation of mitochondrial protein import. OMA1 activation restricts the import of newly synthesized proteins, affecting specifically the biogenesis of OXPHOS complexes under stress. This effect is mediated by the selective proteolytic processing of DNAJC15 by OMA1, which facilitates its subsequent degradation by AFG3L2. Although the cleaved form of DNAJC15 is rapidly degraded, our findings suggest that it retains a transient, but functionally relevant role in coenzyme Q metabolism. This is reminiscent of the dual functionality for its yeast homolog Pam18 in OXPHOS assembly and mitochondrial protein import regulation [211]. Furthermore, we showed that depletion of TIMM17A, but not TIMM17B, further exacerbates this effect, suggesting a functional cooperation of DNAJC15 and TIMM17A in regulating mitochondrial protein import. Although DNAJC15 and its paralog DNAJC19 have partially overlapping functions, only DNAJC15 exerts a broad impact on mitochondrial protein import. Our data suggest that under stress conditions, mitochondria actively limit mitochondrial import capacity to reshape their proteome. Non-imported mitochondrial proteins are enriched for factors with short apparent half-lives and for components involved in OXPHOS biogenesis. This enables a rapid and flexible response to environmental challenges beyond transcriptional control. We propose that this adaptation persists until mitochondrial homeostasis is restored, or alternatively, until dysfunctional organelles are removed via mitophagy.

Impaired mitochondrial protein import, caused by DNAJC15 loss, results in the accumulation of mitochondrial precursor proteins at the ER, triggering an ATF6-regulated UPR. We propose that the ER may serve as a transient buffering compartment for non-imported mitochondrial proteins, facilitating cellular adaptation during mitochondrial stress. Similar buffering mechanisms for non-imported mitochondrial proteins have been described in yeast, including MitoStores [240], which are cytosolic accumulations of mitochondrial proteins, as well as the use of the ER as a transient storage compartment [265]. Through unbiased proteome-wide screening and genetic interaction analysis of the mitochondrial co-chaperone,

DNAJC15, our study is the first to prove a mitochondrial protein relocalisation to the ER in mammalian cells. The mechanisms by which mitochondrial precursors are sequestered at the ER, as well as whether these non-imported precursors retain import competence to enable rapid recovery of OXPHOS function after stress, remain to be elucidated.

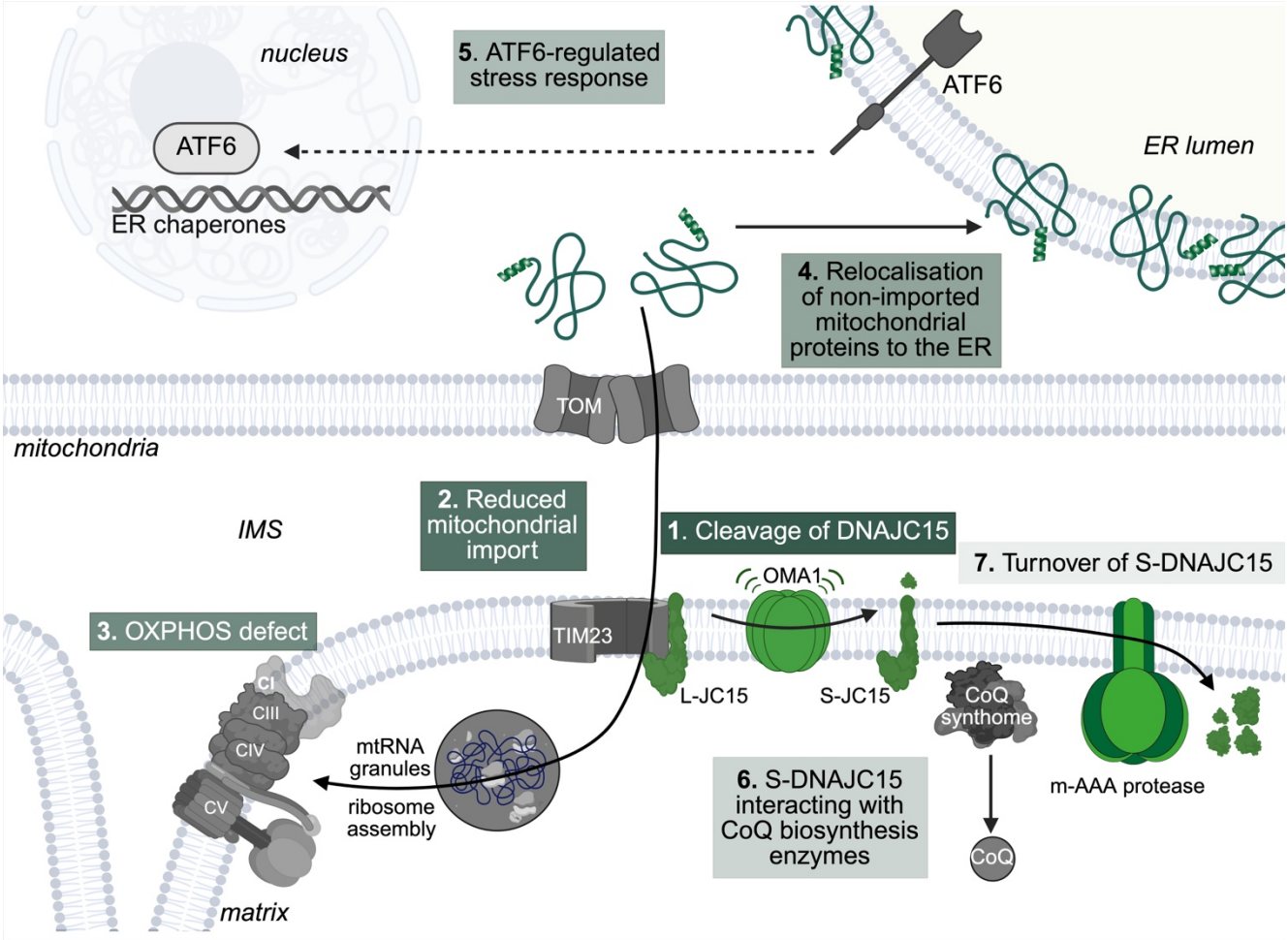

Figure 15. Schematic representation of the functions of DNAJC15 under stress conditions. Under physiological conditions, DNAJC15 functions as a component of the mitochondrial protein import machinery, promoting the import of proteins essential for OXPHOS biogenesis, including those involved in mtRNA granule formation and ribosome assembly. Upon mitochondrial stress, DNAJC15 is N-terminally cleaved by OMA1, resulting in its dissociation from the TIM23 translocase. This impairs the import of DNAJC15-dependent substrate proteins, leading to reduced mitochondrial respiration. Unimported mitochondrial precursor proteins accumulate at the ER and trigger an ATF6-mediated UPR. The cleaved, stress-induced form of DNAJC15 (S-DNAJC15) interacts with enzymes of the coenzyme Q biosynthesis pathway and is rapidly degraded by the m-AAA protease.

5.1 Regulation of the TIM23-dependent protein import by DNAJC15 proteolysis

Mitochondrial protein import is critical, as >99% of the mitochondrial proteins are nuclear-encoded and must be translocated across both mitochondrial membranes to reach their site of function. Dynamic modulation of the import machinery therefore enables mitochondria to adapt their proteome in response to metabolic and cellular stress. Consistent with this, mitochondrial protein import is recognized as a central and initial signaling hub that integrates stress signals to coordinate adaptive responses [242, 362, 363]. The TIM23 complex is regulated by several mitochondrial proteases, including the stress-responsive peptidase OMA1 and the AAA proteases, which expose their catalytic domains to either the IMS or the matrix [219, 222, 224].

OMA1 plays a central role in coordinating mitochondrial dynamics and the stress response under conditions of mitochondrial dysfunction [34, 36, 37, 44, 48, 56-58, 339, 340]. Stress conditions, such as the loss of MMP, oxidative stress, heat shock, or inhibition of respiratory chain complexes, activate OMA1 [33-36, 313]. Although the exact mechanism of activation remains unclear, it is thought to involve a sensing mechanism mediated by the N- and C-terminal extensions and redox-sensitive sites in OMA1 [36, 37]. Here, we extended the known functions of OMA1 and demonstrated that its activation induces the targeted cleavage of DNAJC15, promoting its degradation by the m-AAA protease and limiting mitochondrial protein import.

This distinct proteolysis profile is specific to DNAJC15 but not to its paralog, DNAJC19, despite the presence of conserved structural domains. The apparent half-lives of these proteins differ significantly; DNAJC15 exhibits a half-life of 15.7 h, while DNAJC19 demonstrates a substantially longer half-life of 164.9 h [76]. This disparity in protein stability may arise from subtle structural differences, particularly within the un-conserved extended N-terminal region or the linker region, connecting the transmembrane segment to the J-domain. An alternative explanation is that differences in their interactomes may contribute to the distinct stability of these proteins (s. chapter 5.2.4).

To dissect the structural determinants underlying functional differences between DNAJC15 and DNAJC19, we generated chimeric constructs by swapping their N-

terminal regions (Extended Data Fig. 7). Substitution of the N-terminus of DNAJC15 with that of DNAJC19 did not alter the kinetics of the AFG3L2-dependent DNAJC15 decay. Therefore, we propose that the adjacent unstructured linker region serves as the primary target for m-AAA protease-mediated degradation of DNAJC15. This unconserved structural feature may contribute to the reduced stability of DNAJC15, as unstructured domains are known to facilitate protease recognition and initiation of degradation [364, 365]. Studies on the substrate specificity of AFG3L2, based on the proteolysis of MRPL32 and SLC25A39, have shown that substrate accessibility can be limited by binding motifs that sterically hinder AFG3L2 degradation [29, 366]. A conserved CX_2C-X_9-CX_2C motif in MRPL32 with presumed metal-binding capacity prevents degradation by forming tight bonds [367]. In SLC25A39, a similar mechanism involving conformational changes has been proposed. High iron availability induces iron-sulfur cluster binding involving four matrix-localised cysteines in Loop1, which blocks AFG3L2-mediated degradation [28]. The sequence of SLC25A39 is composed of a CX_3C-X_9-CX_5C motif. Although no analogous mechanism or structural features have been identified for DNAJC15, conformational changes in its linker region may facilitate AFG3L2 recognition and subsequent degradation.

Additionally, we sought to investigate the underlying stability differences between L-DNAJC15 and S-DNAJC15. AAA proteases are known to generate mechanical pulling forces through ATP hydrolysis alleviating the dislocation of substrates from the membrane bilayer [30, 367]. Since the region of DNAJC15 cleaved by OMA1 represents the minimal domain required for interaction with TIMM17A [213], cleavage might promote the dissociation of DNAJC15 from the TIM23 complex. It is therefore plausible that dissociation from the TIM23 complex enhances sterical access of the substrate for the protease [364, 365, 368]. An alternative explanation for the different apparent half-lives of DNAJC15 isoforms is that cleavage of the N-terminal domain may alter the overall charge properties or membrane integration of the protein. OMA1-mediated cleavage of the N-terminal 19 AA of DNAJC15 increases the hydrophilicity of S-DNAJC15 without affecting its net charge, likely reducing its membrane retention. This change in biochemical properties may facilitate AFG3L2-mediated extraction and degradation [368].

Taken together, these findings support the concept that proteolytic surveillance of the mitochondrial import machinery constitutes a key regulatory node in

mitochondrial biogenesis. OMA1 emerges as a central regulator that triggers DNAJC15 turnover through targeted cleavage, enabling AFG3L2-mediated degradation. Structural or biochemical features likely account for the distinct half-lives of L-DNAJC15 and S-DNAJC15, and may also explain the stability difference between DNAJC15 and its long-lived paralog DNAJC19.

5.2 The function of human TIM23 paralogs in mitochondrial protein import

The TIM23 translocase includes several human paralogs with high structural similarity. The functional roles and evolutionary divergence of these subunits remain incompletely understood. This study focuses on TIMM17A, TIMM17B, DNAJC15, and DNAJC19 to define their specific contributions to mitochondrial protein import. We assessed the impact of their depletion on import efficiency and examined how functional differences correlate with their distinct interactome and expression profiles across cell types.

5.2.1 Comparative analysis of TIM23 paralogs in mitochondrial protein import

To elucidate the functional significance of the human paralogs in regulating mitochondrial import, we employed a whole cell proteomics, as well as an unbiased SILAC-based mitochondrial proteomics approach. Targeted depletion of DNAJC15, DNAJC19, TIMM17A, and TIMM17B allowed us to characterize the impact of their loss on the mitochondrial proteome.

We showed that acute depletion of DNAJC15 broadly impaired mitochondrial protein import, an effect not observed upon acute depletion of DNAJC19. These findings suggest that DNAJC15 may serve as the primary import-associated co-chaperone under the conditions tested. This is further supported by data demonstrating that DNAJC15 exhibits a stronger ATPase-stimulating activity compared to DNAJC19 [215], consistent with its ability to rescue the lethal phenotype associated with *Pam18* deletion in yeast, a function that DNAJC19 is unable to perform [207]. However, it is important to note that the effects observed upon acute depletion of

DNAJC15 are not recapitulated in chronic knockout models, suggesting the presence of compensatory mechanisms. Such discrepancies between acute and chronic loss-of-function approaches are well-documented in the field [369-373]. In our case, the genetic redundancy between DNAJC15 and its paralog DNAJC19 implies that DNAJC19 sustains import homeostasis under those conditions, despite unaltered steady-state expression levels of DNAJC19. Previous studies support this hypothesis, showing that in the absence of one J-domain protein, the other can functionally compensate by binding to its non-preferred TIMM17 subunit in the mitochondrial import machinery [213].

Acute depletion of TIMM17A, but not TIMM17B, resulted in a marked downregulation of the mitochondrial proteome on whole cell level, indicating distinct functional roles for these paralogs in mitochondrial protein import. The impact of TIMM17A depletion on import regulation was further exacerbated by the concurrent loss of DNAJC15. However, co-depletion of TIMM17B and DNAJC15 did not downregulate the mitochondrial proteome. These observations suggest that DNAJC15 and TIMM17A functionally cooperate, potentially as components of a transient, stress-responsive variant of the TIM23 complex. Alternatively, DNAJC15 and TIMM17A may act within distinct, functionally specialized translocase assemblies. The latter hypothesis is supported by our genetic interaction screen, which revealed that combined loss of both proteins severely compromises cell viability.

Consistent with a functional interdependence, acute depletion of DNAJC15 also downregulated TIMM17A levels in isolated mitochondria. These findings indicate that DNAJC15 and TIMM17A are coordinately regulated and critical for maintaining mitochondrial import capacity. Simultaneous disruption of these subunits synergistically amplifies import defects. The relatively short half-life of these proteins further supports a model in which selective turnover of specific import subunits enables dynamic adjustment of mitochondrial import in response to metabolic or environmental cues (s. chapter 5.2.2).

Together, our data challenge the prevailing view that import efficiency is predominantly determined by TIMM17B and DNAJC19 [213]. Instead, we highlight a regulatory role for stress-responsive subunits, such as TIMM17A and DNAJC15, whose dynamic abundance appears to support both basal and stress-adaptive

import functions. While prior studies have suggested a physical interaction between DNAJC15 and TIMM17A [213, 215], further work is needed to elucidate the structural and regulatory organization of the TIM23 complex, particularly under diverse stress conditions (s. chapter 5.2.4).

5.2.2 Proteolytic regulation of the TIM23 complex

Beyond their role in regulating DNAJC15 abundance, both proteases, OMA1 and AFG3L2, have been implicated in the broader control of mitochondrial protein import [63, 224, 374]. OMA1, in particular, resolves import blockages caused by clogged precursor proteins through targeted proteolytic cleavage, thereby safeguarding mitochondrial integrity both at basal and stressed conditions [318]. AFG3L2 contributes to import regulation by degrading additional components of the TIM23 complex, such as PAM16 and TIMM17A, both of which accumulate in a time-dependent manner in its absence [224]. The regulation of TIMM17A abundance is further modulated by YME1L, which mediates its targeted degradation to limit mitochondrial import in response to acute oxidative stress, hypoxia, or nutrient starvation [222, 375, 376]. This degradation of TIMM17A under stress conditions is known to activate the mitochondrial UPR, enhancing cellular resilience [222, 375]. This goes in line with YME1L further degrading TIMM23 under conditions where mitochondrial protein import is impaired by a human clogger, assuming a protective role of YME1L [223]. However, YME1L has been further linked to mitochondrial protein import by targeted degradation of ROMO1 [222]. This mitochondrial membrane protein contributes to membrane integrity by enhancing import efficiency. While dispensable for general import, ROMO1 shields the TIMM17-formed half-channel and recruits TIMM21 to the TIM23 complex, facilitating lateral sorting [185, 203-205].

The proteolytic degradation of mitochondrial import subunits aligns with recent studies investigating the mitochondrial proteome dynamics in human cell lines [377]. Morgenstern *et al.* proposed a model in which protein instability within complexes acts as a regulatory sensor, modulating mitochondrial biogenesis in response to cellular stress [377]. Within the mitochondrial protein import machinery, some subunits of the TIM23-PAM complex exist as isoforms with markedly different apparent degradation rates, proposing the presence of distinct protein complexes. Proteins,

such as TIMM17A, DNAJC15, and GRPEL2 are short-lived, while their paralogs, TIMM17B, DNAJC19, and GRPEL1, are more stable. This indicates a layered regulatory system in which short-lived isoforms by targeted proteolytic degradation support rapid functional adjustments, whereas long-lived counterparts are suggested to maintain baseline functionality [213, 377].

As mentioned, this disparity is also characteristic of the paralogs, TIMM17A and TIMM17B. They share significant structural similarities with each other and with the yeast Tim17 homolog, including conserved features, such as a negatively charged residues, hydrophobic lining of the lateral cavity, and a disulfide bridge. Both human homologs are proposed to form functional complexes with TIMM23, suggesting overlapping roles in mitochondrial protein translocation [378]. Although TIMM17A and TIMM17B have a high degree of sequence similarity and functional overlap, they are subject to distinct regulatory mechanisms. It is therefore plausible that the different proteolytic regulations of TIMM17A and TIMM17B arise from specific interactions with unique regulatory factors or binding partners. For example, OCIAD1 has been shown to selectively modulate TIMM17A without affecting TIMM17B, underscoring paralog-specific regulation [379]. Elucidating the structural organization and regulatory dynamics of mitochondrial translocase complexes will provide critical insight into the functional specialization of TIMM17A and TIMM17B, and the other known paralogs with distinct proteolytic regulations.

Taken together, these findings show that the TIM23 complex is tightly regulated by proteolytic mechanisms, enabling rapid adaptation to changing environmental conditions via post-translational modification. Defining the molecular determinants of TIM23 paralog-specific regulation is therefore essential to elucidate their distinct functional roles.

5.2.3 Expression profiles of human TIM23 subunits across cell lines

In our study, we observed that the expression of specific subunits of the TIM23 mitochondrial import machinery varies considerably across different human and mouse cell lines. Understanding how changes in the stoichiometry of import machinery components, particularly between different paralogs, shape

mitochondrial identity is essential to uncover mitochondrial plasticity in various tissues and cell types.

It is evident, that the short-lived proteins, such as TIMM17A and DNAJC15, are also considerably less abundant than their long-lived paralogs, TIMM17B and DNAJC19, in HeLa, HEK293T and MEF cells. This difference among the paralogs suggests potential specialization across tissues or cellular contexts. For example, in our model system, we observe a critical role for DNAJC15 in maintaining mitochondrial protein import, as its loss leads to broad import defects. However, this may not universally apply across all cell types. For instance, in HEK293T cells, DNAJC15 expression is undetectable, while DNAJC19 remains robustly expressed. Given that J-domain proteins are central regulators of mitochondrial protein import [214], our findings suggest that the dominant co-chaperone within the TIM23 translocase may vary depending on the cellular context. The genetic interaction and partially redundant functions of DNAJC15 and DNAJC19 support the notion that their relevance in mitochondrial protein import is determined by cell-type-specific regulatory programs. In humans, DNAJC19 is expressed universally, whereas DNAJC15 is enriched in metabolically active tissues, such as the heart and liver [380]. This suggests that DNAJC15 may enable rapid modulation of mitochondrial protein import in response to environmental or cellular stress in these high-demand tissues. However, the data on TIM subunit expression in tissues from mice or humans is quite limited, which makes it critical to better define their abundance across organs in the future. Core components of the TIM23 complex, including HSPA9, TIMM50, TIMM44, and TIMM23, were uniformly and robustly expressed across all tested cell types. This underscores their essential and constitutive role in maintaining mitochondrial import capacity under a wide range of physiological conditions [203-205].

The functional importance of TIM subunit composition becomes particularly evident in cancer. Published studies have shown that PAM16, a mitochondrial co-chaperone and substrate of AFG3L2 [224], is overexpressed in several malignancies, including prostate cancer, pituitary adenomas, and ovarian carcinomas [381-384]. PAM16 recruits J-domain proteins like DNAJC15 and DNAJC19 to the import machinery, modulating the activity of distinct translocase variants [385]. Overexpression of PAM16 might therefore be relevant to promote the recruitment of the co-chaperones to the TIM23 translocase differently. In this context, TIMM17A, is also upregulated in breast

cancer and correlates with poor clinical outcomes and tumor aggressiveness. Functional studies show that downregulation of TIMM17A reduces migration and invasion in breast cancer cells, pointing to a pro-oncogenic role for this isoform [386-388]. In the context of disease, particularly cancer, these findings underscore the importance of modulating the composition of mitochondrial import subunits. Such alterations may confer selective growth advantages or enhance cellular adaptability, further emphasizing the critical role of the relative expression levels of translocase components in regulating mitochondrial function and influencing cell fate decisions.

Taken together, our findings, in conjunction with existing literature, support a model in which the relative expression levels of TIM23 complex subunits functions as a dynamic modulator, fine-tuning mitochondrial protein translocation. The composition of TIM translocases appears to vary in a context- and cell-type-specific manner, highlighting the need for further investigation into its regulatory mechanisms and functional consequences.

5.2.4 Distinct interaction networks of the human J-domain paralogs

The human J-domain protein paralogs exhibit distinct proteolytic processing patterns and expression profiles, which are consistent with their divergent functional effects on mitochondrial protein import. However, they also share common features, particularly with respect to their interactomes.

It is important to recognize that DNAJC19 functions beyond its role in mitochondrial protein translocation. In particular, its binding to the PHB complex contributes to cardiolipin remodeling, and mutations in DNAJC19 are associated with dilated cardiomyopathy with ataxia [191, 389-391]. These observations support a dual role for DNAJC19 in coordinating both cardiolipin homeostasis and mitochondrial protein import. A similar functional duality may also be plausible for DNAJC15. This is supported not only by the interaction of PHB1, PHB2, and AFG3L2 to DNAJC15, but also by the high structural similarity between DNAJC15 and DNAJC19, particularly in their conserved J-domains. J-domains are known to preferentially engage in homo-, or heterodimers [214, 385, 392]. As DNAJC19 is also an interactor of DNAJC15, it is likely, that they form dimers and potentially act within the same regulatory networks, particularly in the context of the PHB-AFG3L2 complex.

This dimerization process is also critical for dual regulatory functions of the yeast homolog of DNAJC15 and DNAJC19, Pam18. Pam18 forms either a regulatory heterodimer with Pam16, thereby modulating mitochondrial protein import, or acts as a homodimer involved in OXPHOS assembly [211]. Given that PAM16, a J-like domain-containing protein, also emerged as one of the most prominent interactors of DNAJC15, it is likely that similar dimerization events occur constitutively in human cells and contribute to the dual functions of DNAJC15 (s. chapter 5.4). Notably, DNAJC15 interacts with multiple factors involved in mitochondrial biogenesis, including the interactors of the m-AAA protease, MAIP1 and TMBIM5, and other proteases, like the i-AAA protease YME1L, the CLPB chaperone, and scaffold proteins such as SLP2.

DNAJC15 cooperates with the TIM23 complex during protein import. Although no significant interaction has been detected between DNAJC15 and either TIMM17A or TIMM17B, DNAJC15 consistently co-purifies with components of the PAM complex. PAM16 and TIMM44 represent the most prominent interaction partners. Additional enriched proteins included key constituents of the TIM23 translocase, such as TIMM50, TIMM23, DNAJC19, and TIMM21. These interactions were detectable only in the presence of a chemical crosslinker and were observed at relatively low abundance, suggesting their association to be transiently regulated. The lack of evidence of a detectable interaction between DNAJC15 and either TIMM17A or TIMM17B underscores the importance of dissecting the structural organization and regulatory dynamics of mitochondrial translocase complexes, particularly in contexts where selective import subunits, like DNAJC15, are absent. However, such mechanistic insights would require extensive biochemical and structural analyses that fall beyond the scope of the current study.

In summary, DNAJC15 co-purifies robustly with components of the PAM complex, supporting its critical role in the regulation of mitochondrial protein import. Notably, several other mitochondrial biogenesis factors were also enriched, reflecting functional overlap with its paralog DNAJC19. While many of these interactions and functional implications require further investigation, it is important to emphasize that the potential dual functionality of DNAJC15 and DNAJC19 is likely context-dependent and may be shaped by their relative expression levels, localization, and complex assembly dynamics.

5.3 DNAJC15-dependent import of mitochondrial proteins involved in OXPHOS biogenesis

Unbiased mitochondrial import assays demonstrated that acute depletion of DNAJC15 constrains mitochondrial import capacity, with a preferential impact on short-lived proteins. Among the most affected proteins are factors involved in the assembly of OXPHOS complexes, such as COX18 (complex IV) and SDHAF4 (complex II), as well as proteins implicated in mitochondrial calcium handling (e.g. TMBIM5, MCU, TMEM65) and coenzyme Q biosynthesis (e.g. COQ10B). These proteins frequently serve as integral subunits of larger multi-protein complexes, where strict stoichiometric balance is required for proper assembly, stability, and function. In addition to this broad import restriction, a degree of specificity toward OXPHOS-associated proteins, specifically of proteins involved in mitochondrial ribosome assembly and mtRNA granule formation, was observed. However, the mechanistic basis for this selectivity remains unclear. Our analysis ruled out confounding effects related to MTS structure or length, overall protein length, or steady-state protein abundance. An alternative hypothesis for the selective import impairment on OXPHOS biogenesis factors is that these pathways might be enriched for short-lived proteins. However, since not all DNAJC15-dependent import substrates are short-lived, additional regulatory mechanisms likely contribute to the selective import defects observed upon DNAJC15 loss.

This selective import defect leads to impaired mitochondrial respiration in isolated mitochondria, with a significant reduction in complex I activity. This finding aligns with studies in human cancer cells, where loss of the import subunit DNAJC15 was also shown to reduce mitochondrial respiration downstream [213]. However, this respiratory defect is contradicting to previous studies, that have implicated DNAJC15 in the repression of respiratory chain supercomplex assembly, with its loss enhancing mitochondrial respiration and ATP production *in vivo*. This metabolic effect has been associated with beneficial outcomes, including improved energy metabolism and reduced inflammation, particularly in hepatic tissue and various immune cells [216, 358-360, 393]. However, its potential role in regulating mitochondrial protein import in these settings remains uncharacterized. Furthermore, mitochondrial respiration in these studies was evaluated exclusively at the cellular level. We, however, showed that the mitochondrial respiratory defect in DNAJC15-

depleted conditions is detectable only at the level of isolated mitochondria, while cellular respiration remains largely unaffected. This is due to the compensatory increase in mitochondrial mass, confirmed by our proteomic analysis, which sustains overall cellular energy production. Increased mitochondrial mass may obscure import-related deficiencies at the cellular level, underscoring the importance of mitochondrial-level assessments to reveal intrinsic functional impairments.

Our findings support a revised model for the role of DNAJC15 in mitochondrial homeostasis. We show that acute depletion of DNAJC15 causes a global mitochondrial translocation defect, with a pronounced impairment in the import of short-lived proteins. Notably, through a mechanism that remains to be elucidated, DNAJC15 exhibits substrate specificity by selectively reducing the import of proteins critical for OXPHOS biogenesis. This selective import defect results in a measurable respiratory impairment at the mitochondrial level. Notably, a similar effect has been linked to TIMM17A, the proposed interaction partner of DNAJC15 [213, 215], that is associated with impaired import of proteins essential for mitochondrial respiration [213, 394].

5.4 S-DNAJC15 is associated with the coenzyme Q biosynthesis complex

The OMA1-mediated cleavage of DNAJC15 introduces an additional regulatory layer to its function. Our data support a model in which proteolytic processing of OMA1 converts the full-length, translocase-associated form into a truncated and translocase-disassociated form. Different interaction profiles suggest potentially divergent functions of L- and S-DNAJC15. Notably, the N-terminal region of DNAJC15, the target of the OMA1-dependent cleavage, is required for its interaction with TIMM17A [213]. The cleavage presumably initiates a dissociation from the TIM23 complex suggesting that S-DNAJC15 may engage in alternative roles beyond mitochondrial protein import. Due to its rapid degradation by the m-AAA protease, direct interaction analysis of S-DNAJC15 was not feasible. However, proteomic analyses of the L-DNAJC15 reveal a distinct interactome compared to the non-cleavable DNAJC15 mutant. The data supports a model in which S-DNAJC15 is

associated with the coenzyme Q biosynthesis complex. We specifically demonstrated that the interactions of COQ5, COQ6, COQ7, and COQ8B are dependent on OMA1-mediated cleavage. These enzymes contribute to distinct steps in the biosynthesis of coenzyme Q, including C-methylation (COQ5) and ring hydroxylation (COQ6, COQ7) [395]. COQ8B, in particular, has been proposed to play a central role in stabilizing the CoQ complex, potentially through an ATPase or kinase-like function, although the precise mechanism remains unknown [396]. The CoQ complex, often referred to as the CoQ synthome [397], is believed to be organized through protein-protein interactions among the COQ3 to COQ9 proteins [398, 399]. Disruptions in CoQ biosynthetic enzymes can have profound consequences due to their association in OXPHOS biogenesis. For instance, COQ6 deficiency has been associated with nephrotic syndrome and sensorineural deficits, including hearing and vision impairments [400]. Many various factors, including lipids, CoQ intermediates, and accessory proteins, are known to associate with the complex [401]. Given the structural and functional complexity of this multi-subunit complex, it is plausible that S-DNAJC15 may also be a constituent, which would explain the ability of DNAJC15 to co-purify with several of its key components. Importantly, since S-DNAJC15 retains its functional J-domain, it is conceivable that it may exert an active, stimulatory role in coenzyme Q biosynthesis.

Therefore, OMA1 processing of DNAJC15 initiates the removal of DNAJC15 from the translocase complex and redirects DNAJC15 towards coenzyme Q biosynthesis. The exact function in this pathway remains an open question. However, this model supports a stress-responsive mechanism in which proteolytic processing enables a functional shift toward metabolic remodeling, underscoring the role of DNAJC15 in the regulation of the mitochondrial respiration [402, 403]. This model aligns with the dual functionality described for the yeast homolog Pam18, which shifts between import-related activity, when bound to Pam16, and respiratory complex assembly, when present as homodimer [404]. We propose a similar functional bifurcation for mammalian DNAJC15, in which OMA1-dependent cleavage serves as a molecular switch that decouples DNAJC15 from the TIM23 complex and repurposes it for coenzyme Q biosynthesis.

In this context, the fate and potential function of the IMS-localised 19-AA peptide, generated by OMA1 cleavage, remain unclear and warrant further investigation.

Similar cleavage fragments, for example the one from OPA1 have demonstrated distinct colocalization profiles with the mtDNA [405], indicating that the DNAJC15-derived peptide may also have a functional significance.

Collectively, our findings establish DNAJC15 as a dynamic regulator of OXPHOS biogenesis and mitochondrial protein import. Its activity is modulated by OMA1-dependent proteolytic cleavage in a stress-sensitive manner, allowing DNAJC15 to alternate between roles in import regulation and metabolic adaptation. Such functional versatility is critical for maintaining mitochondrial homeostasis during physiological conditions, cellular stress, disease progression, and ageing.

5.5 Cellular outcomes of mitochondrial import dysfunction

Mitochondrial protein import is necessary for sustaining both mitochondrial integrity and cellular homeostasis. However, it is also a highly vulnerable process. Mitochondrial protein import regulation involves the translocation of thousands of nuclear-encoded proteins from the cytosol into a double-membrane-bound organelle, across complex translocase systems, such as TOM and TIM [105, 242, 406]. The fidelity of this import machinery is critical; even subtle defects can have profound consequences for cellular homeostasis [357].

To prevent such dysfunction, cells have evolved stress response pathways that monitor and react to mitochondrial import stress. MitoTAD is a constitutive surveillance mechanism of the TOM complex that ensures efficient protein import under normal conditions [243, 244, 246, 357]. However, under severe import stress, this system fails, leading to the activation of the mitoCPR pathway [357]. In this context, the AAA-ATPase Msp1 removes clogged precursor proteins from translocases during import blockages induced by artificial clogging systems [257, 258, 407]. Since these stress pathways often act locally, this might suggest that the effects of mitochondrial stress are confined to the organelle. However, emerging evidence [264-267], including our findings on DNAJC15, challenges this view. Instead, the evidence suggests that import stress can extend beyond mitochondria, activating alternative stress responses that originate in other cellular compartments [264-267]. These cellular responses are commonly activated by the accumulation of unfolded proteins or distinct metabolic cues, and are not restricted to stimuli originating from

mitochondria. They involve pathways, such as the UPR and ISR, which can also be activated by mitochondrial dysfunction. Examples of this include the ISR^{mt} and the UPR^{mt} [314, 327, 408, 409].

In this study, we examined the functional consequences of DNAJC15 depletion. This resulted in a selective impairment of the import of precursor proteins targeted to the inner mitochondrial membrane and matrix. Unlike previous studies that used artificial clogger systems to induce a complete blockage of mitochondrial protein import, our work is the first to analyse the consequences of a partial impairment of mitochondrial protein import. This endogenous and partial import block reveals a novel, physiologically relevant mechanism for modulating mitochondrial protein import. Upon complete blockage of the import machinery, non-imported mitochondrial proteins usually accumulate in the cytosol and are targeted for proteasomal degradation [228, 240, 241]. However, under conditions of acute DNAJC15 depletion, we observe a partial accumulation of non-imported precursor proteins at the mitochondrial surface and a partial engagement of mitochondrial proteins with the ER. Therefore, our data argues against a cytosolic stress response driven by toxic aggregates of non-imported mitochondrial proteins in the cytosol [410]. This also rules out activation of cytosolic pathways, such as mPOS, that gets activated by mistargeted proteins in the cytosol [411, 412].

Moreover, the DNAJC15-dependent relocalisation of un-imported proteins to the ER induces a specific ER stress response, namely the activation of the ATF6 branch of the UPR, with no changes to the other two canonical branches of the UPR of the ER, IRE1/XBP1 and PERK. Targeted downregulation of the cytosolic HSP40 protein, DNAJA1, that is known to be involved in the UPR^{mt} [408], did not affect the ATF6-regulated signaling under the conditions tested (Extended Data Fig. 8a). The observed ATF6-regulated UPR further seemed to be independent of the ISR initiated by the retrotranslocation of DELE1 [56-59, 219]. These findings prompt a broader consideration of how cells coordinate mitochondrial and cytosolic stress signaling in response to impaired mitochondrial protein import.

Although the mechanisms underlying the relocalisation of mitochondrial proteins to the ER remain unclear, we have no evidence for the involvement of established mitochondrial biogenesis pathways, such as the ER-SURF pathway [264-266] (Extended Data Fig. 8b), as well as the involvement of biogenesis factors like

ATAD1 (Extended Data Fig. 8c). Furthermore, it is important to note that our proteomic approach does not distinguish between precursor and mature forms of these proteins, leaving open the possibility that proteins engage with the ER prior to mitochondrial import. Therefore, it is crucial to investigate whether proteins are retained in an import-competent state, allowing for re-import once the stress subsides. Such a mechanism would imply the existence of unknown factors capable of sensing mitochondrial import stress and relaying this signal to the ER.

In our genetic model, the selective activation of ATF6 rather than IRE1 or PERK presents a unique opportunity to investigate the relatively understudied ATF6-regulated branch of the UPR in a physiological context. It is thought that ATF6 functions as an early responder to mild proteostatic disturbances by promoting the upregulation of chaperones and enhancing protein folding capacity, without triggering translational arrest or broader cellular stress signaling [413, 414]. In contrast, activation of IRE1 and PERK typically requires more severe or prolonged stress [299, 415]. Their lack of activation in our system suggests that the accumulation of mitochondrial precursors at the ER is mild and does not exceed the threshold necessary to trigger a full-scale UPR. This hierarchical activation mechanism enables the cell to mount a proportionate response, thereby preserving resources and avoiding the potentially harmful consequences of fully activating the UPR when a more limited adaptive program is sufficient [416]. It is important to note that our analysis relies on a set of proteins presumed to be specific to ATF6 signaling [417]. However, given the limited understanding and underrepresentation of ATF6 in the context of the UPR, further validation is required. This could include targeted knockdown approaches of ATF6, the use of specific ATF6 inhibitors or live-cell imaging of ATF6 relocalisation using GFP-tagged constructs.

In summary, this study demonstrates that mitochondrial import defects are regulated through inter-organellar communication rather than isolated surveillance pathways. We demonstrate that ER-mediated responses can mitigate mitochondrial stress, highlighting the need to consider cellular stress mechanisms as integrated networks. Establishing whether this mechanism operates *in vivo*, during development, ageing, or disease, will be essential to define its physiological significance.

5.6 The role of OMA1 in maintaining mitochondrial plasticity

OMA1-dependent proteolysis is critical for mitochondrial plasticity and cellular homeostasis. In response to stress, such as OXPHOS dysfunction, OMA1 mediates mitochondrial rewiring at multiple levels to reduce mitochondrial burden and preserve cellular viability [418-420]. OMA1 cleaves OPA1 to promote mitochondrial fragmentation and enable selective mitophagy [36, 41-44, 51, 420-422], and it cleaves DELE1 to activate the ISR and attenuate global translation [56-59]. We expanded the repertoire of OMA1 functions by identifying DNAJC15 as a novel substrate that links OMA1 to mitochondrial protein import. Under mitochondrial stress, OMA1 limits protein import by cleaving DNAJC15, which impairs the import of OXPHOS biogenesis factors and reduces respiratory capacity. Although these OMA1-regulated pathways act independently [45, 73], they converge to form an integrated mitochondrial stress response that repurposes mitochondria to mitigate the OXPHOS burden.

By dynamically coordinating mitochondrial morphology, mitochondrial protein import, and metabolism [73], OMA1 serves as a stress-protective protease that dynamically remodels the mitochondrial proteome upon mitochondrial insults to promote cellular adaptation and survival.

6. List of references

1. Deshwal, S., Fiedler, K.U. & Langer, T. Mitochondrial Proteases: Multifaceted Regulators of Mitochondrial Plasticity. *Annu Rev Biochem* **89**, 501-528 (2020).
2. Sun, N., Youle, R.J. & Finkel, T. The Mitochondrial Basis of Aging. *Mol Cell* **61**, 654-666 (2016).
3. Reddy, P.H. Role of mitochondria in neurodegenerative diseases: mitochondria as a therapeutic target in Alzheimer's disease. *CNS Spectr* **14**, 8-13; discussion 16-18 (2009).
4. Leonhard, K. *et al.* Membrane protein degradation by AAA proteases in mitochondria: extraction of substrates from either membrane surface. *Mol Cell* **5**, 629-638 (2000).
5. Gerdes, F., Tatsuta, T. & Langer, T. Mitochondrial AAA proteases--towards a molecular understanding of membrane-bound proteolytic machines. *Biochim Biophys Acta* **1823**, 49-55 (2012).
6. Leonhard, K., Stiegler, A., Neupert, W. & Langer, T. Chaperone-like activity of the AAA domain of the yeast Yme1 AAA protease. *Nature* **398**, 348-351 (1999).
7. Lee, S. *et al.* Electron cryomicroscopy structure of a membrane-anchored mitochondrial AAA protease. *J Biol Chem* **286**, 4404-4411 (2011).
8. Koppen, M., Metodiev, M.D., Casari, G., Rugarli, E.I. & Langer, T. Variable and tissue-specific subunit composition of mitochondrial m-AAA protease complexes linked to hereditary spastic paraplegia. *Mol Cell Biol* **27**, 758-767 (2007).
9. Janska, H., Kwasniak, M. & Szczepanowska, J. Protein quality control in organelles — AAA/FtsH story. *Biochimica et Biophysica Acta (BBA) - Molecular Cell Research* **1833**, 381-387 (2013).
10. Piechota, J., Kolodziejczak, M., Juszczak, I., Sakamoto, W. & Janska, H. Identification and characterization of high molecular weight complexes formed by matrix AAA proteases and prohibitins in mitochondria of Arabidopsis thaliana. *J Biol Chem* **285**, 12512-12521 (2010).
11. Wai, T. *et al.* The membrane scaffold SLP2 anchors a proteolytic hub in mitochondria containing PARL and the i-AAA protease YME1L. *EMBO Rep* **17**, 1844-1856 (2016).
12. Tatsuta, T. & Langer, T. Prohibitins. *Curr Biol* **27**, R629-r631 (2017).
13. Steglich, G., Neupert, W. & Langer, T. Prohibitins regulate membrane protein degradation by the m-AAA protease in mitochondria. *Mol Cell Biol* **19**, 3435-3442 (1999).
14. Merkwirth, C. & Langer, T. Prohibitin function within mitochondria: essential roles for cell proliferation and cristae morphogenesis. *Biochim Biophys Acta* **1793**, 27-32 (2009).
15. Osman, C. *et al.* The genetic interactome of prohibitins: coordinated control of cardiolipin and phosphatidylethanolamine by conserved regulators in mitochondria. *J Cell Biol* **184**, 583-596 (2009).
16. Casari, G. *et al.* Spastic paraplegia and OXPHOS impairment caused by mutations in paraplegin, a nuclear-encoded mitochondrial metalloprotease. *Cell* **93**, 973-983 (1998).

17. Di Bella, D. *et al.* Mutations in the mitochondrial protease gene AFG3L2 cause dominant hereditary ataxia SCA28. *Nat Genet* **42**, 313-321 (2010).
18. Pierson, T.M. *et al.* Whole-exome sequencing identifies homozygous AFG3L2 mutations in a spastic ataxia-neuropathy syndrome linked to mitochondrial m-AAA proteases. *PLoS Genet* **7**, e1002325 (2011).
19. Koppen, M., Bonn, F., Ehses, S. & Langer, T. Autocatalytic processing of m-AAA protease subunits in mitochondria. *Mol Biol Cell* **20**, 4216-4224 (2009).
20. Nolden, M. *et al.* The m-AAA protease defective in hereditary spastic paraplegia controls ribosome assembly in mitochondria. *Cell* **123**, 277-289 (2005).
21. Tsai, C.-W. *et al.* Proteolytic control of the mitochondrial calcium uniporter complex. *Proceedings of the National Academy of Sciences* **114**, 4388-4393 (2017).
22. König, T. *et al.* The m-AAA Protease Associated with Neurodegeneration Limits MCU Activity in Mitochondria. *Mol Cell* **64**, 148-162 (2016).
23. Tsai, M.-F. *et al.* Dual functions of a small regulatory subunit in the mitochondrial calcium uniporter complex. *eLife* **5**, e15545 (2016).
24. Patron, M. *et al.* Regulation of mitochondrial proteostasis by the proton gradient. *Embo j* **41**, e110476 (2022).
25. Hornig-Do, H.T. *et al.* Nonsense mutations in the COX1 subunit impair the stability of respiratory chain complexes rather than their assembly. *Embo j* **31**, 1293-1307 (2012).
26. Zurita Rendón, O. & Shoubridge, E.A. Early complex I assembly defects result in rapid turnover of the ND1 subunit. *Hum Mol Genet* **21**, 3815-3824 (2012).
27. Tröder, S.E. A protective function against apoptosis revealed by the neuronal interactome of the mitochondrial m-AAA protease. (2014).
28. Wang, T. *et al.* C9orf72 regulates energy homeostasis by stabilizing mitochondrial complex I assembly. *Cell Metab* **33**, 531-546.e539 (2021).
29. Shi, X. *et al.* Dual regulation of SLC25A39 by AFG3L2 and iron controls mitochondrial glutathione homeostasis. *Mol Cell* **84**, 802-810.e806 (2024).
30. Herrmann, J.M. A Force-Generating Machine in the Plant's Powerhouse: A Pulling AAA-ATPase Motor Drives Protein Translocation into Chloroplasts. *The Plant Cell* **30**, 2646-2647 (2018).
31. Kikuchi, S. *et al.* A Ycf2-FtsHi Heteromeric AAA-ATPase Complex Is Required for Chloroplast Protein Import. *The Plant Cell* **30**, 2677-2703 (2018).
32. Kaser, M., Kambacheld, M., Kisters-Woike, B. & Langer, T. Oma1, a novel membrane-bound metallopeptidase in mitochondria with activities overlapping with the m-AAA protease. *J Biol Chem* **278**, 46414-46423 (2003).
33. Rainbolt, T.K., Lebeau, J., Puchades, C. & Wiseman, R.L. Reciprocal Degradation of YME1L and OMA1 Adapts Mitochondrial Proteolytic Activity during Stress. *Cell Rep* **14**, 2041-2049 (2016).
34. Zhang, K., Li, H. & Song, Z. Membrane depolarization activates the mitochondrial protease OMA1 by stimulating self-cleavage. *EMBO Rep* **15**, 576-585 (2014).
35. Murata, D. *et al.* Mitochondrial Safeguard: a stress response that offsets extreme fusion and protects respiratory function via flickering-induced Oma1 activation. *EMBO J* **39**, e105074 (2020).

36. Baker, M.J. *et al.* Stress-induced OMA1 activation and autocatalytic turnover regulate OPA1-dependent mitochondrial dynamics. *Embo j* **33**, 578-593 (2014).
37. Bohovych, I., Donaldson, G., Christianson, S., Zahayko, N. & Khalimonchuk, O. Stress-triggered activation of the metalloprotease Oma1 involves its C-terminal region and is important for mitochondrial stress protection in yeast. *J Biol Chem* **289**, 13259-13272 (2014).
38. Miallot, R. *et al.* An OMA1 redox site controls mitochondrial homeostasis, sarcoma growth, and immunogenicity. *Life Sci Alliance* **6** (2023).
39. Bohovych, I., Dietz, J.V., Swenson, S., Zahayko, N. & Khalimonchuk, O. Redox Regulation of the Mitochondrial Quality Control Protease Oma1. *Antioxid Redox Signal* **31**, 429-443 (2019).
40. Ohba, Y., MacVicar, T. & Langer, T. Regulation of mitochondrial plasticity by the i-AAA protease YME1L. *Biol Chem* **401**, 877-890 (2020).
41. MacVicar, T. & Langer, T. OPA1 processing in cell death and disease - the long and short of it. *J Cell Sci* **129**, 2297-2306 (2016).
42. Quirós, P.M. *et al.* Loss of mitochondrial protease OMA1 alters processing of the GTPase OPA1 and causes obesity and defective thermogenesis in mice. *Embo j* **31**, 2117-2133 (2012).
43. Jiang, X., Jiang, H., Shen, Z. & Wang, X. Activation of mitochondrial protease OMA1 by Bax and Bak promotes cytochrome c release during apoptosis. *Proc Natl Acad Sci U S A* **111**, 14782-14787 (2014).
44. Frezza, C. *et al.* OPA1 controls apoptotic cristae remodeling independently from mitochondrial fusion. *Cell* **126**, 177-189 (2006).
45. Ahola, S. *et al.* Opa1 processing is dispensable in mouse development but is protective in mitochondrial cardiomyopathy. *Science Advances* **10**, eadp0443 (2024).
46. Lee, H., Smith, S.B. & Yoon, Y. The short variant of the mitochondrial dynamin OPA1 maintains mitochondrial energetics and cristae structure. *J Biol Chem* **292**, 7115-7130 (2017).
47. Ban, T. *et al.* Molecular basis of selective mitochondrial fusion by heterotypic action between OPA1 and cardiolipin. *Nat Cell Biol* **19**, 856-863 (2017).
48. Anand, R. *et al.* The i-AAA protease YME1L and OMA1 cleave OPA1 to balance mitochondrial fusion and fission. *J Cell Biol* **204**, 919-929 (2014).
49. Ge, Y. *et al.* Two forms of Opa1 cooperate to complete fusion of the mitochondrial inner-membrane. *Elife* **9** (2020).
50. Suga, S. *et al.* An interactive deep learning-based approach reveals mitochondrial cristae topologies. *PLoS Biol* **21**, e3002246 (2023).
51. Fry, M.Y. *et al.* In situ architecture of Opa1-dependent mitochondrial cristae remodeling. *Embo j* **43**, 391-413 (2024).
52. Tang, J. *et al.* Sam50-Mic19-Mic60 axis determines mitochondrial cristae architecture by mediating mitochondrial outer and inner membrane contact. *Cell Death Differ* **27**, 146-160 (2020).
53. Korwitz, A. *et al.* Loss of OMA1 delays neurodegeneration by preventing stress-induced OPA1 processing in mitochondria. *J Cell Biol* **212**, 157-166 (2016).
54. Viana, M.P., Levytskyy, R.M., Anand, R., Reichert, A.S. & Khalimonchuk, O. Protease OMA1 modulates mitochondrial bioenergetics and ultrastructure through dynamic association with MICOS complex. *iScience* **24**, 102119 (2021).

55. Guo, X. *et al.* Mitochondrial stress is relayed to the cytosol by an OMA1–DELE1–HRI pathway. *Nature* **579**, 427-432 (2020).
56. Guo, X. *et al.* Mitochondrial stress is relayed to the cytosol by an OMA1-DELE1-HRI pathway. *Nature* **579**, 427-432 (2020).
57. Fessler, E. *et al.* A pathway coordinated by DELE1 relays mitochondrial stress to the cytosol. *Nature* **579**, 433-437 (2020).
58. Fessler, E., Krumwiede, L. & Jae, L.T. DELE1 tracks perturbed protein import and processing in human mitochondria. *Nat Commun* **13**, 1853 (2022).
59. Sekine, Y. *et al.* A mitochondrial iron-responsive pathway regulated by DELE1. *Mol Cell* **83**, 2059-2076.e2056 (2023).
60. Sekine, S. *et al.* Reciprocal Roles of Tom7 and OMA1 during Mitochondrial Import and Activation of PINK1. *Mol Cell* **73**, 1028-1043 e1025 (2019).
61. Tanaka, A. *et al.* Proteasome and p97 mediate mitophagy and degradation of mitofusins induced by Parkin. *J Cell Biol* **191**, 1367-1380 (2010).
62. Yamada, T. *et al.* Dual regulation of mitochondrial fusion by Parkin–PINK1 and OMA1. *Nature* **639**, 776-783 (2025).
63. Krakowczyk, M. *et al.* OMA1 protease eliminates arrested protein import intermediates upon mitochondrial depolarization. *J Cell Biol* **223** (2024).
64. Quiros, P.M. *et al.* Loss of mitochondrial protease OMA1 alters processing of the GTPase OPA1 and causes obesity and defective thermogenesis in mice. *EMBO J* **31**, 2117-2133 (2012).
65. Wai, T. *et al.* Imbalanced OPA1 processing and mitochondrial fragmentation cause heart failure in mice. *Science* **350**, aad0116 (2015).
66. Acin-Perez, R. *et al.* Ablation of the stress protease OMA1 protects against heart failure in mice. *Sci Transl Med* **10** (2018).
67. Korwitz, A. *et al.* Loss of OMA1 delays neurodegeneration by preventing stress-induced OPA1 processing in mitochondria. *J Cell Biol* **212**, 157-166 (2016).
68. Nan, J. *et al.* EGCG protects cardiomyocytes against hypoxia-reperfusion injury through inhibition of OMA1 activation. *J Cell Sci* **132** (2019).
69. Xiao, X. *et al.* OMA1 mediates OPA1 proteolysis and mitochondrial fragmentation in experimental models of ischemic kidney injury. *Am J Physiol Renal Physiol* **306**, F1318-1326 (2014).
70. Li, X. *et al.* Ischemia-induced cleavage of OPA1 at S1 site aggravates mitochondrial fragmentation and reperfusion injury in neurons. *Cell Death Dis* **13**, 321 (2022).
71. Ahola, S. *et al.* OMA1-mediated integrated stress response protects against ferroptosis in mitochondrial cardiomyopathy. *Cell Metab* **34**, 1875-1891.e1877 (2022).
72. Sprenger, H.G. *et al.* Loss of the mitochondrial i-AAA protease YME1L leads to ocular dysfunction and spinal axonopathy. *EMBO Mol Med* **11** (2019).
73. Rivera-Mejías, P. *et al.* The mitochondrial protease OMA1 acts as a metabolic safeguard upon nuclear DNA damage. *Cell Rep* **42**, 112332 (2023).
74. Wu, Z. *et al.* OMA1 reprograms metabolism under hypoxia to promote colorectal cancer development. *EMBO Rep* **22**, e50827 (2021).
75. Daverey, A. *et al.* Depletion of mitochondrial protease OMA1 alters proliferative properties and promotes metastatic growth of breast cancer cells. *Sci Rep* **9**, 14746 (2019).

76. Morgenstern, M. *et al.* Quantitative high-confidence human mitochondrial proteome and its dynamics in cellular context. *Cell Metab* **33**, 2464-2483 e2418 (2021).
77. Lopez, M.F. *et al.* High-throughput profiling of the mitochondrial proteome using affinity fractionation and automation. *Electrophoresis* **21**, 3427-3440 (2000).
78. Callegari, S., Cruz-Zaragoza, L.D. & Rehling, P. From TOM to the TIM23 complex - handing over of a precursor. *Biol Chem* **401**, 709-721 (2020).
79. Herrmann, J.M. & Bykov, Y. Protein translocation in mitochondria: Sorting out the Toms, Tims, Pams, Sams and Mia. *FEBS Lett* **597**, 1553-1554 (2023).
80. Bolender, N., Sickmann, A., Wagner, R., Meisinger, C. & Pfanner, N. Multiple pathways for sorting mitochondrial precursor proteins. *EMBO Rep* **9**, 42-49 (2008).
81. Shiota, T. *et al.* Molecular architecture of the active mitochondrial protein gate. *Science* **349**, 1544-1548 (2015).
82. Araiso, Y. *et al.* Structure of the mitochondrial import gate reveals distinct preprotein paths. *Nature* **575**, 395-401 (2019).
83. Tucker, K. & Park, E. Cryo-EM structure of the mitochondrial protein-import channel TOM complex at near-atomic resolution. *Nat Struct Mol Biol* **26**, 1158-1166 (2019).
84. Araiso, Y. & Endo, T. Structural overview of the translocase of the mitochondrial outer membrane complex. *Biophys Physicobiol* **19**, e190022 (2022).
85. Wang, W. *et al.* Atomic structure of human TOM core complex. *Cell Discovery* **6**, 67 (2020).
86. Wang, W. *et al.* Atomic structure of human TOM core complex. *Cell Discov* **6**, 67 (2020).
87. Chacinska, A., Koehler, C.M., Milenkovic, D., Lithgow, T. & Pfanner, N. Importing mitochondrial proteins: machineries and mechanisms. *Cell* **138**, 628-644 (2009).
88. Dutta, D. *et al.* De novo mutations in TOMM70, a receptor of the mitochondrial import translocase, cause neurological impairment. *Hum Mol Genet* **29**, 1568-1579 (2020).
89. Wei, X. *et al.* Mutations in TOMM70 lead to multi-OXPHOS deficiencies and cause severe anemia, lactic acidosis, and developmental delay. *J Hum Genet* **65**, 231-240 (2020).
90. Palmer, C.S., Anderson, A.J. & Stojanovski, D. Mitochondrial protein import dysfunction: mitochondrial disease, neurodegenerative disease and cancer. *FEBS Lett* **595**, 1107-1131 (2021).
91. Yamamoto, H. *et al.* Roles of Tom70 in import of presequence-containing mitochondrial proteins. *J Biol Chem* **284**, 31635-31646 (2009).
92. Yamano, K. *et al.* Tom20 and Tom22 share the common signal recognition pathway in mitochondrial protein import. *J Biol Chem* **283**, 3799-3807 (2008).
93. Abe, Y. *et al.* Structural basis of presequence recognition by the mitochondrial protein import receptor Tom20. *Cell* **100**, 551-560 (2000).
94. Gupta, A. & Becker, T. Mechanisms and pathways of mitochondrial outer membrane protein biogenesis. *Biochimica et Biophysica Acta (BBA) - Bioenergetics* **1862**, 148323 (2021).

95. Brix, J., Dietmeier, K. & Pfanner, N. Differential recognition of preproteins by the purified cytosolic domains of the mitochondrial import receptors Tom20, Tom22, and Tom70. *J Biol Chem* **272**, 20730-20735 (1997).
96. Periasamy, A. *et al.* Structure of an ex vivoDrosophila TOM complex determined by single-particle cryoEM. *IUCrJ* **12**, 49-61 (2025).
97. Nussberger, S., Ghosh, R. & Wang, S. New insights into the structure and dynamics of the TOM complex in mitochondria. *Biochem Soc Trans* **52**, 911-922 (2024).
98. Zhou, X. *et al.* Molecular pathway of mitochondrial preprotein import through the TOM–TIM23 supercomplex. *Nature Structural & Molecular Biology* **30**, 1996-2008 (2023).
99. Honlinger, A. *et al.* Tom7 modulates the dynamics of the mitochondrial outer membrane translocase and plays a pathway-related role in protein import. *EMBO J* **15**, 2125-2137 (1996).
100. Dietmeier, K. *et al.* Tom5 functionally links mitochondrial preprotein receptors to the general import pore. *Nature* **388**, 195-200 (1997).
101. Becker, T. *et al.* Biogenesis of Mitochondria: Dual Role of Tom7 in Modulating Assembly of the Preprotein Translocase of the Outer Membrane. *Journal of Molecular Biology* **405**, 113-124 (2011).
102. Su, J. *et al.* Structural basis of Tom20 and Tom22 cytosolic domains as the human TOM complex receptors. *Proceedings of the National Academy of Sciences* **119**, e2200158119 (2022).
103. Gomkale, R. *et al.* Mapping protein interactions in the active TOM-TIM23 supercomplex. *Nat Commun* **12**, 5715 (2021).
104. Sinzel, M. *et al.* Mcp3 is a novel mitochondrial outer membrane protein that follows a unique IMP-dependent biogenesis pathway. *EMBO Rep* **17**, 965-981 (2016).
105. Wiedemann, N. & Pfanner, N. Mitochondrial Machineries for Protein Import and Assembly. *Annu Rev Biochem* **86**, 685-714 (2017).
106. Qi, L. *et al.* Cryo-EM structure of the human mitochondrial translocase TIM22 complex. *Cell Research* **31**, 369-372 (2021).
107. Kang, Y. *et al.* Tim29 is a novel subunit of the human TIM22 translocase and is involved in complex assembly and stability. *eLife* **5**, e17463 (2016).
108. Vukotic, M. *et al.* Acylglycerol Kinase Mutated in Sengers Syndrome Is a Subunit of the TIM22 Protein Translocase in Mitochondria. *Mol Cell* **67**, 471-483.e477 (2017).
109. Okamoto, H., Miyagawa, A., Shiota, T., Tamura, Y. & Endo, T. Intramolecular disulfide bond of Tim22 protein maintains integrity of the TIM22 complex in the mitochondrial inner membrane. *J Biol Chem* **289**, 4827-4838 (2014).
110. Gebert, N. *et al.* Dual function of Sdh3 in the respiratory chain and TIM22 protein translocase of the mitochondrial inner membrane. *Mol Cell* **44**, 811-818 (2011).
111. Dudek, J., Rehling, P. & van der Laan, M. Mitochondrial protein import: Common principles and physiological networks. *Biochimica et Biophysica Acta (BBA) - Molecular Cell Research* **1833**, 274-285 (2013).
112. Wu, Y. & Sha, B. Crystal structure of yeast mitochondrial outer membrane translocon member Tom70p. *Nat Struct Mol Biol* **13**, 589-593 (2006).
113. Curran, S.P., Leuenberger, D., Schmidt, E. & Koehler, C.M. The role of the Tim8p-Tim13p complex in a conserved import pathway for mitochondrial polytopic inner membrane proteins. *J Cell Biol* **158**, 1017-1027 (2002).

114. Milenkovic, D. *et al.* Biogenesis of the Essential Tim9–Tim10 Chaperone Complex of Mitochondria: SITE-SPECIFIC RECOGNITION OF CYSTEINE RESIDUES BY THE INTERMEMBRANE SPACE RECEPTOR Mia40*. *Journal of Biological Chemistry* **282**, 22472-22480 (2007).
115. Anderson, A.J. *et al.* Human Tim8a, Tim8b and Tim13 are auxiliary assembly factors of mature Complex IV. *EMBO reports* **24**, e56430 (2023).
116. Wrobel, L., Trojanowska, A., Sztolsztener, M.E. & Chacinska, A. Mitochondrial protein import: Mia40 facilitates Tim22 translocation into the inner membrane of mitochondria. *Mol Biol Cell* **24**, 543-554 (2013).
117. Badrie, S., Hell, K. & Mokranjac, D. Dbi1 is an oxidoreductase and an assembly chaperone for mitochondrial inner membrane proteins. *EMBO reports* **26**, 911-928 (2025).
118. Stroud, D.A. *et al.* Accessory subunits are integral for assembly and function of human mitochondrial complex I. *Nature* **538**, 123-126 (2016).
119. Kang, Y. *et al.* Sengers Syndrome-Associated Mitochondrial Acylglycerol Kinase Is a Subunit of the Human TIM22 Protein Import Complex. *Mol Cell* **67**, 457-470.e455 (2017).
120. Haghighi, A. *et al.* Sengers syndrome: six novel AGK mutations in seven new families and review of the phenotypic and mutational spectrum of 29 patients. *Orphanet Journal of Rare Diseases* **9**, 119 (2014).
121. Vukotic, M. *et al.* Acylglycerol Kinase Mutated in Sengers Syndrome Is a Subunit of the TIM22 Protein Translocase in Mitochondria. *Mol Cell* **67**, 471-483 e477 (2017).
122. Esaki, M. *et al.* Tom40 protein import channel binds to non-native proteins and prevents their aggregation. *Nat Struct Biol* **10**, 988-994 (2003).
123. Künkele, K.-P. *et al.* The Preprotein Translocation Channel of the Outer Membrane of Mitochondria. *Cell* **93**, 1009-1019 (1998).
124. Wiedemann, N. *et al.* Machinery for protein sorting and assembly in the mitochondrial outer membrane. *Nature* **424**, 565-571 (2003).
125. Curran, S.P., Leuenberger, D., Oppliger, W. & Koehler, C.M. The Tim9p-Tim10p complex binds to the transmembrane domains of the ADP/ATP carrier. *Embo j* **21**, 942-953 (2002).
126. Vasiljev, A. *et al.* Reconstituted TOM core complex and Tim9/Tim10 complex of mitochondria are sufficient for translocation of the ADP/ATP carrier across membranes. *Mol Biol Cell* **15**, 1445-1458 (2004).
127. Webb, C.T., Gorman, M.A., Lazarou, M., Ryan, M.T. & Gulbis, J.M. Crystal structure of the mitochondrial chaperone TIM9.10 reveals a six-bladed alpha-propeller. *Mol Cell* **21**, 123-133 (2006).
128. Paschen, S.A. *et al.* Evolutionary conservation of biogenesis of beta-barrel membrane proteins. *Nature* **426**, 862-866 (2003).
129. Kutik, S. *et al.* Dissecting membrane insertion of mitochondrial beta-barrel proteins. *Cell* **132**, 1011-1024 (2008).
130. Kozjak, V. *et al.* An essential role of Sam50 in the protein sorting and assembly machinery of the mitochondrial outer membrane. *J Biol Chem* **278**, 48520-48523 (2003).
131. Kutik, S. *et al.* Dissecting Membrane Insertion of Mitochondrial β-Barrel Proteins. *Cell* **132**, 1011-1024 (2008).
132. Kozjak-Pavlovic, V. *et al.* Conserved roles of Sam50 and metaxins in VDAC biogenesis. *EMBO Rep* **8**, 576-582 (2007).

133. Milenkovic, D. *et al.* Sam35 of the Mitochondrial Protein Sorting and Assembly Machinery Is a Peripheral Outer Membrane Protein Essential for Cell Viability*. *Journal of Biological Chemistry* **279**, 22781-22785 (2004).
134. Chan, N.C. & Lithgow, T. The peripheral membrane subunits of the SAM complex function codependently in mitochondrial outer membrane biogenesis. *Mol Biol Cell* **19**, 126-136 (2008).
135. Ellenrieder, L. *et al.* Separating mitochondrial protein assembly and endoplasmic reticulum tethering by selective coupling of Mdm10. *Nature Communications* **7**, 13021 (2016).
136. Becker, T. *et al.* Biogenesis of mitochondria: dual role of Tom7 in modulating assembly of the preprotein translocase of the outer membrane. *J Mol Biol* **405**, 113-124 (2011).
137. Qiu, J. *et al.* Coupling of mitochondrial import and export translocases by receptor-mediated supercomplex formation. *Cell* **154**, 596-608 (2013).
138. Sideris, D.P. *et al.* A novel intermembrane space-targeting signal docks cysteines onto Mia40 during mitochondrial oxidative folding. *J Cell Biol* **187**, 1007-1022 (2009).
139. Zarges, C. & Riemer, J. Oxidative protein folding in the intermembrane space of human mitochondria. *FEBS Open Bio* **14**, 1610-1626 (2024).
140. Dickson-Murray, E., Nedara, K., Modjtahedi, N. & Tokatlidis, K. The Mia40/CHCHD4 Oxidative Folding System: Redox Regulation and Signaling in the Mitochondrial Intermembrane Space. *Antioxidants (Basel)* **10** (2021).
141. von der Malsburg, K. *et al.* Dual role of mitofilin in mitochondrial membrane organization and protein biogenesis. *Dev Cell* **21**, 694-707 (2011).
142. Longen, S., Woellhaf, M.W., Petrungaro, C., Riemer, J. & Herrmann, J.M. The disulfide relay of the intermembrane space oxidizes the ribosomal subunit mrp10 on its transit into the mitochondrial matrix. *Dev Cell* **28**, 30-42 (2014).
143. Ramesh, A. *et al.* A disulfide bond in the TIM23 complex is crucial for voltage gating and mitochondrial protein import. *J Cell Biol* **214**, 417-431 (2016).
144. Terziyska, N., Grumbt, B., Kozany, C. & Hell, K. Structural and functional roles of the conserved cysteine residues of the redox-regulated import receptor Mia40 in the intermembrane space of mitochondria. *J Biol Chem* **284**, 1353-1363 (2009).
145. Chacinska, A. *et al.* Essential role of Mia40 in import and assembly of mitochondrial intermembrane space proteins. *EMBO J* **23**, 3735-3746 (2004).
146. Grumbt, B., Stroobant, V., Terziyska, N., Israel, L. & Hell, K. Functional characterization of Mia40p, the central component of the disulfide relay system of the mitochondrial intermembrane space. *J Biol Chem* **282**, 37461-37470 (2007).
147. Allen, S., Balabanidou, V., Sideris, D.P., Lisowsky, T. & Tokatlidis, K. Erv1 mediates the Mia40-dependent protein import pathway and provides a functional link to the respiratory chain by shuttling electrons to cytochrome c. *J Mol Biol* **353**, 937-944 (2005).
148. Bien, M. *et al.* Mitochondrial disulfide bond formation is driven by intersubunit electron transfer in Erv1 and proofread by glutathione. *Mol Cell* **37**, 516-528 (2010).
149. Mesecke, N. *et al.* The zinc-binding protein Hot13 promotes oxidation of the mitochondrial import receptor Mia40. *EMBO Rep* **9**, 1107-1113 (2008).

150. Rothemann, R.A. *et al.* Interaction with the cysteine-free protein HAX1 expands the substrate specificity and function of MIA40 beyond protein oxidation. *Febs j* **291**, 5506-5522 (2024).
151. Murschall, L.M. *et al.* The C-terminal region of the oxidoreductase MIA40 stabilizes its cytosolic precursor during mitochondrial import. *BMC Biol* **18**, 96 (2020).
152. Hangen, E. *et al.* Interaction between AIF and CHCHD4 Regulates Respiratory Chain Biogenesis. *Mol Cell* **58**, 1001-1014 (2015).
153. Salscheider, S.L. *et al.* AIFM1 is a component of the mitochondrial disulfide relay that drives complex I assembly through efficient import of NDUFS5. *EMBO J* **41**, e110784 (2022).
154. Brosey, C.A. *et al.* Defining NADH-Driven Allostery Regulating Apoptosis-Inducing Factor. *Structure* **24**, 2067-2079 (2016).
155. Rinaldi, C. *et al.* Cowchock syndrome is associated with a mutation in apoptosis-inducing factor. *Am J Hum Genet* **91**, 1095-1102 (2012).
156. Ardissone, A. *et al.* A slowly progressive mitochondrial encephalomyopathy widens the spectrum of AIFM1 disorders. *Neurology* **84**, 2193-2195 (2015).
157. Mierzewska, H. *et al.* Spondyloepimetaphyseal dysplasia with neurodegeneration associated with AIFM1 mutation - a novel phenotype of the mitochondrial disease. *Clin Genet* **91**, 30-37 (2017).
158. Susin, S.A. *et al.* Molecular characterization of mitochondrial apoptosis-inducing factor. *Nature* **397**, 441-446 (1999).
159. Heimer, G. *et al.* Mutations in AIFM1 cause an X-linked childhood cerebellar ataxia partially responsive to riboflavin. *Eur J Paediatr Neurol* **22**, 93-101 (2018).
160. Popov-Celeketić, J., Waizenegger, T. & Rapaport, D. Mim1 functions in an oligomeric form to facilitate the integration of Tom20 into the mitochondrial outer membrane. *J Mol Biol* **376**, 671-680 (2008).
161. Hulett, J.M. *et al.* The transmembrane segment of Tom20 is recognized by Mim1 for docking to the mitochondrial TOM complex. *J Mol Biol* **376**, 694-704 (2008).
162. Otera, H. *et al.* A novel insertion pathway of mitochondrial outer membrane proteins with multiple transmembrane segments. *J Cell Biol* **179**, 1355-1363 (2007).
163. Becker, T. *et al.* The mitochondrial import protein Mim1 promotes biogenesis of multispanning outer membrane proteins. *J Cell Biol* **194**, 387-395 (2011).
164. Papić, D. *et al.* The role of Djp1 in import of the mitochondrial protein Mim1 demonstrates specificity between a cochaperone and its substrate protein. *Mol Cell Biol* **33**, 4083-4094 (2013).
165. Opalinski, L. *et al.* Recruitment of Cytosolic J-Proteins by TOM Receptors Promotes Mitochondrial Protein Biogenesis. *Cell Rep* **25**, 2036-2043 e2035 (2018).
166. Vogtle, F.N. *et al.* The fusogenic lipid phosphatidic acid promotes the biogenesis of mitochondrial outer membrane protein Ugo1. *J Cell Biol* **210**, 951-960 (2015).
167. Sauerwald, J. *et al.* Genome-Wide Screens in Saccharomyces cerevisiae Highlight a Role for Cardiolipin in Biogenesis of Mitochondrial Outer Membrane Multispan Proteins. *Mol Cell Biol* **35**, 3200-3211 (2015).

168. Becker, T. *et al.* Biogenesis of the mitochondrial TOM complex: Mim1 promotes insertion and assembly of signal-anchored receptors. *J Biol Chem* **283**, 120-127 (2008).
169. Doan, K.N. *et al.* The Mitochondrial Import Complex MIM Functions as Main Translocase for α-Helical Outer Membrane Proteins. *Cell Reports* **31**, 107567 (2020).
170. Labbe, K. *et al.* The modified mitochondrial outer membrane carrier MTCH2 links mitochondrial fusion to lipogenesis. *J Cell Biol* **220** (2021).
171. Guna, A. *et al.* MTCH2 is a mitochondrial outer membrane protein insertase. *Science* **378**, 317-322 (2022).
172. Dimogkioka, A.R., Elias, A. & Rapaport, D. The mammalian protein MTCH1 can function as an insertase. *bioRxiv*, 2024.2012.2011.627916 (2024).
173. Makki, A. & Rehling, P. Protein transport along the presequence pathway. *Biological Chemistry* **404**, 807-812 (2023).
174. van der Laan, M. *et al.* Motor-free mitochondrial presequence translocase drives membrane integration of preproteins. *Nat Cell Biol* **9**, 1152-1159 (2007).
175. Rada, P. *et al.* N-Terminal Presequence-Independent Import of Phosphofructokinase into Hydrogenosomes of Trichomonas vaginalis. *Eukaryot Cell* **14**, 1264-1275 (2015).
176. Bykov, Y.S. *et al.* Widespread use of unconventional targeting signals in mitochondrial ribosome proteins. *EMBO J* **41**, e109519 (2022).
177. Glick, B.S. *et al.* Cytochromes c1 and b2 are sorted to the intermembrane space of yeast mitochondria by a stop-transfer mechanism. *Cell* **69**, 809-822 (1992).
178. Pfanner, N., Warscheid, B. & Wiedemann, N. Mitochondrial proteins: from biogenesis to functional networks. *Nat Rev Mol Cell Biol* **20**, 267-284 (2019).
179. Araiso, Y. *et al.* Structure of the mitochondrial import gate reveals distinct preprotein paths. *Nature* **575**, 395-401 (2019).
180. Mokranjac, D. *et al.* Tim50, a novel component of the TIM23 preprotein translocase of mitochondria. *EMBO J* **22**, 816-825 (2003).
181. Chacinska, A. *et al.* Mitochondrial Presequence Translocase: Switching between TOM Tethering and Motor Recruitment Involves Tim21 and Tim17. *Cell* **120**, 817-829 (2005).
182. Yamamoto, H. *et al.* Tim50 is a subunit of the TIM23 complex that links protein translocation across the outer and inner mitochondrial membranes. *Cell* **111**, 519-528 (2002).
183. Mick, D.U. *et al.* MITRAC links mitochondrial protein translocation to respiratory-chain assembly and translational regulation. *Cell* **151**, 1528-1541 (2012).
184. Matta, S.K., Kumar, A. & D'Silva, P. Mgr2 regulates mitochondrial preprotein import by associating with channel-forming Tim23 subunit. *Mol Biol Cell* **31**, 1112-1123 (2020).
185. Gebert, M. *et al.* Mgr2 promotes coupling of the mitochondrial presequence translocase to partner complexes. *J Cell Biol* **197**, 595-604 (2012).
186. Mapa, K. *et al.* The conformational dynamics of the mitochondrial Hsp70 chaperone. *Mol Cell* **38**, 89-100 (2010).
187. Slutsky-Leiderman, O. *et al.* The interplay between components of the mitochondrial protein translocation motor studied using purified components. *J Biol Chem* **282**, 33935-33942 (2007).

188. D'Silva, P.D., Schilke, B., Walter, W., Andrew, A. & Craig, E.A. J protein cochaperone of the mitochondrial inner membrane required for protein import into the mitochondrial matrix. *Proc Natl Acad Sci U S A* **100**, 13839-13844 (2003).
189. Frazier, A.E. *et al.* Pam16 has an essential role in the mitochondrial protein import motor. *Nat Struct Mol Biol* **11**, 226-233 (2004).
190. Marada, A. *et al.* Mge1, a nucleotide exchange factor of Hsp70, acts as an oxidative sensor to regulate mitochondrial Hsp70 function. *Mol Biol Cell* **24**, 692-703 (2013).
191. Richter-Dennerlein, R. *et al.* DNAJC19, a mitochondrial cochaperone associated with cardiomyopathy, forms a complex with prohibitins to regulate cardiolipin remodeling. *Cell Metab* **20**, 158-171 (2014).
192. Moosa, S. *et al.* A novel homozygous PAM16 mutation in a patient with a milder phenotype and longer survival. *Am J Med Genet A* **170**, 2436-2439 (2016).
193. Mégarbané, A., Dagher, R. & Melki, I. Sib pair with previously unreported skeletal dysplasia. *Am J Med Genet A* **146a**, 2916-2919 (2008).
194. Mégarbané, A., Mehawej, C., El Zahr, A., Haddad, S. & Cormier-Daire, V. A second family with autosomal recessive spondylometaphyseal dysplasia and early death. *Am J Med Genet A* **164a**, 1010-1014 (2014).
195. Mehawej, C. *et al.* The impairment of MAGMAS function in human is responsible for a severe skeletal dysplasia. *PLoS Genet* **10**, e1004311 (2014).
196. Tort, F. *et al.* Mutations in TIMM50 cause severe mitochondrial dysfunction by targeting key aspects of mitochondrial physiology. *Hum Mutat* **40**, 1700-1712 (2019).
197. Reyes, A. *et al.* Mutations in TIMM50 compromise cell survival in OxPhos-dependent metabolic conditions. *EMBO Mol Med* **10** (2018).
198. Shahrour, M.A. *et al.* Mitochondrial epileptic encephalopathy, 3-methylglutaconic aciduria and variable complex V deficiency associated with TIMM50 mutations. *Clin Genet* **91**, 690-696 (2017).
199. Joshi, M. *et al.* Mutations in the substrate binding glycine-rich loop of the mitochondrial processing peptidase-α protein (PMPCA) cause a severe mitochondrial disease. *Cold Spring Harb Mol Case Stud* **2**, a000786 (2016).
200. Vögtle, F.N. *et al.* Mutations in PMPCB Encoding the Catalytic Subunit of the Mitochondrial Presequence Protease Cause Neurodegeneration in Early Childhood. *Am J Hum Genet* **102**, 557-573 (2018).
201. Choquet, K. *et al.* Autosomal recessive cerebellar ataxia caused by a homozygous mutation in PMPCA. *Brain* **139**, e19 (2016).
202. Jobling, R.K. *et al.* PMPCA mutations cause abnormal mitochondrial protein processing in patients with non-progressive cerebellar ataxia. *Brain* **138**, 1505-1517 (2015).
203. Fielden, L.F. *et al.* Central role of Tim17 in mitochondrial presequence protein translocation. *Nature* **621**, 627-634 (2023).
204. Sim, S.I., Chen, Y., Lynch, D.L., Gumbart, J.C. & Park, E. Structural basis of mitochondrial protein import by the TIM23 complex. *Nature* **621**, 620-626 (2023).
205. Zhou, X. *et al.* Molecular pathway of mitochondrial preprotein import through the TOM-TIM23 supercomplex. *Nat Struct Mol Biol* **30**, 1996-2008 (2023).

206. Žárský, V. & Doležal, P. Evolution of the Tim17 protein family. *Biology Direct* **11**, 54 (2016).
207. Schusdziarra, C., Blamowska, M., Azem, A. & Hell, K. Methylation-controlled J-protein MCJ acts in the import of proteins into human mitochondria. *Hum Mol Genet* **22**, 1348-1357 (2013).
208. Truscott, K.N. *et al.* A J-protein is an essential subunit of the presequence translocase-associated protein import motor of mitochondria. *J Cell Biol* **163**, 707-713 (2003).
209. Kampinga, H.H. *et al.* Function, evolution, and structure of J-domain proteins. *Cell Stress and Chaperones* **24**, 7-15 (2019).
210. Hatle, K.M. *et al.* Methylation-controlled J protein promotes c-Jun degradation to prevent ABCB1 transporter expression. *Mol Cell Biol* **27**, 2952-2966 (2007).
211. Priesnitz, C. *et al.* Coupling to Pam16 differentially controls the dual role of Pam18 in protein import and respiratory chain formation. *Cell Rep* **39**, 110619 (2022).
212. Schendzielorz, A.B. *et al.* Motor recruitment to the TIM23 channel's lateral gate restricts polypeptide release into the inner membrane. *Nat Commun* **9**, 4028 (2018).
213. Sinha, D., Srivastava, S., Krishna, L. & D'Silva, P. Unraveling the intricate organization of mammalian mitochondrial presequence translocases: existence of multiple translocases for maintenance of mitochondrial function. *Mol Cell Biol* **34**, 1757-1775 (2014).
214. Sinha, D., Srivastava, S. & D'Silva, P. Functional Diversity of Human Mitochondrial J-proteins Is Independent of Their Association with the Inner Membrane Presequence Translocase. *J Biol Chem* **291**, 17345-17359 (2016).
215. Waingankar, T.P. & D'Silva, P. Multiple variants of the human presequence translocase motor subunit Magmas govern the mitochondrial import. *J Biol Chem* **297**, 101349 (2021).
216. Hatle, K.M. *et al.* MCJ/DnaJC15, an endogenous mitochondrial repressor of the respiratory chain that controls metabolic alterations. *Mol Cell Biol* **33**, 2302-2314 (2013).
217. Miglietta, S. *et al.* Mitochondrial chaperonin DNAJC15 promotes vulnerability to ferroptosis of chemoresistant ovarian cancer cells. *Open Biol* **15**, 240151 (2025).
218. Cicuéndez, B. *et al.* Absence of MCJ/DnaJC15 promotes brown adipose tissue thermogenesis. *Nat Commun* **16**, 229 (2025).
219. Rainbolt, T.K., Atanassova, N., Genereux, J.C. & Wiseman, R.L. Stress-regulated translational attenuation adapts mitochondrial protein import through Tim17A degradation. *Cell Metab* **18**, 908-919 (2013).
220. Stiburek, L. *et al.* YME1L controls the accumulation of respiratory chain subunits and is required for apoptotic resistance, cristae morphogenesis, and cell proliferation. *Mol Biol Cell* **23**, 1010-1023 (2012).
221. Richter, F. *et al.* ROMO1 is a constituent of the human presequence translocase required for YME1L protease import. *J Cell Biol* **218**, 598-614 (2019).
222. MacVicar, T. *et al.* Lipid signalling drives proteolytic rewiring of mitochondria by YME1L. *Nature* **575**, 361-365 (2019).

223. Hsu, M.C. *et al.* Mitochondrial YME1L1 governs unoccupied protein translocase channels. *Nat Cell Biol* **27**, 309-321 (2025).
224. Chandragiri, S. *et al.* AFG3L2-mediated proteolysis restricts mitochondrial biogenesis and gene expression in hypoxia. *bioRxiv*, 2024.2009.2027.615438 (2024).
225. Freeman, B.C. & Morimoto, R.I. The human cytosolic molecular chaperones hsp90, hsp70 (hsc70) and hdj-1 have distinct roles in recognition of a non-native protein and protein refolding. *Embo j* **15**, 2969-2979 (1996).
226. Balchin, D., Hayer-Hartl, M. & Hartl, F.U. Recent advances in understanding catalysis of protein folding by molecular chaperones. *FEBS Lett* **594**, 2770-2781 (2020).
227. Drwesh, L. *et al.* A network of cytosolic (co)chaperones promotes the biogenesis of mitochondrial signal-anchored outer membrane proteins. *Elife* **11** (2022).
228. Maruszczak, K.K., Ayyamperumal, S. & Chacinska, A. Defective mitochondrial import as a challenge for cellular protein homeostasis. *FEBS Lett* **597**, 1555-1568 (2023).
229. den Brave, F. *et al.* Chaperone-Mediated Protein Disaggregation Triggers Proteolytic Clearance of Intra-nuclear Protein Inclusions. *Cell Rep* **31**, 107680 (2020).
230. Coux, O., Tanaka, K. & Goldberg, A.L. Structure and functions of the 20S and 26S proteasomes. *Annu Rev Biochem* **65**, 801-847 (1996).
231. Collins, G.A. & Goldberg, A.L. The Logic of the 26S Proteasome. *Cell* **169**, 792-806 (2017).
232. Livneh, I., Cohen-Kaplan, V., Cohen-Rosenzweig, C., Avni, N. & Ciechanover, A. The life cycle of the 26S proteasome: from birth, through regulation and function, and onto its death. *Cell Res* **26**, 869-885 (2016).
233. Hahn, J.S., Neef, D.W. & Thiele, D.J. A stress regulatory network for co-ordinated activation of proteasome expression mediated by yeast heat shock transcription factor. *Mol Microbiol* **60**, 240-251 (2006).
234. Akerfelt, M. *et al.* Heat shock transcription factor 1 localizes to sex chromatin during meiotic repression. *J Biol Chem* **285**, 34469-34476 (2010).
235. Muller, L. & Hoppe, T. UPS-dependent strategies of protein quality control degradation. *Trends Biochem Sci* **49**, 859-874 (2024).
236. Swatek, K.N. & Komander, D. Ubiquitin modifications. *Cell Res* **26**, 399-422 (2016).
237. Kowalski, L. *et al.* Determinants of the cytosolic turnover of mitochondrial intermembrane space proteins. *BMC Biol* **16**, 66 (2018).
238. Habich, M. *et al.* Vectorial Import via a Metastable Disulfide-Linked Complex Allows for a Quality Control Step and Import by the Mitochondrial Disulfide Relay. *Cell Rep* **26**, 759-774 e755 (2019).
239. Amponsah, P.S. *et al.* Aneuploidy-induced proteostasis disruption impairs mitochondrial functions and mediates aggregation of mitochondrial precursor proteins through SQSTM1/p62. *bioRxiv*, 2024.2007.2029.605607 (2024).
240. Kramer, L. *et al.* MitoStores: chaperone-controlled protein granules store mitochondrial precursors in the cytosol. *EMBO J* **42**, e112309 (2023).
241. Nowicka, U. *et al.* Cytosolic aggregation of mitochondrial proteins disrupts cellular homeostasis by stimulating the aggregation of other proteins. *Elife* **10** (2021).

242. Pfanner, N., den Brave, F. & Becker, T. Mitochondrial protein import stress. *Nature Cell Biology* **27**, 188-201 (2025).
243. Martensson, C.U. *et al.* Mitochondrial protein translocation-associated degradation. *Nature* **569**, 679-683 (2019).
244. Schuberth, C. & Buchberger, A. Membrane-bound Ubx2 recruits Cdc48 to ubiquitin ligases and their substrates to ensure efficient ER-associated protein degradation. *Nat Cell Biol* **7**, 999-1006 (2005).
245. Wang, C.-W. & Lee, S.-C. The ubiquitin-like (UBX)-domain-containing protein Ubx2/Ubxd8 regulates lipid droplet homeostasis. *Journal of cell science* **125**, 2930-2939 (2012).
246. Neuber, O., Jarosch, E., Volkwein, C., Walter, J. & Sommer, T. Ubx2 links the Cdc48 complex to ER-associated protein degradation. *Nat Cell Biol* **7**, 993-998 (2005).
247. Ishii, T., Funakoshi, M. & Kobayashi, H. Yeast Pth2 is a UBL domain-binding protein that participates in the ubiquitin-proteasome pathway. *EMBO J* **25**, 5492-5503 (2006).
248. Schulte, U. *et al.* Mitochondrial complexome reveals quality-control pathways of protein import. *Nature* **614**, 153-159 (2023).
249. Lapointe, C.P. *et al.* Multi-omics Reveal Specific Targets of the RNA-Binding Protein Puf3p and Its Orchestration of Mitochondrial Biogenesis. *Cell Syst* **6**, 125-135 e126 (2018).
250. Williams, C.C., Jan, C.H. & Weissman, J.S. Targeting and plasticity of mitochondrial proteins revealed by proximity-specific ribosome profiling. *Science* **346**, 748-751 (2014).
251. Filbeck, S., Cerullo, F., Pfeffer, S. & Joazeiro, C.A.P. Ribosome-associated quality-control mechanisms from bacteria to humans. *Mol Cell* **82**, 1451-1466 (2022).
252. Izawa, T., Park, S.H., Zhao, L., Hartl, F.U. & Neupert, W. Cytosolic Protein Vms1 Links Ribosome Quality Control to Mitochondrial and Cellular Homeostasis. *Cell* **171**, 890-903 e818 (2017).
253. Verma, R. *et al.* Vms1 and ANKZF1 peptidyl-tRNA hydrolases release nascent chains from stalled ribosomes. *Nature* **557**, 446-451 (2018).
254. Zurita Rendón, O. *et al.* Vms1p is a release factor for the ribosome-associated quality control complex. *Nat Commun* **9**, 2197 (2018).
255. Kuroha, K., Zinoviev, A., Hellen, C.U.T. & Pestova, T.V. Release of Ubiquitinated and Non-ubiquitinated Nascent Chains from Stalled Mammalian Ribosomal Complexes by ANKZF1 and Ptrh1. *Mol Cell* **72**, 286-302.e288 (2018).
256. Su, T. *et al.* Structure and function of Vms1 and Arb1 in RQC and mitochondrial proteome homeostasis. *Nature* **570**, 538-542 (2019).
257. Weidberg, H. & Amon, A. MitoCPR-A surveillance pathway that protects mitochondria in response to protein import stress. *Science* **360** (2018).
258. Chen, Y.C. *et al.* Msp1/ATAD1 maintains mitochondrial function by facilitating the degradation of mislocalized tail-anchored proteins. *EMBO J* **33**, 1548-1564 (2014).
259. Okreglak, V. & Walter, P. The conserved AAA-ATPase Msp1 confers organelle specificity to tail-anchored proteins. *Proc Natl Acad Sci U S A* **111**, 8019-8024 (2014).

260. Wohlever, M.L., Mateja, A., McGilvray, P.T., Day, K.J. & Keenan, R.J. Msp1 Is a Membrane Protein Dislocase for Tail-Anchored Proteins. *Mol Cell* **67**, 194-202 e196 (2017).
261. Basch, M. *et al.* Msp1 cooperates with the proteasome for extraction of arrested mitochondrial import intermediates. *Mol Biol Cell* **31**, 753-767 (2020).
262. Xiao, T., Shakya, V.P. & Hughes, A.L. ER targeting of non-imported mitochondrial carrier proteins is dependent on the GET pathway. *Life Sci Alliance* **4** (2021).
263. Schuldiner, M. *et al.* The GET complex mediates insertion of tail-anchored proteins into the ER membrane. *Cell* **134**, 634-645 (2008).
264. Hansen, K.G. *et al.* An ER surface retrieval pathway safeguards the import of mitochondrial membrane proteins in yeast. *Science* **361**, 1118-1122 (2018).
265. Knöringer, K. *et al.* The unfolded protein response of the endoplasmic reticulum supports mitochondrial biogenesis by buffering nonimported proteins. *Mol Biol Cell* **34**, ar95 (2023).
266. Koch, C. *et al.* The ER-SURF pathway uses ER-mitochondria contact sites for protein targeting to mitochondria. *EMBO Rep* **25**, 2071-2096 (2024).
267. Hees, J.T. *et al.* ER-associated biogenesis of PINK1 preprotein for neuronal mitophagy. *bioRxiv*, 2024.2006.2021.600039 (2024).
268. Hoj, J.P., Mayro, B. & Pendergast, A.M. The ABL2 kinase regulates an HSF1-dependent transcriptional program required for lung adenocarcinoma brain metastasis. *Proc Natl Acad Sci U S A* **117**, 33486-33495 (2020).
269. Kim, E. *et al.* NEDD4-mediated HSF1 degradation underlies alpha-synucleinopathy. *Hum Mol Genet* **25**, 211-222 (2016).
270. Singh, I.S. & Hasday, J.D. Fever, hyperthermia and the heat shock response. *Int J Hyperthermia* **29**, 423-435 (2013).
271. Cotto, J.J. & Morimoto, R.I. Stress-induced activation of the heat-shock response: cell and molecular biology of heat-shock factors. *Biochem Soc Symp* **64**, 105-118 (1999).
272. Zuo, J., Rungger, D. & Voellmy, R. Multiple layers of regulation of human heat shock transcription factor 1. *Mol Cell Biol* **15**, 4319-4330 (1995).
273. Farkas, T., Kutskova, Y.A. & Zimarino, V. Intramolecular repression of mouse heat shock factor 1. *Mol Cell Biol* **18**, 906-918 (1998).
274. Singh, M.K. *et al.* Heat Shock Response and Heat Shock Proteins: Current Understanding and Future Opportunities in Human Diseases. *Int J Mol Sci* **25** (2024).
275. Masser, A.E., Ciccarelli, M. & Andreasson, C. Hsf1 on a leash - controlling the heat shock response by chaperone titration. *Exp Cell Res* **396**, 112246 (2020).
276. Atlante, A. *et al.* Cytochrome c is released from mitochondria in a reactive oxygen species (ROS)-dependent fashion and can operate as a ROS scavenger and as a respiratory substrate in cerebellar neurons undergoing excitotoxic death. *J Biol Chem* **275**, 37159-37166 (2000).
277. Meyer, M., Schreck, R. & Baeuerle, P.A. H2O2 and antioxidants have opposite effects on activation of NF-kappa B and AP-1 in intact cells: AP-1 as secondary antioxidant-responsive factor. *Embo j* **12**, 2005-2015 (1993).
278. Zhang, Y. & Wong, H.S. Are mitochondria the main contributor of reactive oxygen species in cells? *J Exp Biol* **224** (2021).

279. Swindell, W.R., Huebner, M. & Weber, A.P. Transcriptional profiling of Arabidopsis heat shock proteins and transcription factors reveals extensive overlap between heat and non-heat stress response pathways. *BMC Genomics* **8**, 125 (2007).
280. Gorman, A.M., Heavey, B., Creagh, E., Cotter, T.G. & Samali, A. Antioxidant-mediated inhibition of the heat shock response leads to apoptosis. *FEBS Lett* **445**, 98-102 (1999).
281. Gorman, A.M., Szegezdi, E., Quigney, D.J. & Samali, A. Hsp27 inhibits 6-hydroxydopamine-induced cytochrome c release and apoptosis in PC12 cells. *Biochem Biophys Res Commun* **327**, 801-810 (2005).
282. Cullinan, S.B. & Diehl, J.A. Coordination of ER and oxidative stress signaling: the PERK/Nrf2 signaling pathway. *Int J Biochem Cell Biol* **38**, 317-332 (2006).
283. Chen, X., Shi, C., He, M., Xiong, S. & Xia, X. Endoplasmic reticulum stress: molecular mechanism and therapeutic targets. *Signal Transduction and Targeted Therapy* **8**, 352 (2023).
284. Read, A. & Schröder, M. The Unfolded Protein Response: An Overview. *Biology (Basel)* **10** (2021).
285. Urano, F. *et al.* Coupling of Stress in the ER to Activation of JNK Protein Kinases by Transmembrane Protein Kinase IRE1. *Science* **287**, 664-666 (2000).
286. Oikawa, D., Kimata, Y., Kohno, K. & Iwawaki, T. Activation of mammalian IRE1alpha upon ER stress depends on dissociation of BiP rather than on direct interaction with unfolded proteins. *Exp Cell Res* **315**, 2496-2504 (2009).
287. Korennykh, A.V. *et al.* The unfolded protein response signals through high-order assembly of Ire1. *Nature* **457**, 687-693 (2009).
288. Tirasophon, W., Lee, K., Callaghan, B., Welihinda, A. & Kaufman, R.J. The endoribonuclease activity of mammalian IRE1 autoregulates its mRNA and is required for the unfolded protein response. *Genes Dev* **14**, 2725-2736 (2000).
289. Oikawa, D., Kitamura, A., Kinjo, M. & Iwawaki, T. Direct association of unfolded proteins with mammalian ER stress sensor, IRE1β. *PLoS One* **7**, e51290 (2012).
290. Bao, Y. *et al.* IRE1B degrades RNAs encoding proteins that interfere with the induction of autophagy by ER stress in Arabidopsis thaliana. *Autophagy* **14**, 1562-1573 (2018).
291. Hollien, J. & Weissman, J.S. Decay of Endoplasmic Reticulum-Localized mRNAs During the Unfolded Protein Response. *Science* **313**, 104-107 (2006).
292. Guo, J. & Polymenis, M. Dcr2 targets Ire1 and downregulates the unfolded protein response in Saccharomyces cerevisiae. *EMBO Rep* **7**, 1124-1127 (2006).
293. Welihinda, A.A., Tirasophon, W., Green, S.R. & Kaufman, R.J. Protein serine/threonine phosphatase Ptc2p negatively regulates the unfolded-protein response by dephosphorylating Ire1p kinase. *Mol Cell Biol* **18**, 1967-1977 (1998).
294. Lu, P.D., Harding, H.P. & Ron, D. Translation reinitiation at alternative open reading frames regulates gene expression in an integrated stress response. *J Cell Biol* **167**, 27-33 (2004).

295. Gordiyenko, Y., Llácer, J.L. & Ramakrishnan, V. Structural basis for the inhibition of translation through eIF2α phosphorylation. *Nature Communications* **10**, 2640 (2019).
296. Adomavicius, T. *et al.* The structural basis of translational control by eIF2 phosphorylation. *Nature Communications* **10**, 2136 (2019).
297. Dever, T.E., Ivanov, I.P. & Hinnebusch, A.G. Translational regulation by uORFs and start codon selection stringency. *Genes Dev* **37**, 474-489 (2023).
298. Novoa, I., Zeng, H., Harding, H.P. & Ron, D. Feedback inhibition of the unfolded protein response by GADD34-mediated dephosphorylation of eIF2alpha. *J Cell Biol* **153**, 1011-1022 (2001).
299. Lin, J.H., Li, H., Zhang, Y., Ron, D. & Walter, P. Divergent effects of PERK and IRE1 signaling on cell viability. *PLoS One* **4**, e4170 (2009).
300. Lin, J.H. *et al.* IRE1 signaling affects cell fate during the unfolded protein response. *Science* **318**, 944-949 (2007).
301. Ye, J. *et al.* ER stress induces cleavage of membrane-bound ATF6 by the same proteases that process SREBPs. *Mol Cell* **6**, 1355-1364 (2000).
302. Oka, O.B. *et al.* ERp18 regulates activation of ATF6α during unfolded protein response. *The EMBO Journal* **38**, e100990 (2019).
303. Rawson, R.B. *et al.* Complementation cloning of S2P, a gene encoding a putative metalloprotease required for intramembrane cleavage of SREBPs. *Mol Cell* **1**, 47-57 (1997).
304. Bommiasamy, H. *et al.* ATF6alpha induces XBP1-independent expansion of the endoplasmic reticulum. *J Cell Sci* **122**, 1626-1636 (2009).
305. Shoulders, M.D. *et al.* Stress-independent activation of XBP1s and/or ATF6 reveals three functionally diverse ER proteostasis environments. *Cell Rep* **3**, 1279-1292 (2013).
306. Wang, Y. *et al.* Activation of ATF6 and an ATF6 DNA binding site by the endoplasmic reticulum stress response. *J Biol Chem* **275**, 27013-27020 (2000).
307. Thuerauf, D.J., Morrison, L. & Glembotski, C.C. Opposing roles for ATF6alpha and ATF6beta in endoplasmic reticulum stress response gene induction. *J Biol Chem* **279**, 21078-21084 (2004).
308. Yoshida, H. *et al.* A time-dependent phase shift in the mammalian unfolded protein response. *Dev Cell* **4**, 265-271 (2003).
309. Qu, J., Zou, T. & Lin, Z. The Roles of the Ubiquitin-Proteasome System in the Endoplasmic Reticulum Stress Pathway. *Int J Mol Sci* **22** (2021).
310. Ong, G. *et al.* IRE1 signaling increases PERK expression during chronic ER stress. *Cell Death & Disease* **15**, 276 (2024).
311. Chang, T.-K. *et al.* Coordination between Two Branches of the Unfolded Protein Response Determines Apoptotic Cell Fate. *Molecular Cell* **71**, 629-636.e625 (2018).
312. Acosta-Alvear, D. Common signaling principles and interconnectivity in the ISR-UPR networks. *The FASEB Journal* **36** (2022).
313. Dey, M. *et al.* PKR and GCN2 kinases and guanine nucleotide exchange factor eukaryotic translation initiation factor 2B (eIF2B) recognize overlapping surfaces on eIF2alpha. *Mol Cell Biol* **25**, 3063-3075 (2005).
314. Mick, E. *et al.* Distinct mitochondrial defects trigger the integrated stress response depending on the metabolic state of the cell. *Elife* **9** (2020).
315. Chen, J.J. Regulation of protein synthesis by the heme-regulated eIF2alpha kinase: relevance to anemias. *Blood* **109**, 2693-2699 (2007).

316. Lee, Y.Y., Cevallos, R.C. & Jan, E. An upstream open reading frame regulates translation of GADD34 during cellular stresses that induce eIF2alpha phosphorylation. *J Biol Chem* **284**, 6661-6673 (2009).
317. Han, J. *et al.* ER-stress-induced transcriptional regulation increases protein synthesis leading to cell death. *Nat Cell Biol* **15**, 481-490 (2013).
318. Ye, J. *et al.* Pyruvate kinase M2 promotes de novo serine synthesis to sustain mTORC1 activity and cell proliferation. *Proc Natl Acad Sci U S A* **109**, 6904-6909 (2012).
319. Li, X. *et al.* ATF3 promotes the serine synthesis pathway and tumor growth under dietary serine restriction. *Cell Rep* **36**, 109706 (2021).
320. Ryoo, H.D. The integrated stress response in metabolic adaptation. *J Biol Chem* **300**, 107151 (2024).
321. Fessler, E., Krumwiede, L. & Jae, L.T. DELE1 tracks perturbed protein import and processing in human mitochondria. *Nature Communications* **13**, 1853 (2022).
322. Yang, J. *et al.* DELE1 oligomerization promotes integrated stress response activation. *Nat Struct Mol Biol* **30**, 1295-1302 (2023).
323. Bi, P.Y. *et al.* Cytosolic retention of HtrA2 during mitochondrial protein import stress triggers the DELE1-HRI pathway. *Commun Biol* **7**, 391 (2024).
324. Wang, X. & Zhang, G. The mitochondrial integrated stress response: A novel approach to anti-aging and pro-longevity. *Ageing Research Reviews* **103**, 102603 (2025).
325. Forsström, S. *et al.* Fibroblast Growth Factor 21 Drives Dynamics of Local and Systemic Stress Responses in Mitochondrial Myopathy with mtDNA Deletions. *Cell Metab* **30**, 1040-1054.e1047 (2019).
326. Ahola, S. *et al.* OMA1-mediated integrated stress response protects against ferroptosis in mitochondrial cardiomyopathy. *Cell Metab* **34**, 1875-1891 e1877 (2022).
327. Han, S. *et al.* Mitochondrial integrated stress response controls lung epithelial cell fate. *Nature* **620**, 890-897 (2023).
328. Ahola, S. & Langer, T. Ferroptosis in mitochondrial cardiomyopathy. *Trends Cell Biol* **34**, 150-160 (2024).
329. Dey, S. *et al.* ATF4-dependent induction of heme oxygenase 1 prevents anoikis and promotes metastasis. *J Clin Invest* **125**, 2592-2608 (2015).
330. Verginadis, II *et al.* A stromal Integrated Stress Response activates perivascular cancer-associated fibroblasts to drive angiogenesis and tumour progression. *Nat Cell Biol* **24**, 940-953 (2022).
331. Ma, T. *et al.* Suppression of eIF2alpha kinases alleviates Alzheimer's disease-related plasticity and memory deficits. *Nat Neurosci* **16**, 1299-1305 (2013).
332. Yang, W. *et al.* Repression of the eIF2alpha kinase PERK alleviates mGluR-LTD impairments in a mouse model of Alzheimer's disease. *Neurobiol Aging* **41**, 19-24 (2016).
333. Zhu, P.J. *et al.* Activation of the ISR mediates the behavioral and neurophysiological abnormalities in Down syndrome. *Science* **366**, 843-849 (2019).
334. Hughes, C.S. *et al.* Ultrasensitive proteome analysis using paramagnetic bead technology. *Molecular Systems Biology* **10** (2014).

335. Ishihama, Y., Rappsilber, J. & Mann, M. Modular stop and go extraction tips with stacked disks for parallel and multidimensional Peptide fractionation in proteomics. *J Proteome Res* **5**, 988-994 (2006).
336. Nolte, H., MacVicar, T.D., Tellkamp, F. & Krüger, M. Instant Clue: A Software Suite for Interactive Data Visualization and Analysis. *Scientific Reports* **8**, 12648 (2018).
337. Cox, J. & Mann, M. MaxQuant enables high peptide identification rates, individualized p.p.b.-range mass accuracies and proteome-wide protein quantification. *Nature Biotechnology* **26**, 1367-1372 (2008).
338. Nolte, H., MacVicar, T.D., Tellkamp, F. & Kruger, M. Instant Clue: A Software Suite for Interactive Data Visualization and Analysis. *Sci Rep* **8**, 12648 (2018).
339. Ehses, S. *et al.* Regulation of OPA1 processing and mitochondrial fusion by m-AAA protease isoenzymes and OMA1. *J Cell Biol* **187**, 1023-1036 (2009).
340. Yamada, T. *et al.* Dual regulation of mitochondrial fusion by Parkin-PINK1 and OMA1. *Nature* (2025).
341. Ahola, S. *et al.* Opa1 processing is dispensable in mouse development but is protective in mitochondrial cardiomyopathy. *Sci Adv* **10**, eadp0443 (2024).
342. Lin, H.P. *et al.* DELE1 maintains muscle proteostasis to promote growth and survival in mitochondrial myopathy. *EMBO J* **43**, 5548-5585 (2024).
343. Shammas, M.K. *et al.* OMA1 mediates local and global stress responses against protein misfolding in CHCHD10 mitochondrial myopathy. *J Clin Invest* **132** (2022).
344. Rath, S. *et al.* MitoCarta3.0: an updated mitochondrial proteome now with sub-organelle localization and pathway annotations. *Nucleic Acids Res* **49**, D1541-d1547 (2021).
345. Busch, J.D., Fielden, L.F., Pfanner, N. & Wiedemann, N. Mitochondrial protein transport: Versatility of translocases and mechanisms. *Mol Cell* **83**, 890-910 (2023).
346. Mokranjac, D., Sichting, M., Neupert, W. & Hell, K. Tim14, a novel key component of the import motor of the TIM23 protein translocase of mitochondria. *EMBO J* **22**, 4945-4956 (2003).
347. Kohler, A. *et al.* Early fate decision for mitochondrially encoded proteins by a molecular triage. *Mol Cell* **83**, 3470-3484 e3478 (2023).
348. Patron, M. *et al.* Regulation of mitochondrial proteostasis by the proton gradient. *The EMBO Journal* **41**, e110476 (2022).
349. Christie, D.A. *et al.* Stomatin-like protein 2 binds cardiolipin and regulates mitochondrial biogenesis and function. *Mol Cell Biol* **31**, 3845-3856 (2011).
350. Crameri, J.J. *et al.* Reduced Protein Import via TIM23 SORT Drives Disease Pathology in TIMM50-Associated Mitochondrial Disease. *Mol Cell Biol* **44**, 226-244 (2024).
351. Acosta-Alvear, D., Harnoss, J.M., Walter, P. & Ashkenazi, A. Homeostasis control in health and disease by the unfolded protein response. *Nat Rev Mol Cell Biol* (2024).
352. Wiseman, R.L., Mesgarzadeh, J.S. & Hendershot, L.M. Reshaping endoplasmic reticulum quality control through the unfolded protein response. *Mol Cell* **82**, 1477-1491 (2022).
353. Grandjean, J.M.D. *et al.* Deconvoluting Stress-Responsive Proteostasis Signaling Pathways for Pharmacologic Activation Using Targeted RNA Sequencing. *ACS Chemical Biology* **14**, 784-795 (2019).

354. Madrazo, N., Khattar, Z., Powers, E.T., Rosarda, J.D. & Wiseman, R.L. Mapping Stress-Responsive Signaling Pathways Induced by Mitochondrial Proteostasis Perturbations. *bioRxiv*, 2024.2001.2030.577830 (2024).
355. Sutandy, F.X.R., Gossner, I., Tascher, G. & Munch, C. A cytosolic surveillance mechanism activates the mitochondrial UPR. *Nature* **618**, 849-854 (2023).
356. Michaelis, J.B. *et al.* Protein import motor complex reacts to mitochondrial misfolding by reducing protein import and activating mitophagy. *Nature Communications* **13**, 5164 (2022).
357. Pfanner, N., den Brave, F. & Becker, T. Mitochondrial protein import stress. *Nat Cell Biol* **27**, 188-201 (2025).
358. Navasa, N. *et al.* Regulation of oxidative stress by methylation-controlled J protein controls macrophage responses to inflammatory insults. *J Infect Dis* **211**, 135-145 (2015).
359. Wu, M.H. *et al.* Deleting the mitochondrial respiration negative regulator MCJ enhances the efficacy of CD8(+) T cell adoptive therapies in pre-clinical studies. *Nat Commun* **15**, 4444 (2024).
360. Champagne, D.P. *et al.* Fine-Tuning of CD8(+) T Cell Mitochondrial Metabolism by the Respiratory Chain Repressor MCJ Dictates Protection to Influenza Virus. *Immunity* **44**, 1299-1311 (2016).
361. Eiyama, A., Aaltonen, M.J., Nolte, H., Tatsuta, T. & Langer, T. Disturbed intramitochondrial phosphatidic acid transport impairs cellular stress signaling. *J Biol Chem* **296**, 100335 (2021).
362. Bi, P.Y. *et al.* Cytosolic retention of HtrA2 during mitochondrial protein import stress triggers the DELE1-HRI pathway. *Communications Biology* **7**, 391 (2024).
363. Lionaki, E., Gkikas, I. & Tavernarakis, N. Mitochondrial protein import machinery conveys stress signals to the cytosol and beyond. *Bioessays* **45**, e2200160 (2023).
364. Leonhard, K. *et al.* Membrane Protein Degradation by AAA Proteases in Mitochondria: Extraction of Substrates from Either Membrane Surface. *Molecular Cell* **5**, 629-638 (2000).
365. Tatsuta, T., Augustin, S., Nolden, M., Friedrichs, B. & Langer, T. m-AAA protease-driven membrane dislocation allows intramembrane cleavage by rhomboid in mitochondria. *EMBO J* **26**, 325-335 (2007).
366. Bonn, F., Tatsuta, T., Petrungaro, C., Riemer, J. & Langer, T. Presequence‐dependent folding ensures MrpL32 processing by the m‐AAA protease in mitochondria. *The EMBO Journal* **30**, 2545-2556 (2011).
367. Kikuchi, S. *et al.* A Ycf2-FtsHi Heteromeric AAA-ATPase Complex Is Required for Chloroplast Protein Import. *Plant Cell* **30**, 2677-2703 (2018).
368. Botelho, S.C., Tatsuta, T., von Heijne, G. & Kim, H. Dislocation by the m-AAA protease increases the threshold hydrophobicity for retention of transmembrane helices in the inner membrane of yeast mitochondria. *J Biol Chem* **288**, 4792-4798 (2013).
369. Rossi, A. *et al.* Genetic compensation induced by deleterious mutations but not gene knockdowns. *Nature* **524**, 230-233 (2015).
370. Kawai, Y. *et al.* A genome-wide CRISPR/Cas9 knockout screen identifies SEMA3F gene for resistance to cyclin-dependent kinase 4 and 6 inhibitors in breast cancer. *Breast Cancer* **32**, 120-131 (2025).

371. Khan, F.J., Yuen, G. & Luo, J. Multiplexed CRISPR/Cas9 gene knockout with simple crRNA:tracrRNA co-transfection. *Cell & Bioscience* **9**, 41 (2019).
372. Shalem, O. *et al.* Genome-Scale CRISPR-Cas9 Knockout Screening in Human Cells. *Science* **343**, 84-87 (2014).
373. Meng, H. *et al.* Application of CRISPR-Cas9 gene editing technology in basic research, diagnosis and treatment of colon cancer. *Front Endocrinol (Lausanne)* **14**, 1148412 (2023).
374. Sekine, S. *et al.* Reciprocal Roles of Tom7 and OMA1 during Mitochondrial Import and Activation of PINK1. *Mol Cell* **73**, 1028-1043.e1025 (2019).
375. Rainbolt, T.K., Saunders, J.M. & Wiseman, R.L. YME1L degradation reduces mitochondrial proteolytic capacity during oxidative stress. *EMBO Rep* **16**, 97-106 (2015).
376. Opalińska, M., Parys, K., Murcha, M.W. & Jańska, H. The plant i-AAA protease controls the turnover of an essential mitochondrial protein import component. *Journal of Cell Science* **131**, jcs200733 (2018).
377. Morgenstern, M. *et al.* Quantitative high-confidence human mitochondrial proteome and its dynamics in cellular context. *Cell Metabolism* **33**, 2464-2483.e2418 (2021).
378. Maruszczak, K.K., Draczkowski, P., Wnorowski, A. & Chacinska, A. Structure prediction analysis of human core TIM23 complex reveals conservation of the protein translocation mechanism. *FEBS Open Bio* **14**, 1656-1667 (2024).
379. Elancheliyan, P. *et al.* OCIAD1 and prohibitins regulate the stability of the TIM23 protein translocase. *Cell Rep* **43**, 115038 (2024).
380. Hatle, K. *et al.* MCJ/DnaJC15, an Endogenous Mitochondrial Repressor of the Respiratory Chain That Controls Metabolic Alterations. *Molecular and cellular biology* **33** (2013).
381. Di, K., Lomeli, N., Bota, D.A. & Das, B.C. Magmas inhibition as a potential treatment strategy in malignant glioma. *Journal of Neuro-Oncology* **141**, 267-276 (2019).
382. Tagliati, F. *et al.* Magmas, a Gene Newly Identified as Overexpressed in Human and Mouse ACTH-Secreting Pituitary Adenomas, Protects Pituitary Cells from Apoptotic Stimuli. *Endocrinology* **151**, 4635-4642 (2010).
383. Jubinsky, P.T. *et al.* Magmas expression in neoplastic human prostate. *J Mol Histol* **36**, 69-75 (2005).
384. Jubinsky, P.T. *et al.* Identification and characterization of Magmas, a novel mitochondria-associated protein involved in granulocyte-macrophage colony-stimulating factor signal transduction. *Exp Hematol* **29**, 1392-1402 (2001).
385. Sinha, D., Joshi, N., Chittoor, B., Samji, P. & D'Silva, P. Role of Magmas in protein transport and human mitochondria biogenesis. *Human Molecular Genetics* **19**, 1248-1262 (2010).
386. Yang, X. *et al.* The Impact of TIMM17A on Aggressiveness of Human Breast Cancer Cells. *Anticancer Res* **36**, 1237-1241 (2016).
387. Cai, J. *et al.* A TIMM17A Regulatory Network Contributing to Breast Cancer. *Front Genet* **12**, 658154 (2021).
388. Xu, X. *et al.* Quantitative proteomics study of breast cancer cell lines isolated from a single patient: discovery of TIMM17A as a marker for breast cancer. *Proteomics* **10**, 1374-1390 (2010).

389. Ojala, T. *et al.* New mutation of mitochondrial DNAJC19 causing dilated and noncompaction cardiomyopathy, anemia, ataxia, and male genital anomalies. *Pediatr Res* **72**, 432-437 (2012).
390. Al Tuwaijri, A. *et al.* Novel homozygous pathogenic mitochondrial DNAJC19 variant in a patient with dilated cardiomyopathy and global developmental delay. *Mol Genet Genomic Med* **10**, e1969 (2022).
391. Janz, A. *et al.* Mutations in DNAJC19 cause altered mitochondrial structure and increased mitochondrial respiration in human iPSC-derived cardiomyocytes. *Mol Metab* **79**, 101859 (2024).
392. Kampinga, H.H. *et al.* Function, evolution, and structure of J-domain proteins. *Cell Stress Chaperones* **24**, 7-15 (2019).
393. Giddings, E.L. *et al.* Mitochondrial ATP fuels ABC transporter-mediated drug efflux in cancer chemoresistance. *Nature Communications* **12**, 2804 (2021).
394. Wang, G. *et al.* An MCIA-like complex is required for mitochondrial complex I assembly and seed development in maize. *Molecular Plant* **15**, 1470-1487 (2022).
395. Stefely, J.A. & Pagliarini, D.J. Biochemistry of Mitochondrial Coenzyme Q Biosynthesis. *Trends Biochem Sci* **42**, 824-843 (2017).
396. He, C.H., Xie, L.X., Allan, C.M., Tran, U.C. & Clarke, C.F. Coenzyme Q supplementation or over-expression of the yeast Coq8 putative kinase stabilizes multi-subunit Coq polypeptide complexes in yeast coq null mutants. *Biochimica et Biophysica Acta (BBA) - Molecular and Cell Biology of Lipids* **1841**, 630-644 (2014).
397. Nguyen, T.P. *et al.* Molecular characterization of the human COQ5 C-methyltransferase in coenzyme Q10 biosynthesis. *Biochim Biophys Acta* **1841**, 1628-1638 (2014).
398. Yen, H.-C. *et al.* Disruption of the human COQ5-containing protein complex is associated with diminished coenzyme Q10 levels under two different conditions of mitochondrial energy deficiency. *Biochimica et Biophysica Acta (BBA) - General Subjects* **1860**, 1864-1876 (2016).
399. Floyd, B.J. *et al.* Mitochondrial Protein Interaction Mapping Identifies Regulators of Respiratory Chain Function. *Mol Cell* **63**, 621-632 (2016).
400. Heeringa, S.F. *et al.* COQ6 mutations in human patients produce nephrotic syndrome with sensorineural deafness. *J Clin Invest* **121**, 2013-2024 (2011).
401. Stefely, J.A. *et al.* Cerebellar Ataxia and Coenzyme Q Deficiency through Loss of Unorthodox Kinase Activity. *Mol Cell* **63**, 608-620 (2016).
402. Guarás, A. *et al.* The CoQH2/CoQ Ratio Serves as a Sensor of Respiratory Chain Efficiency. *Cell Reports* **15**, 197-209 (2016).
403. Enriquez, J.A. & Lenaz, G. Coenzyme q and the respiratory chain: coenzyme q pool and mitochondrial supercomplexes. *Mol Syndromol* **5**, 119-140 (2014).
404. Priesnitz, C. *et al.* Coupling to Pam16 differentially controls the dual role of Pam18 in protein import and respiratory chain formation. *Cell Rep* **39**, 110619 (2022).
405. Elachouri, G. *et al.* OPA1 links human mitochondrial genome maintenance to mtDNA replication and distribution. *Genome Res* **21**, 12-20 (2011).
406. Maity, S. & Chakrabarti, O. Mitochondrial protein import as a quality control sensor. *Biol Cell* **113**, 375-400 (2021).
407. Desai, R. & Campanella, M. MitoCPR: Meticulous Monitoring of Mitochondrial Proteostasis. *Mol Cell* **71**, 8-9 (2018).

408. Sutandy, F.X.R., Gößner, I., Tascher, G. & Münch, C. A cytosolic surveillance mechanism activates the mitochondrial UPR. *Nature* **618**, 849-854 (2023).
409. Shpilka, T. & Haynes, C.M. The mitochondrial UPR: mechanisms, physiological functions and implications in ageing. *Nature Reviews Molecular Cell Biology* **19**, 109-120 (2018).
410. Nowicka, U. *et al.* Cytosolic aggregation of mitochondrial proteins disrupts cellular homeostasis by stimulating the aggregation of other proteins. *eLife* **10**, e65484 (2021).
411. Wrobel, L. *et al.* Mistargeted mitochondrial proteins activate a proteostatic response in the cytosol. *Nature* **524**, 485-488 (2015).
412. Wang, X. & Chen, X.J. A cytosolic network suppressing mitochondria-mediated proteostatic stress and cell death. *Nature* **524**, 481-484 (2015).
413. Blackwood, E.A. *et al.* ATF6 Regulates Cardiac Hypertrophy by Transcriptional Induction of the mTORC1 Activator, Rheb. *Circ Res* **124**, 79-93 (2019).
414. Blackwood, E.A., Bilal, A.S., Stauffer, W.T., Arrieta, A. & Glembotski, C.C. Designing Novel Therapies to Mend Broken Hearts: ATF6 and Cardiac Proteostasis. *Cells* **9**, 602 (2020).
415. Lin, J.H. *et al.* IRE1 Signaling Affects Cell Fate During the Unfolded Protein Response. *Science* **318**, 944-949 (2007).
416. Walter, F., Schmid, J., Düssmann, H., Concannon, C.G. & Prehn, J.H.M. Imaging of single cell responses to ER stress indicates that the relative dynamics of IRE1/XBP1 and PERK/ATF4 signalling rather than a switch between signalling branches determine cell survival. *Cell Death & Differentiation* **22**, 1502-1516 (2015).
417. Plate, L. *et al.* Small molecule proteostasis regulators that reprogram the ER to reduce extracellular protein aggregation. *eLife* **5**, e15550 (2016).
418. Zanfardino, P., Amati, A., Perrone, M. & Petruzzella, V. The Balance of MFN2 and OPA1 in Mitochondrial Dynamics, Cellular Homeostasis, and Disease. *Biomolecules* **15**, 433 (2025).
419. Cogliati, S., Enriquez, J.A. & Scorrano, L. Mitochondrial Cristae: Where Beauty Meets Functionality. *Trends in Biochemical Sciences* **41**, 261-273 (2016).
420. Youle, R.J. & van der Bliek, A.M. Mitochondrial Fission, Fusion, and Stress. *Science* **337**, 1062-1065 (2012).
421. Guillery, O. *et al.* Metalloprotease-mediated OPA1 processing is modulated by the mitochondrial membrane potential. *Biol Cell* **100**, 315-325 (2008).
422. Head, B., Griparic, L., Amiri, M., Gandre-Babbe, S. & van der Bliek, A.M. Inducible proteolytic inactivation of OPA1 mediated by the OMA1 protease in mammalian cells. *J Cell Biol* **187**, 959-966 (2009).
423. Bayne, A.N., Dong, J., Amiri, S., Farhan, S.M.K. & Trempe, J.-F. MTSviewer: A database to visualize mitochondrial targeting sequences, cleavage sites, and mutations on protein structures. *PLOS ONE* **18**, e0284541 (2023).
424. Torrence, M.E. *et al.* The mTORC1-mediated activation of ATF4 promotes protein and glutathione synthesis downstream of growth signals. *eLife* **10**, e63326 (2021).

7. Extended figures

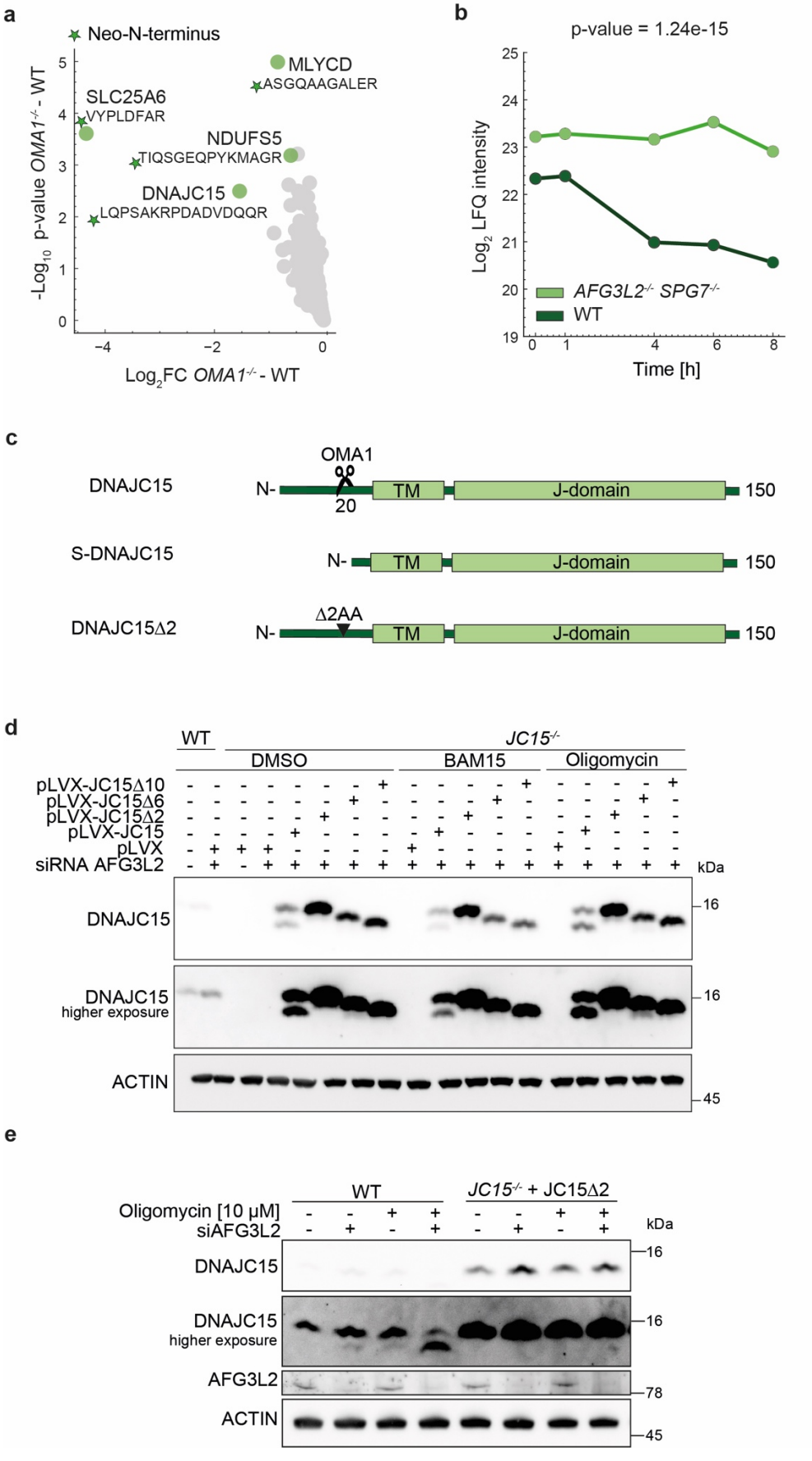

7. Extended figures

Extended Data Figure 1. **a**, Volcano plot of the Neo-N-terminal proteome of wild-type (WT) and *OMA1*$^{-/-}$ HeLa cells, highlighting significantly affected mitochondrial proteins in green (FDR < 0.05; MitoCarta 3.0). (n = 5, biologically independent samples). **b**, Stability of DNAJC15 in WT and *AFG3L2*$^{-/-}$ *SPG7*$^{-/-}$ HeLa cells (FDR < 0.05; n = 5, biologically independent samples). **c**, Schematic representation of the different DNAJC15 variants (TM = transmembrane domain). **d**, Western blot analysis of WT and *DNAJC15*$^{-/-}$ HeLa cells, which transiently express DNAJC15 or DNAJC15 variants lacking two (19/20), six (17-22) or ten (15-24) amino acids. After siRNA-mediated depletion of AFG3L2 for 72 h and treatment with oligomycin (10 µM) or Bam15 (10 µM) for 2 h, cells were lysed and analysed by SDS-PAGE and immunoblotting. **e**, Western blot analysis of WT and *DNAJC15*$^{-/-}$ HeLa cells stably expressing DNAJC15Δ2 following treatment with siRNA directed against AFG3L2 for 72 h and with oligomycin (10 µM) for 16 h as indicated.

7. Extended figures

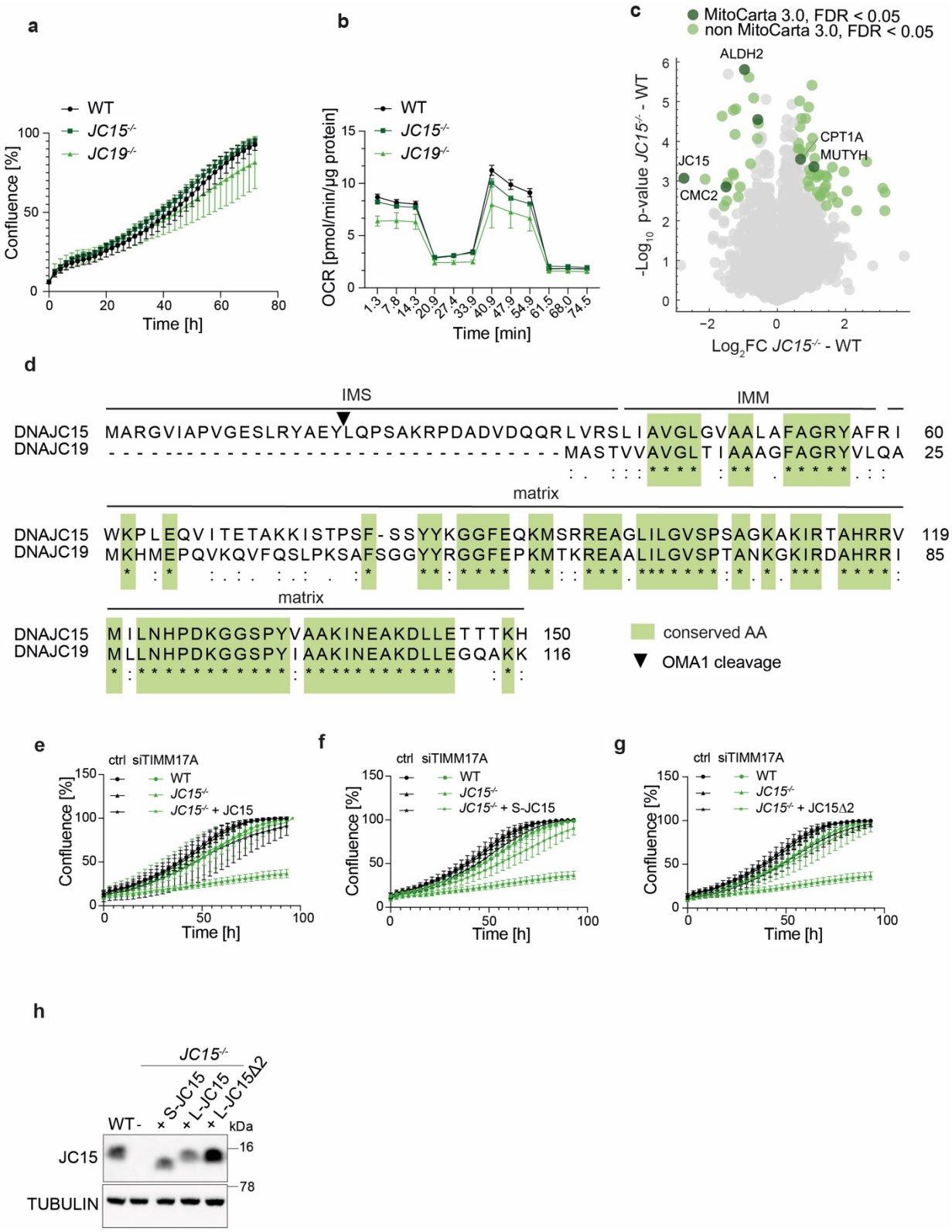

7. Extended figures

Extended Data Figure 2. **a**, Cell growth of wild-type (WT), *DNAJC15*$^{-/-}$, and *DNAJC19*$^{-/-}$ HeLa cells (n = 3, biologically independent samples). Data are presented as means +/- SD. **b**, Oxygen consumption rate (OCR) of WT, *DNAJC15*$^{-/-}$, and *DNAJC19*$^{-/-}$ cells after the addition of oligomycin, FCCP, and antimycin A (n = 3, biologically independent samples). **c**, Volcano plot of cellular proteomes of wild-type and *DNAJC15*$^{-/-}$ HeLa cells. Significantly affected proteins (FDR < 0.05) are shown in green, significantly changed MitoCarta 3.0-annotated proteins in dark green (n = 5, biologically independent samples). **d**, Sequence alignment of human DNAJC15 and DNAJC19. Conserved amino acids are highlighted in green. IMS, intermembrane space; IM, inner mitochondrial membrane. **e-g**, Growth of wild-type (WT) cells, *DNAJC15*$^{-/-}$ cells and *DNAJC15*$^{-/-}$ cells expressing (e) DNAJC15, (f) cleaved DNAJC15 (S-DNAJC15) or (g) DNAJC15Δ2, which were treated with siRNA targeting TIMM17A for 72 h (n = 3, biologically independent samples). Data are presented as means +/- SD. **h**, Expression of DNAJC15 and variants in different HeLa cell lines monitored by Western Blot.

7. Extended figures

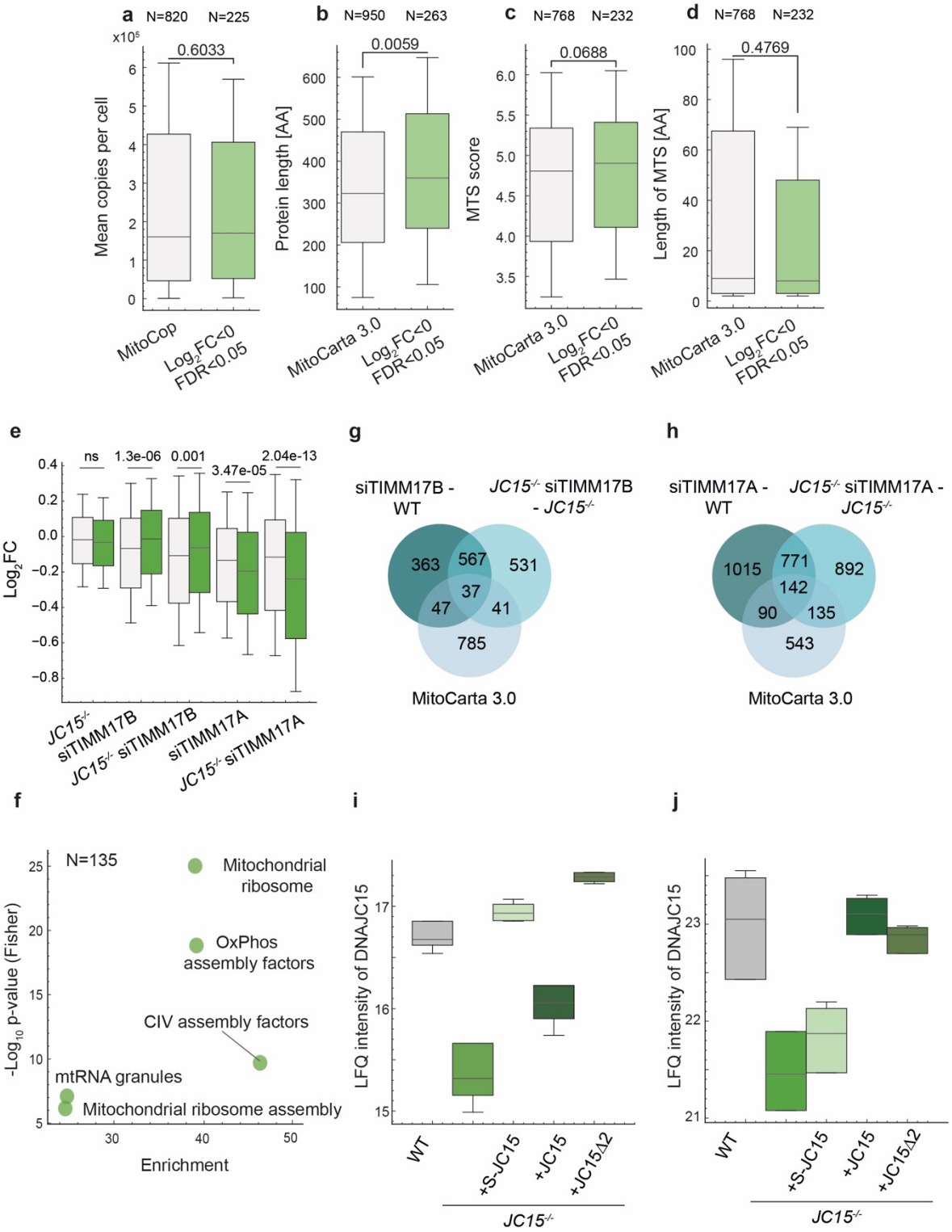

7. Extended figures

Extended Data Figure 3. **a**, Boxplot visualizing the distribution of significantly downregulated proteins in the mitochondrial fraction ($log_2FC < 0$, FDR < 0.05) compared to all MitoCop or MitoCarta 3.0-annotated fractions. Mann-Whitney U-test was performed. Quantile box plot show median (n = 5, biologically independent samples). The distribution indicates the mean copies per cell, extracted from Morgenstern *et al*. [76], in **a**, the protein length in **b**, the highest calculated MTS score in **c** and the length of the MTS with the highest MTS score in **d**, both extracted from the MTSviewer platform [423]. **e**, Boxplot visualizing the distribution of mitochondrial proteins (MitoCarta 3.0) compared to all identified proteins in the whole cell fraction in HeLa WT and *DNAJC15*$^{-/-}$ cells, treated with siRNA targeting TIMM17A or TIMM17B. Mann-Whitney U-test was performed. Quantile box plot show median, 25th and 75th (n = 5, biologically independent samples). **f**, MitoPathways enrichment analysis of the significant mitochondrial (according to MitoCarta 3.0) proteins, that are specifically affected in *DNAJC15*$^{-/-}$ treated with siRNA targeting TIMM17A (s. Fig. 3c, FDR < 0.05). Pathways are enriched with FDR < 0.02. **g**, Venn diagram visualizing the overlap of the significantly changed proteins of WT and *DNAJC15*$^{-/-}$ cells, treated with siRNA targeting TIMM17B, and MitoCarta 3.0-annotated protein groups (FDR < 0.05). **h**, Venn diagram visualizing the overlap of the significantly changed proteins of WT and *DNAJC15*$^{-/-}$ cells, treated with siRNA targeting TIMM17A, and MitoCarta 3.0- annotated protein groups (FDR < 0.05). **i**, Boxplot visualizing the LFQ intensity of all identified DNAJC15 peptides in the different cell lines from the input fraction after crosslinking with 2 mM DSP (n = 4, biologically independent samples). **j**, Boxplot visualizing the LFQ intensity of all identified DNAJC15 peptides in the different cell lines in the elution fraction after crosslinking with 2 mM DSP (n = 4, biologically independent samples).

7. Extended figures

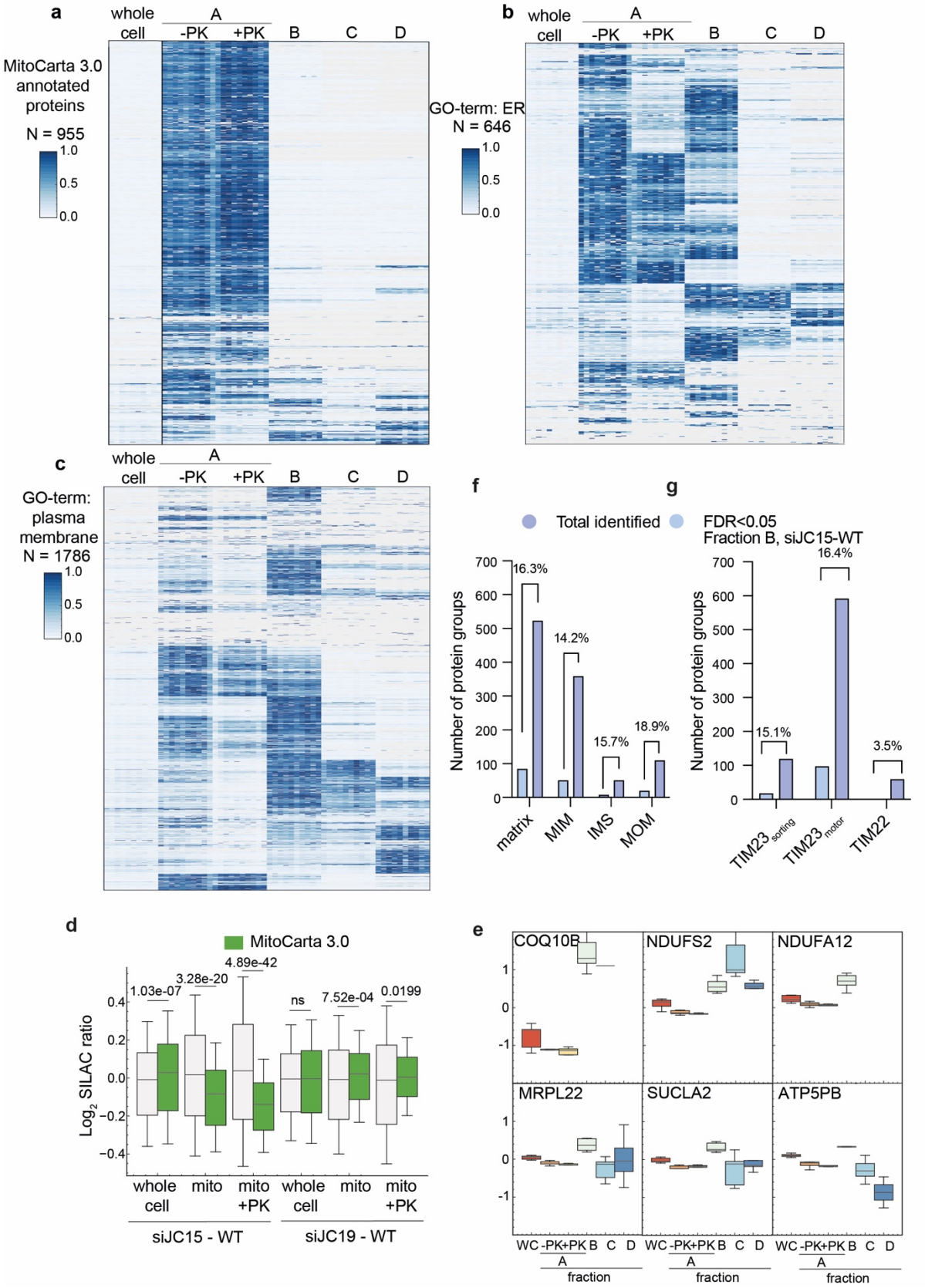

7. Extended figures

Extended Data Figure 4. **a**, Heat map showing the intensity-based absolute quantification values of all MitoCarta 3.0 annotated proteins in all extracted fractions according to Fig. 7a (n = 5, biologically independent samples). **b**, Heat map showing the intensity-based absolute quantification values of all proteins annotated with the GO-term 'ER' in all extracted fractions according to Fig. 7a (n = 5, biologically independent samples). **c**, Heat map showing the intensity-based absolute quantification values of all proteins annotated with the GO-term 'plasma membrane' in all extracted fractions according to Fig. 7a (n = 5, biologically independent samples). **d**, Boxplot visualizing the distribution of selected mitochondrial proteins (MitoCarta 3.0) and all identified proteins in the whole cell and in the mitochondrial fractions, which were treated with Proteinase K (PK) when indicated. Mann-Whitney U-test was performed. Quantile box plot show median, 25th and 75th percentiles were adapted to 0.5x fold (n = 5, biologically independent samples). **e**, Panel of significantly downregulated proteins in the mitochondrial fraction treated with PK, that were also significantly upregulated in the 40,000xg fraction upon depletion of DNAJC15 (FDR < 0.05, n = 5, biologically independent samples). **f**, Fraction of significantly changed mitochondrial proteins (FDR < 0.05) within all identified proteins according to the submitochondrial localization of MitoCarta 3.0. **g**, Fraction of significantly changed mitochondrial proteins (FDR < 0.05) within all identified proteins according to their mitochondrial protein import pathway [350].

7. Extended figures

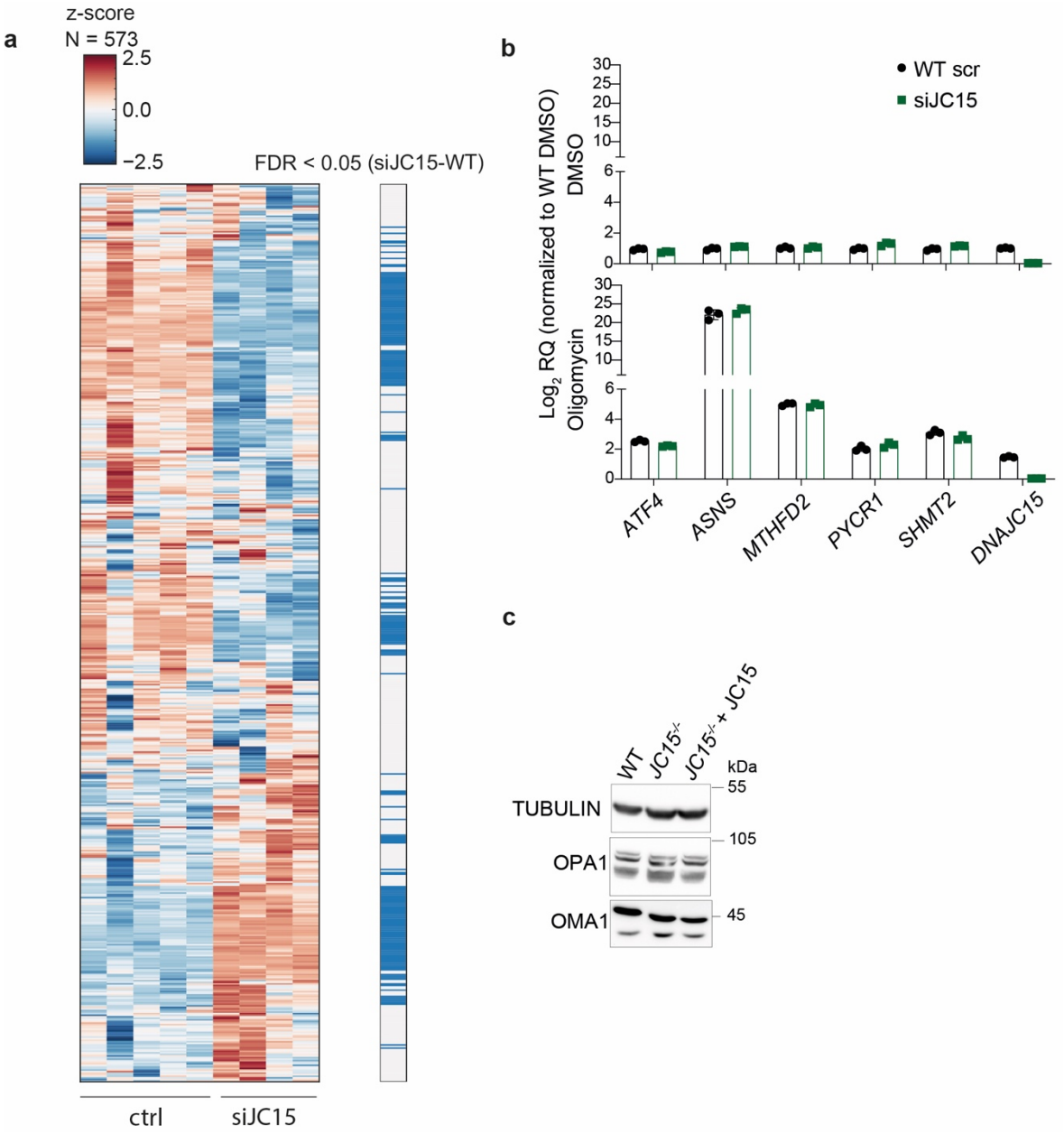

Extended Data Figure 5. **a,** Heat map of ATF4-dependent target genes [424], whose expression in DNAJC15-depleted relative to wild-type (WT) cells (log_2FC) is shown. Genes whose expression was significantly changed after DNAJC15 depletion ($p < 0.05$) are shown in blue. **b**, Log_2 RQ values, normalized to WT cells treated with DMSO (upper panel) or oligomycin (10 µM, lower panel), for cells depleted of DNAJC15 for 48 h (n = 3). **c**, Steady-state levels of OMA1 and OPA1 in WT HeLa, *DNAJC15*$^{-/-}$and *DNAJC15*$^{-/-}$ cells expressing DNAJC15 analysed by Western blot.

7. Extended figures

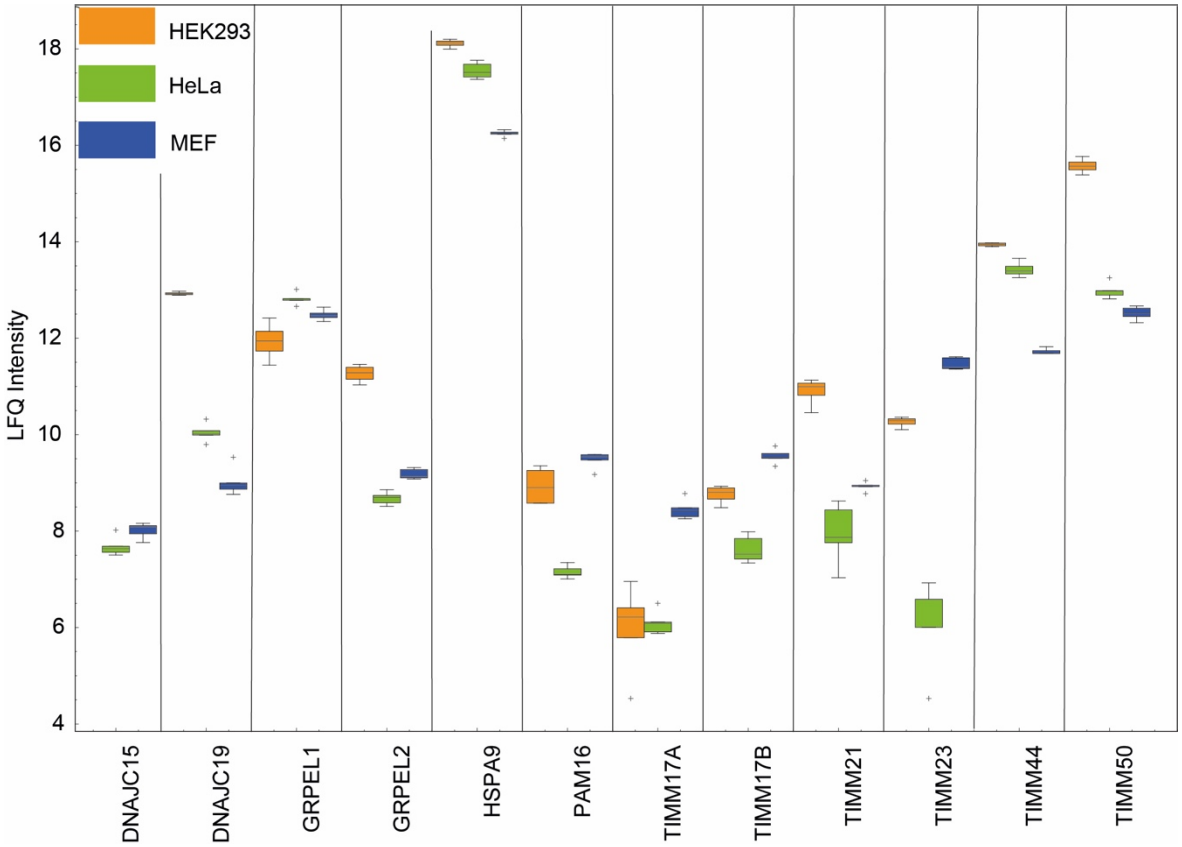

Extended Data Figure 6, Relative expression level of the various subunits of the TIM23 complex in wild-type (WT) Human Embryonic Kidney (HEK) 293, HeLa and Mouse Embyronic Fibroblast (MEF) cell lines (n = 5, biologically independent samples).

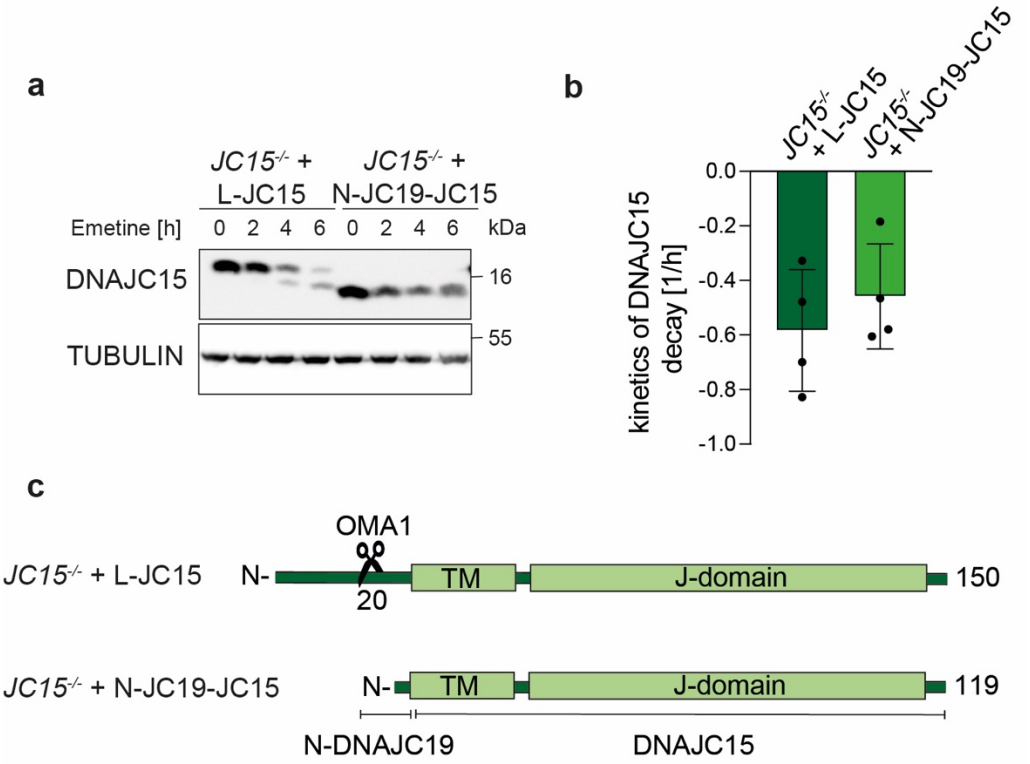

Extended Data Figure 7. **a**, Stability of DNAJC15 in *JC15*$^{-/-}$ + L-JC15 and *JC15*$^{-/-}$ + N-JC19-JC15 HeLa cells after inhibition of cytosolic translation with Emetine for 6h. A representative experiment is shown (n = 4, biologically independent samples). **b**, Degradation rates of DNAJC15 in (a) normalized to time point 0 h. Data are means +/- SD (n = 4, biologically independent samples). Significance was calculated using a two-sided unpaired t-test. **c**, Schematic representation of the different chimeric DNAJC15 variants (TM = transmembrane domain).

7. Extended figures

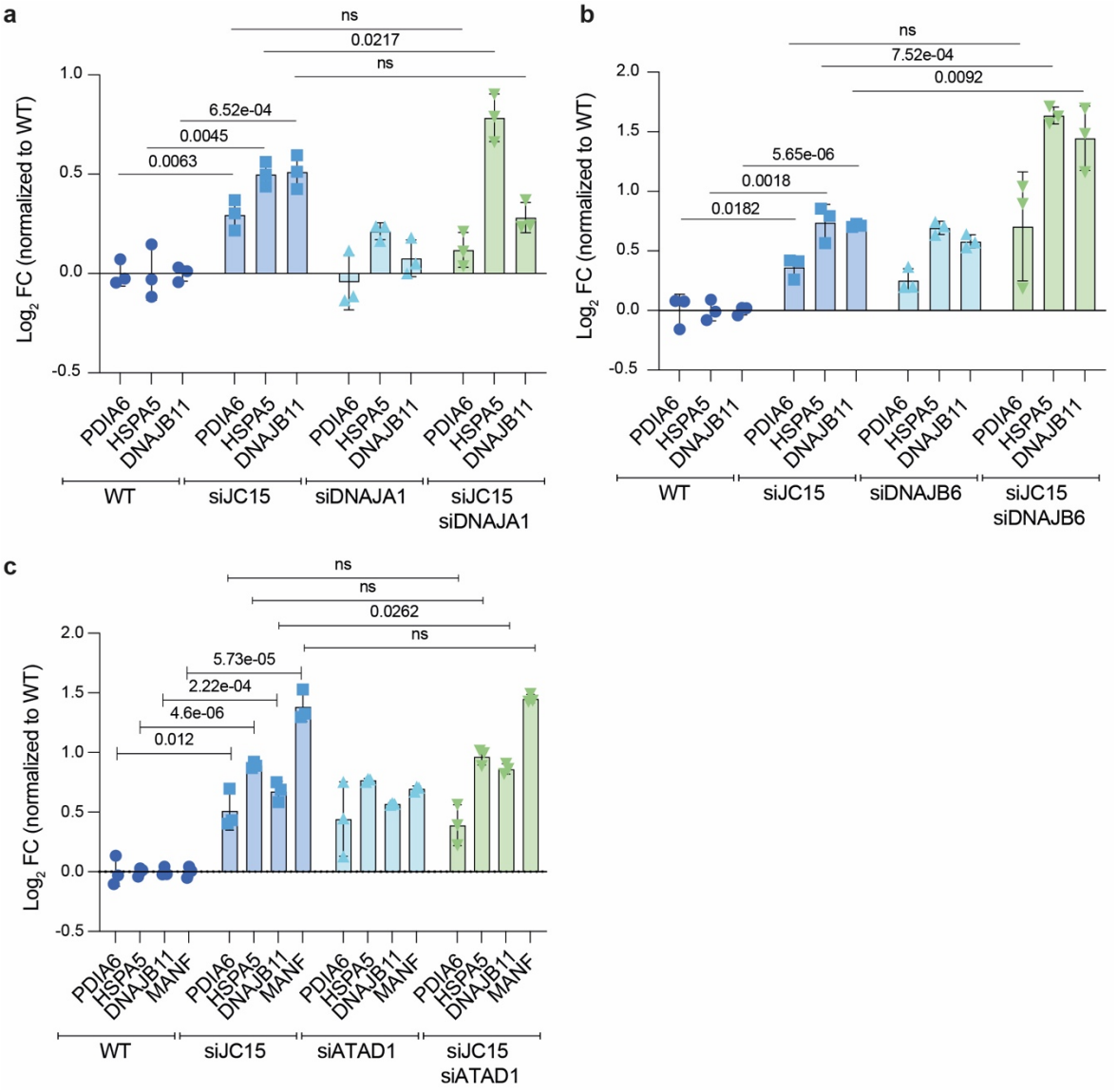

Extended Data Figure 8, Log_2FC values, normalized to HeLa WT cells treated with scr control, for cells depleted of DNAJC15 for 48 h (n = 3, biologically independent samples) and for **a**, DNAJA1 for 72 h (n = 3, biologically independent samples), **b**, DNAJB6 for 72 h (n = 3, biologically independent samples), **c**, ATAD1 for 72 h (n = 3, biologically independent samples). Significance was calculated using a two-sided unpaired t-test.